

11-24-2015

Evaluation of Organic Protective Coatings as Corrosion Prevention for The Interior of Subsea Pipelines in Sour Gas Service

Faris M. Alkordy
falko001@fiu.edu

DOI: 10.25148/etd.FIDC000201

Follow this and additional works at: <https://digitalcommons.fiu.edu/etd>

 Part of the [Other Materials Science and Engineering Commons](#), and the [Polymer and Organic Materials Commons](#)

Recommended Citation

Alkordy, Faris M., "Evaluation of Organic Protective Coatings as Corrosion Prevention for The Interior of Subsea Pipelines in Sour Gas Service" (2015). *FIU Electronic Theses and Dissertations*. 2304.
<https://digitalcommons.fiu.edu/etd/2304>

This work is brought to you for free and open access by the University Graduate School at FIU Digital Commons. It has been accepted for inclusion in FIU Electronic Theses and Dissertations by an authorized administrator of FIU Digital Commons. For more information, please contact dcc@fiu.edu.

FLORIDA INTERNATIONAL UNIVERSITY

Miami, Florida

EVALUATION OF ORGANIC PROTECTIVE COATINGS AS CORROSION
PREVENTION FOR THE INTERIOR OF SUBSEA PIPELINES IN SOUR GAS
SERVICE

A thesis submitted in partial fulfillment of

the requirements for the degree of

MASTER OF SCIENCE

in

MATERIAL SCIENCE AND ENGINEERING

by

Faris Mohammed Alkordy

2015

To: Interim Dean Ranu Jung
College of Engineering and Computing

This thesis, written by Faris Mohammed Alkordy, and entitled Evaluation of Organic Protective Coatings as Corrosion Prevention for The Interior of Subsea Pipelines in Sour Gas Service, having been approved in respect to style and intellectual content, is referred to you for judgment.

We have read this thesis and recommend that it be approved.

Kingsley Lau

Benjamin Boesl

Zhe Cheng

Norman Munroe, Major Professor

Date of Defense: November 24, 2015

The thesis of Faris Mohammed Alkordy is approved.

Interim Dean Ranu Jung
College of Engineering and Computing

Dean Lakshmi N. Reddi
University Graduate School

Florida International University, 2015

© Copyright 2015 by Faris Mohammed Alkordy

All rights reserved.

DEDICATION

I dedicate this thesis to my parents and my lovely wife who have always supported and encouraged me.

ACKNOWLEDGMENTS

Firstly, I would like to express my sincere gratitude to my Major Professor Dr. Norman Munroe for the continuous support of my Master's study and related research. Also, for his patience, motivation, and immense knowledge. His guidance and valuable advice have helped me significantly to achieve the milestones of the research. Besides my advisor, I would like to thank the rest of my thesis committee: Dr. Kingsley Lau, Dr. Benjamin Boesl, and Dr. Zhe Cheng for their insightful comments and advice, which encouraged me to widen my research from various perspectives. I wish to express my sincere appreciation to Dr. Kingsley Lau for his close supervision and continuous guidance throughout the research, and also for allowing me to access the laboratory and use the equipment. Without their precious support and guidance, it would not be possible to complete this research. Lastly, I would like to thank my parents and wife for supporting me spiritually throughout writing this thesis and my life in general.

ABSTRACT OF THE THESIS

EVALUATION OF ORGANIC PROTECTIVE COATINGS AS CORROSION
PREVENTION FOR THE INTERIOR OF SUBSEA PIPELINES IN SOUR GAS
SERVICE

by

Faris Mohammed Alkordy

Florida International University, 2015

Miami, Florida

Professor Norman Munroe, Major Professor

The purpose of this study was to examine the performance of several generic types of organic protective coatings as a corrosion protection method for the interior of subsea pipelines in sour gas media. The sour gas environment was simulated in the laboratory by the use of an Autoclave and the performance of the organic coatings was studied via the use of Electrochemical Impedance Spectroscopy (EIS) and Linear Polarization Resistance (LPR) tests to determine the coatings resistance, capacitance and corrosion behavior before and after the exposure to sour gas environment. The coating degradation and the corrosion products formed were examined by the use of SEM/EDS. The results indicated that both FBE and Novolac Epoxy coatings had excellent adhesion properties and chemical resistance. The Amine-Cured Novolac Epoxy coating exhibited good adhesion properties and chemical resistance. However, the Phenolic Epoxy coating started to degrade over time and corrosion took place under the coating.

TABLE OF CONTENTS

CHAPTER	PAGE
1. INTRODUCTION.....	1
2. LITERATURE REVIEW AND BACKGROUND.....	6
Natural Gas Extraction and Composition.....	6
Corrosion Phenomena in Sour Gas Pipelines.....	7
Corrosiveness of Water (Brine).....	13
CO ₂ Corrosion (Sweet Corrosion).....	15
H ₂ S Corrosion (Sour Corrosion).....	17
Corrosion Control in the Oil and Gas Industry.....	18
3. RESEARCH OBJECTIVES AND HYPOTHESIS.....	22
4. EXPERIMENTAL METHODS AND MATERIALS.....	23
Experimental Methods and Analytical Techniques.....	23
Electrochemical Testing Techniques.....	26
Experimental Procedures and Test Panels Preparation.....	38
Test Matrix.....	45
5. RESULTS AND DISCUSSION.....	47
EIS & LPR Results Before Autoclave.....	47
Chemical Resistance (Autoclave Test) Results.....	55
EIS & LPR Results After Autoclave.....	57
Pull-Off Adhesion Test Results.....	67
SEM/EDS Results.....	71
6. CONCLUSIONS AND RECOMMENDATIONS.....	76
LIST OF REFERENCES.....	79
APPENDICES.....	82

LIST OF TABLES

TABLE	PAGE
1. Generic types of coatings and test names.....	23
2. The common electrical circuit elements.....	30
3. Typical dielectric constants.....	32
4. Autoclave test parameters.....	43
5. Test Matrix.....	45

LIST OF FIGURES

FIGURE	PAGE
1. Natural Gas Offshore Fields in Arabian Gulf.....	4
2. Corrosion Process.....	8
3. Corrosion Mechanisms in a Pipeline.....	9
4. Corrosion rate of Fe in aerated solution at room temperature.....	14
5. Mechanisms for iron dissolution in aqueous solutions containing H ₂ S.....	17
6. Pull-Off Adhesion Tester.....	24
7. Adhesion and cohesive failure of coatings systems.....	24
8. Applied potential vs. Resulting current.....	27
9. Sinusoidal current response to the applied AC potential in a linear system.....	29
10. The equivalent circuit of an organic coating on a metallic substrate.....	31
11. Purely capacitive coating.....	34
12. Simplified Randles Cell.....	34
13. Equivalent Circuit for a Damaged Coating.....	34
14. Nyquist Plot with Impedance Vector.....	34
15. Equivalent Circuit with one time constant.....	34
16. The Bode plot with one time constant.....	35
17. Bode plot for a purely capacitive coating.....	35
18. Nyquist plot for a purely capacitive coating.....	35
19. Nyquist Plot for Randles Cell.....	36

20. Bode Plot for Randles cell.....	36
21. Nyquist Plot for a degraded coating.....	37
22. Bode Plot for a degraded coating.....	37
23. Test Dolly glued on a coated substrate.....	39
24. Schematic view of the three-electrode corrosion cell.....	40
25. Acrylic tubes glued on coated panels.....	41
26. Gamry's Electrochemical Multiplexer ECM.....	41
27. Titanium mesh as a counter and reference electrodes.....	41
28. LPR and EIS experimental setup.....	41
29. Parr Bench Top Reactor and Temperature Controller.....	42
30. Two samples molded in epoxy.....	44
31. Phenolic Epoxy and FBE as received.....	46
32. Amine Novolac and Novolac Epoxy as received.....	46
33. Phenolic and FBE coatings with defect.....	46
34. Amine Novolac and Novolac Epoxy with defect.....	46
35. Bode Plot of all coating for panel #1 in the gas phase.....	48
36. Bode Plot of all coating for panel #1 in the liquid phase.....	49
37. Nyquist Plot of all coating for panel #1 in the gas phase.....	49
38. Nyquist Plot of all coating for panel #1 in the liquid phase.....	50
39. Coating capacitance (F/cm^2) for panels #1 in the gas phase.....	51
40. Coating capacitance (F/cm^2) for panels #1 in the liquid phase.....	52
41. Pore Resistance (R_{po}) for panel #1 in the gas phase.....	52
42. Pore Resistance (R_{po}) for panel #1 in the liquid phase.....	53

43. icorr Vs. Time for panels #10 & #12 in the gas phase.....	54
44. icorr Vs. Time for panels #10 & #12 in the liquid phase.....	55
45. FBE and Phenolic Epoxy coated panels after the autoclave test.....	56
46. Amine Novolac and Novolac Epoxy coated panels after the autoclave test.....	56
47. Bode Plot of all coating for panel #1 in the gas phase.....	57
48. Bode Plot of all coating for panel #1 in the liquid phase.....	58
49. Nyquist Plot of all coating for panel #1 in the gas phase.....	58
50. Nyquist Plot of all coating for panel #1 in the liquid phase.....	59
51. Coating capacitance (F/cm ²) for panels #1 in the gas phase.....	60
52. Coating capacitance (F/cm ²) for panels #1 in the liquid phase.....	61
53. Pore Resistance (R _{po}) for panel #1 in the gas phase.....	61
54. Pore Resistance (R _{po}) for panel #1 in the liquid phase.....	62
55. Logarithmic Coating Impedance Scale.....	63
56. Z (ohm.cm ²) at 0.1 Hz for panel #1 in gas/liquid phases before/after autoclave.	64
57. Z (ohm.cm ²) at 0.1 Hz for panel #3 in gas/liquid phases before/after autoclave.	65
58. icorr Vs. Time for panels #10 & #12 in the gas phase.....	66
59. icorr Vs. Time for panels #10 & #12 in the liquid phase.....	66
60. Pull-Off Adhesion Test results for as-received coatings before autoclave.....	67
61. FBE, Phenolic, Novolac, and Amine Novolac coated panels after pull-off test....	68
62. Pull-Off Adhesion Test results for panel #1 after autoclave.....	68
63. Pull-Off Adhesion Test results for panel #10 after autoclave.....	69
64. Pull-Off Adhesion Test results for panel #12 after autoclave.....	70
65. FBE, Phenolic, Novolac, and Amine Novolac coated panels after pull-off test....	70

66. SEM images of the cross-sectional area of the pinholes.....	71
67. SEM images of the cross-sectional area of the pinholes (FBE).....	72
68. SEM images of the cross-sectional area of the pinholes (Phenolic).....	73
69. SEM images of the cross-sectional area of the pinholes (Novolac).....	74
70. SEM images of the cross-sectional area of the pinholes (Amine Novolac).....	75

CHAPTER 1

INTRODUCTION

The demand for energy is increasing rapidly around the globe as countries and companies are constantly looking for new energy sources. Natural gas is considered to be one of the safest and most reliable energy sources available. Moreover, it is more environmentally friendly than other fossil fuels since it produces relatively low emissions when burned compared to other fossil fuels. In addition, natural gas is mainly composed of methane and thus, it is considered a clean source of energy as it emits roughly half the carbon dioxide of coal and around 30% that of oil. Natural gas also contains varying proportions of ethane, propane, butane and heavier hydrocarbons. Small quantities of nitrogen, oxygen, carbon dioxide, sulfur compounds, and water are also found in natural gas [1].

When it comes to the quality of the extracted gas, it falls within two categories. The first category is called sour gas and it refers to natural gas that contains significant amounts of hydrogen sulfide (> 4 ppm of H_2S). H_2S is flammable, corrosive and extremely poisonous to human even in small quantities. The second category is named sweet gas and it is defined as the natural gas that contains small amounts of hydrogen sulfide (< 4 ppm). Furthermore, natural gas exists in several forms such as dry gas and wet gas. Dry gas consists largely of methane whereas wet gas contains varying proportions of ethane, propane and butane. Moreover, there are two types of natural gas reservoirs known as associated and non-associated natural gas reservoirs. Associated gas refers to the gas that is found dissolved in the crude oil while non-associated gas is the gas that does not contain any hydrocarbon liquids including dry gas wells and wet gas wells (condensate wells) [1].

Many of the new gas fields explored globally are extremely sour in nature. In fact, 30% of the natural gas reserves in the world are of the sour category. The most common contaminants found in sour gas reserves are carbon dioxide (CO₂) and hydrogen sulfide. In the Middle East, approximately 80% of the proven gas reserves contain sour gas. On the other hand, many of the new gas fields are located offshore, which poses a challenge when it comes to transporting the natural gas through sub-sea pipelines to treatment plants and distribution facilities onshore. The pipelines that are used to transport the natural gas are made of carbon steel that are prone to corrosion especially when wet gas that contains CO₂ and H₂S is being transported [1,8].

High concentration of corrosive agents such as CO₂, H₂S, calcium (Ca) and chlorine (Cl) compounds are usually present in the gas stream which accelerate the deterioration of the steel pipe due to several corrosion mechanisms expected to take place throughout the pipe. In addition, the presence of formation water exacerbates the corrosion process. Corrosion products (mainly CaCO₃ and FeCO₃) are usually formed and become deposited on the interior surface of the gas pipeline as scales. At first, the scales act as a protective barrier to prevent corrosion of the steel surface. However, once the scales grow to a certain thickness they become brittle and peel off due to mechanical forces of the gas stream. As a result, the exposed areas are attacked by chloride ions, which result in pitting corrosion that increases the risk of pipeline failure. On the other hand, galvanic corrosion may occur if dissimilar metals are present [2,7,9].

Organic protective coatings are used extensively in the oil and gas industries to protect metallic structures such as pipelines from corrosion due to their durability, corrosion control properties, and ease of application. There are several generic types of pipeline

coatings such as Epoxy, Fusion Bonded Epoxy (FBE), Phenolic Epoxy, Liquid Epoxy, Amine-Cured Novolac Epoxy, and Polyethylene. Each type of coating has its own uses and advantages, which include chemical resistance, durability, flexibility and abrasion resistance. Furthermore, epoxy resins exhibit good abrasive and chemical resistance, in addition to reasonable resistance to humidity. On the other hand, FBE is an epoxy based powder coating that has been used extensively by the oil and gas industries to protect steel pipelines. FBEs are powder mixtures containing epoxy resins, pigments, plasticizers, anti-foaming agents, and curing agents. FBE coatings have been largely used by oil and gas industries in the past decades as a cost-effective means to mitigate corrosion. Since sub-sea trunklines are usually wide in diameter and may reach hundreds of kilometers in length, FBE is certainly considered one of the best solutions available to prevent corrosion along the pipelines [3].

The focus of this thesis is based on recently discovered natural gas offshore fields located in the Arabian Gulf of Saudi Arabia (Figure 1). Usually, the fields lie in medium-depth water in the range of 40-60 meters. The natural gas extracted from each offshore well is transported through dedicated subsea and onshore pipelines for treatment purposes in gas plants. In addition, Mono-Ethylene Glycol (MEG) Injection System is installed to continuously transport MEG and corrosion inhibitor from the onshore treatment plant to each well in order to protect the flowlines and trunklines against hydrates and corrosion [4,5].

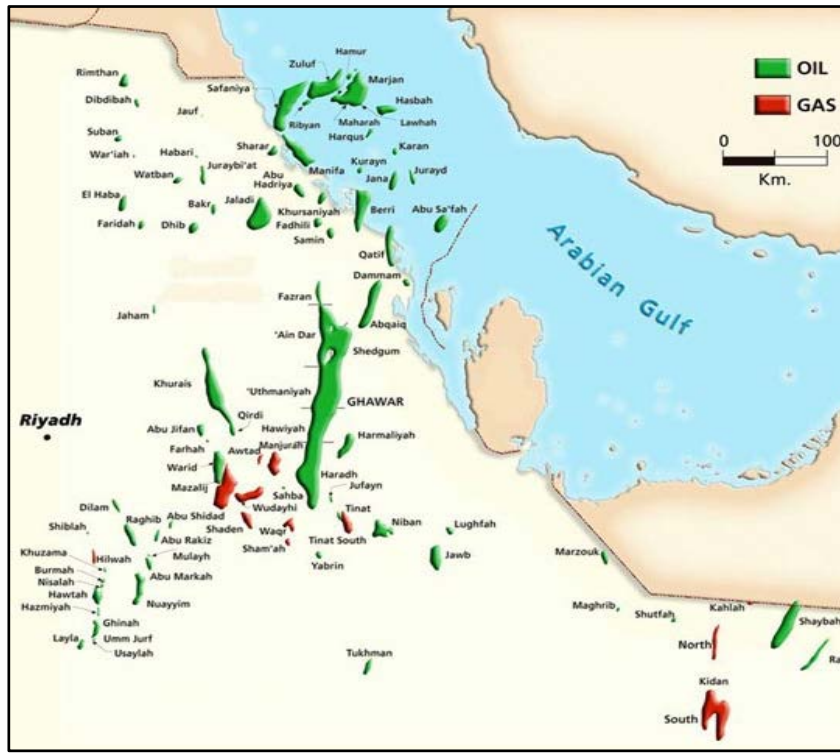


Figure 1: Natural Gas Offshore Fields in Arabian Gulf [17].

Several generic types of coatings such as FBE, Phenolic Epoxy and Novolac Epoxy have been used for a number of years to protect the pipelines carrying oil and gas from corrosion. However, FBE is currently the most common type of coating used to protect the interior of the subsea pipelines that carry sour gas. On the other hand, there is currently no industry standard for testing internal pipe coatings for sour gas delivery. Furthermore, a review of the literature on usage of FBE coatings under anticipated operating conditions does not provide any confidence that coating failure will not occur. All coatings will eventually fail, and there is no evidence to suggest that FBE coatings (or other organic coatings) can survive the design life of 25 years under the anticipated conditions. Several

incidents of FBE coating failures have been reported and the followings are the most common reasons for failure:

- Poor surface preparation (such as contamination, cleanliness and surface profile)
- Inadequate curing procedure (undercure)
- The FBE coating quality and performance differs from one applicator to another

In order to analyze the performance of FBE and several other generic types of coatings (such as Phenolic, Novolac, and Amine-Cured Novolac Epoxies) in a sour environment, there is a need to conduct tests under extreme conditions [6,10]. Thus, the objective of this research is to evaluate the performance of four different generic types of organic coatings in sour gas media. The following generic types were investigated:

- 1) Fusion-Bonded Epoxy (FBE) Coating
- 2) Modified Phenolic Epoxy Coating
- 3) Novolac Epoxy Coating
- 4) Amine-Cured Novolac Epoxy Coating

The sour gas environment was simulated in the laboratory by immersing coated steel samples in a pressurized vessel containing surrogate solutions that represent those encountered in Saudi Arabia. The performance of the organic coatings was studied via Electrochemical Impedance Spectroscopy (EIS), electrochemical polarization resistance and Scanning Electron Microscopy (SEM). Although a few types of epoxy coatings have been approved globally by the oil and gas industries for usage under sour conditions, there are still concerns regarding their long-term behavior and performance. Therefore, long-term evaluation testing under field conditions is needed to examine the stability and adhesion properties of the coatings.

CHAPTER 2

2.0 LITERATURE REVIEW AND BACKGROUND

2.1 Natural Gas Extraction and Composition

Crude oil and natural gas contain several high-impurity products such as carbon dioxide (CO₂), hydrogen sulfide (H₂S) and formation water, which are extremely corrosive in nature. The continuous extraction of such corrosive products can lead to damage of the internal surfaces of components used in the oil and gas industry. Furthermore, extreme conditions of pressure and temperature, fluid compositions, and souring of wells over time exacerbate material degradation of the interior of pipelines. This material degradation then leads to loss of mechanical integrity (ductility and strength), which can lead to critical failures. Therefore, it is very crucial to protect the interior of pipelines by the utilization of metallic cladding and/or protective coatings.

In the extraction of natural gas, the initial temperature at the source is around 95 °C. Further along the pipeline as the flow is cooled down by seawater, it drops down to about 45 °C. The pressure of the process is typically around 2,000 psi. Besides temperature and pressure, there are several other factors that affect the performance of coatings such as, product composition and mono-ethylene glycol (MEG) that is introduced into the process. Protective coatings could work at those temperatures and pressure; however, the main issue is the severity of the entire system. Therefore, metal cladding is typically used for the first few kilometers until the temperature drops to 49 °C. The pipelines are internally cladded with a layer of 3 mm of nickel-based alloy due to its high strength and outstanding corrosion resistance. Below 49 °C, organic coatings are considered cost-effective for

control corrosion. The surrogate solution used in this investigation to simulate gas and liquid phases (sour gas) typically found in pipelines had the following composition:

Gas: H₂S - 5%; CO₂ - 8%; and CH₄ - 87%

Liquid: Mono-Ethylene Glycol - 50%; and Formation Water - 50%

MEG is frequently introduced to the system in order to avoid the formation of hydrates along the pipelines. It captures the water and makes it unavailable for hydrates to form. Furthermore, it also dissolves gas molecules including CO₂, H₂S, and some heavy hydrocarbons [1].

2.2 Corrosion Phenomena in Sour Gas Pipelines

Corrosion is defined as the deterioration of a material via electrochemical reactions with its environment and is considered one of the major challenges encountered in oil and gas production systems and pipelines. Corrosion can take place in any aqueous environment, which is mostly the case in oil and gas production systems and pipelines. The components suffering from corrosion may degrade with time resulting in production disruption as failed or damaged components are replaced. Therefore, the specification for pipelines includes what is referred to as the “corrosion allowance”, which takes into account metal loss throughout the equipment lifespan by ensuring extra wall thickness than is typically required. In fact, the costs associated with corrosion mitigation in industrialized countries represent between 3% to 5% of their Gross National Product (GNP). Furthermore, the oil and gas industries spend billions of dollars annually to treat and mitigate corrosion. The costs associated with corrosion in the US industries is estimated to be \$170 billion a year where half of it is linked to the oil and gas industries [7].

2.2.1 Elements of a Corrosion Cell

Corrosion is an electrochemical process acknowledged by the tendency of a metal to return to its original mineral state. In order for corrosion to occur, the following four elements must always be present: 1) Anode; 2) Cathode; 3) Electrolyte; and 4) Metallic Pathway for electronic conduction. The electrolyte is the liquid medium through which dissolved ions conduct electricity by diffusing to and from the electrodes. In practice, most electrolytes are based on water solutions that contain dissolved ions which carry positive and negative charges. The anode is defined as the part of metal that corrodes by losing electrons thereby producing positively charged ions in the electrolyte. The electrons flow through the metal (or via an external circuit) to the cathode, which is defined as the less active area on the metal where electrons are consumed. Thus, the latter site is protected from corrosion. The metallic pathway between the anodic and cathodic areas enable electrons to flow from the anode to the cathode. Figure 2 is a schematic illustration of the corrosion process of metals [7].

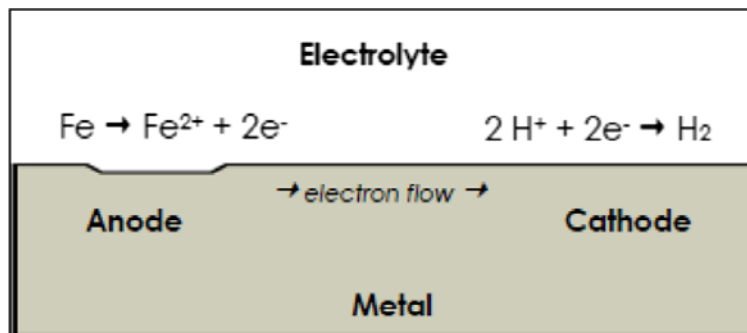


Figure 2: Corrosion Process [18].

2.2.2 Corrosion Mechanisms and Forms

When the extracted natural gas is a wet sour gas, which contains on a molar basis up to 8% CO₂ and 5% H₂S, a predominantly sour corrosion regime can be anticipated. On the other hand, the external environment surrounding the subsea pipelines consists of shallow to medium water depth in which a typical marine type corrosion phenomenon occurs. The different forms of corrosion that may occur internally in a pipeline system is schematically illustrated in Figure 3 [7].

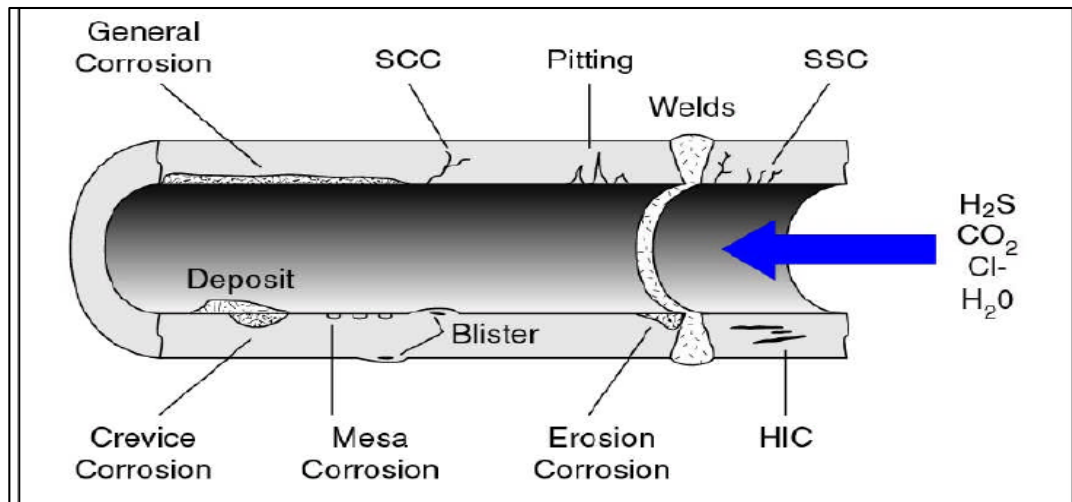


Figure 3: Corrosion Mechanisms in a Pipeline [19].

2.2.2.1 Corrosion Mechanisms

The main types of wet corrosion are: 1) Galvanic Corrosion; and 2) Crevice Corrosion (Concentration Cells). Galvanic Corrosion is defined as an electrochemical process that occurs when two dissimilar metals are electrically coupled in a corrosive electrolyte where the less noble metal (anode) corrodes faster than it would if exposed uncoupled to the same environment, while the more noble metal (cathode) corrodes slower than it would all by itself. Galvanic corrosion can also occur within the same material as a

result of composition and microstructure differences initiated by different thermal or mechanical treatments.

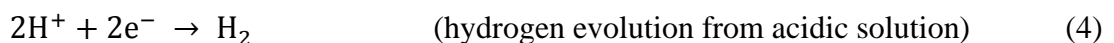
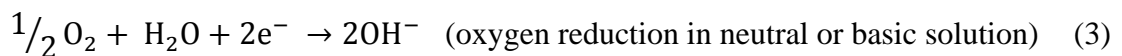
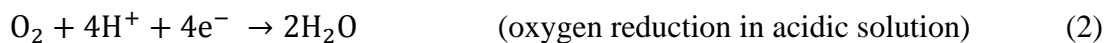
Crevice Corrosion is defined as localized attack due to differential aeration cells which occur in confined spaces (crevices). Because oxygen diffusion is limited within a crevice, the cathodic oxygen reduction reaction is reduced. Thus, the metallic area within a crevice exhibits an anodic character relative to the area outside which produces a concentration cell and the formation of a highly corrosive environment and further metal dissolution. Moreover, the corrosion mechanism depends on several other factors associated with the oil and gas industry such as temperature, fluid composition, geometry, and location [7].

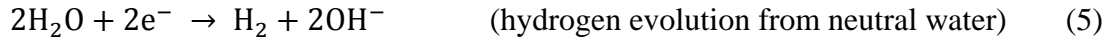
2.2.2.2 Corrosion Forms

Corrosion in the oil and gas industry normally takes place when metallic structures come in contact with aqueous environments. The metal exposed to the corrosive electrolyte loses electrons at the anodic site that are then consumed by reduction reactions at the cathodic site. As a result, the positively charged ions that are released into the electrolyte may bond with the negatively charged ions. The following Reaction (1) illustrates the anodic reaction that occurs with iron and steel.

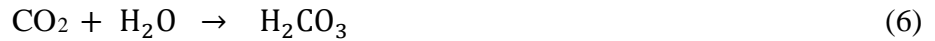


The electrons released are consumed by reduction reactions at the cathodic sites in accordance with the four common cathodic reactions depending on the acidity (pH) of the environment:





Carbon dioxide (CO₂) and hydrogen sulfide (H₂S) present in sour natural gas with formation water as the catalyst for corrosion, react with water as shown in the following reactions:



When both gases are present a combination of the above two reactions might take place. The formed molecules are released into the electrolyte and reduced on cathodic sites. Furthermore, it still remains a challenge to classify the types of corrosion in the oil and gas industry as it could be classified based on the appearance of damage, or the preventive methods, or the mechanism of attack. Besides, there are several types and causes of corrosion. The followings are the main forms of corrosion that are typically present in the oil and gas industries.

1. Uniform Corrosion
 2. Pitting Corrosion (mesa attack)
 3. Crevice Corrosion
 4. Erosion Corrosion
 5. Microbiologically Influenced Corrosion (MIC)
 6. Stress Corrosion Cracking (SCC)
 7. Hydrogen Damage
- Uniform corrosion is defined as the corrosion that is uniformly distributed over the metal surface. It is usually associated with surface roughening and the presence of

corrosion products. The rate at which uniform corrosion proceeds could be predicted and is typically monitored throughout the service life of the pipelines.

- Pitting corrosion is a localized form of corrosion that is initiated by chloride containing water resulting in the formation of acid that lead to the formation of cavities (holes) in the pipelines. Localized corrosion is formed in confined small areas on the metal surface.
- Crevice corrosion is formed on shielded areas on the surface of passive materials that are wetted by chloride containing water under gaskets or seals and in gaps between overlapping surfaces.
- Erosion corrosion is defined as the degradation of metal surfaces as a result of a mechanical action. Erosion corrosion accelerates the corrosion rate since it removes the passive layer formed by the corrosion products on the metal surface. The passive layer stabilizes the corrosion reaction however, and the passive layer could be removed due to turbulence and high shear stress inside the pipelines.
- Microbiologically Induced Corrosion (MIC) is caused by the formation of microorganisms as waste products of CO₂ and H₂S. In addition, the interface between the metal surface and microorganisms' communities may be altered which leads to a very aggressive environment resulting in localized corrosion.
- Stress Corrosion Cracking (SCC) is the cracking which result from the exposure of a specific material to a specific combination of corrosive environment and tensile stress. The required tensile stresses to initiate the crack may be in the form of directly applied stresses or residual stresses. Several types of SCC exist such as Chloride Stress Corrosion Cracking (CSCC) and Sulfide Stress Cracking (SSC).

- Hydrogen damage refers generally to various forms of Environmentally Assisted Cracking (EAC) such as Hydrogen Induced Cracking (HIC), Hydrogen Embrittlement (HE), Sulfides Stress Cracking (SSC), and Stress-Oriented Hydrogen Induced Cracking (SOHIC). Hydrogen damage results from the diffusion of atomic hydrogen into a metal in a corrosive environment. Furthermore, HIC and HE occur typically from stresses developed because of the internal pressure due to the build up of molecular hydrogen, whereas SSC and SOHIC commonly result from the applied or residual stresses. The presence of H₂S and CO₂ are linked to acceleration of hydrogen related cracking phenomena [2,7].

2.3 Corrosiveness of Water (Brine)

The water phase (brine) in oil and gas industry is considered among the most critical environments since it promotes both generalized and localized corrosion by being a good electrolytic conductor. Typically, the water contains ionic species which facilitate the corrosion process. An increase in the concentration of the ionic species lead to an increase in the corrosivity of water. Furthermore, the ionic species affect the corrosion rate due to increased conductivity of water, which participates in the electrochemical corrosion reactions. For example, the cathodic reduction reaction of oxygen that leads to the formation of hydroxyl ion, as well as the role of chloride ions in penetrating oxide surface layers that lead to localized corrosion. Hence, the corrosivity of water depends heavily on the nature and the concentration of both anions and cations.

Figure 4 illustrates the change in the corrosion rate of iron at room temperature immersed in air-saturated distilled water as a function of Cl ion concentration added in the form of NaCl. It can be observed that the corrosion rate increases as the concentration of NaCl increases up to 3% NaCl. In pure distilled water, the oxygen concentration is very high as well as the solution resistance, which means that the solution conductivity is low and as a result the corrosion rate is also low. When NaCl is added to the solution it increases its conductivity, which lead to an increase in the corrosion rate. In addition, the solution conductivity reaches adequate levels for the oxygen effect to become dominant at around 3% NaCl. If the concentration of NaCl is increased above 3%, the amount of oxygen dissolved in the solution decreases, which lead to a decrease in the corrosion rate. Furthermore, chloride ions lead to the formation of localized pitting corrosion by destroying the oxide surface layers.

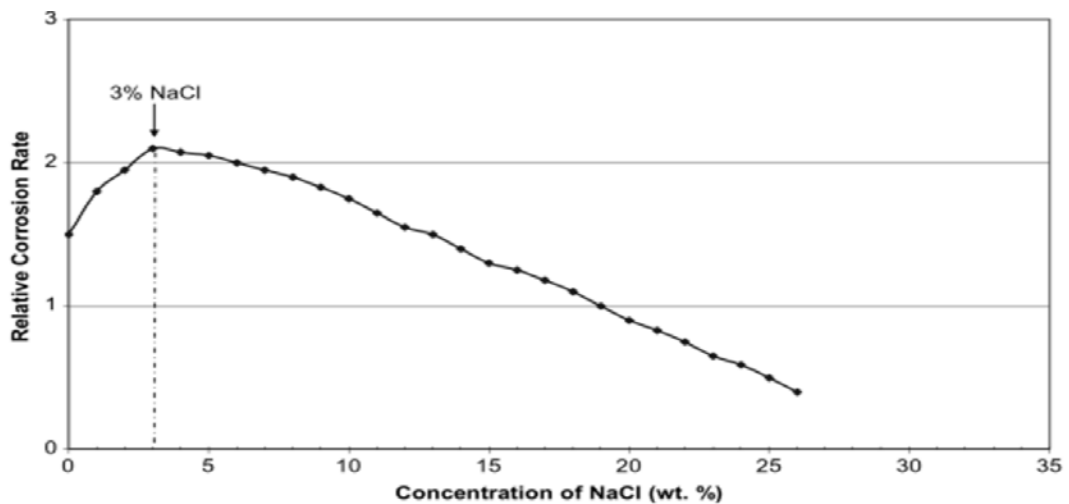


Figure 4: Corrosion rate of Fe in aerated solution at room temperature as a function of NaCl [7].

The following parameters significantly affect the corrosion rate and morphology of iron:

- The chemistry of water is considered to have the most influential effect on corrosion. The condition varies from being simple with only a few carbonic species present to being very complex with several species present for instance in formation water. The pH depends significantly on the water chemistry.
- The pH value has a significant effect on the corrosion rate. A high pH value leads to a decrease in solubility of iron carbonate, which leads to an increase in the precipitation rate and a higher scaling tendency, resulting in a rapid decrease of the corrosion rate.
- Increase in temperature accelerates all of the processes involved in corrosion. The growth of the iron carbonate film also depends on the temperature. When the temperature increases the precipitation rate of iron carbonate increases. The temperature can either increase or decrease the corrosion rate based on the solubility of the protective film. Typically, at low pH the protective films do not form and an increase in the temperature would lead to an increase in the corrosion rate. In contrast, at higher pH values an increase in the temperature would increase the precipitation rate of iron carbonate, which facilitates the formation of protective films, and therefore the corrosion rate is decreased [2,7].

2.4 CO₂ Corrosion (Sweet Corrosion)

Carbon dioxide (CO₂) corrosion is one of the most encountered and recognized form of corrosion in the oil and gas industry over the past decades. Dry CO₂ is not corrosive at the typical temperatures in oil and gas production systems. However, it is corrosive when it dissolves in the water phase and it is known to cause sweet corrosion. When CO₂ dissolves in water it forms carbonic acid, which leads to an increase in the acidity of water.

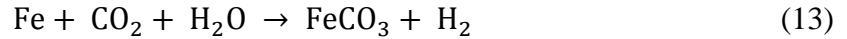
In addition, at high temperatures an iron carbide scale forms on the the pipe and serve as a protective layer. Furthermore, there are two forms of CO₂ corrosion: pitting and mesa attack. The following reactions illustrate the mechanism of the CO₂ corrosion process that was postulated by de Waard et al [2,7,18].



Equation (9) shows the dissolution of CO₂ while Equation (10) displays CO₂ hydration which leads to the formation of carbonic acid. Afterwards, the carbonic acid dissociates into bicarbonate and carbonate as shown in Equations (11) and (12).



The overall electrochemical reaction of CO₂ corrosion is illustrated in Equation (13).

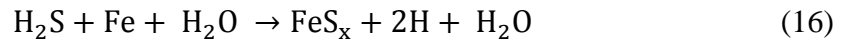


Therefore, the CO₂ corrosion process leads to the formation of the iron carbonate corrosion product (FeCO₃) and when it precipitates it could either form a protective layer or nonprotective scale based on the service conditions. On the other hand, the anodic dissolution of iron at the steel surface is shown in Equation (14) whereas the cathodic reduction reaction (hydrogen evolution) is shown in Equation (15).



2.5 H₂S Corrosion (Sour Corrosion)

Hydrogen sulfide (H₂S) corrosion is considered one of the major corrosion problems in the oil and gas industry. Metals degrade when they are exposed to wet hydrogen sulfide and this phenomenon is known as sour corrosion. H₂S by itself is not corrosive, however when moisture is present it becomes extremely corrosive. When H₂S dissolves in water it forms a weak acid and the corrosion products are iron sulfide (FeS) and hydrogen. In addition, the iron sulfide layers that are formed at low temperature could act as a barrier to slow the corrosion process. There are several forms of sour corrosion including uniform, pitting, and stepwise cracking. The following Equation (16) expresses the general chemical reaction of sour corrosion.



Furthermore, another probable mechanism for iron dissolution in aqueous solutions that contain H₂S is based on the formation of mackinawite film as shown in Figure 5, which was proposed by Sun et al [2,7,12].

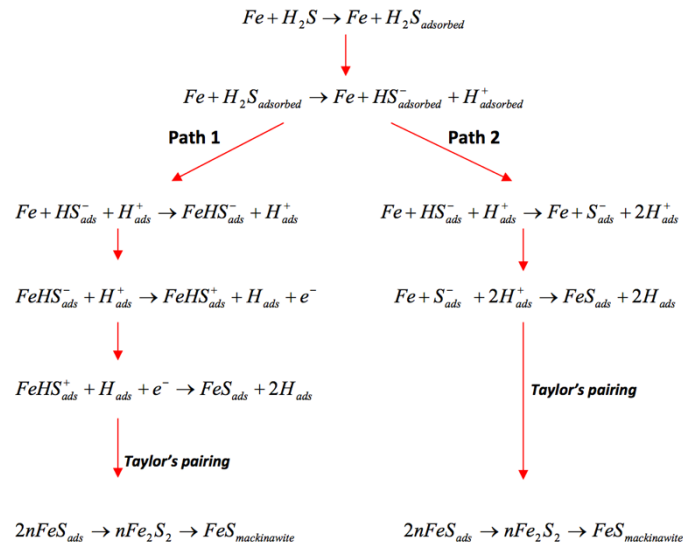


Figure 5: Mechanism for iron dissolution in aqueous solutions containing H₂S

2.6 Corrosion Control in the Oil and Gas Industry

Corrosion causes numerous problems and is considered one of the most challenging issues in the oil and gas industry. Thus, all pieces of equipment used in the oil and gas industry are usually manufactured by taking into consideration the effect of corrosion on the lifespan of the equipment during the industrial design. In fact, several reports and incidents around the globe have illustrated the negative impact of corrosion, which includes its costs, health and safety risks, and environmental pollution due to oil spillage due to rupture of pipelines as a result of corrosion. Therefore, several protection methods and techniques are utilized in the oil and gas industry to mitigate and prevent corrosion [2,7].

2.6.1 Organic Protective Coatings

Organic protective coatings have been used extensively in the oil and gas industry to protect metallic structures against corrosion. These linings control the rate of corrosion by forming a protective barrier separating the metal from the electrolyte. Moreover, coatings have many advantages in comparison to other corrosion control methods used in the oil and gas industry. These advantages include:

- Ease of substrate surface preparation and coating application
- Ease of coating products handling and storage
- Ease of repair and maintenance
- Wide range of application conditions
- Cost effective solution to mitigate corrosion

In order to ensure proper adhesion between the coating and the metal substrate, it is very important to prepare the surface in accordance to well established specifications. A coating system typically consists of multiple layers, which include a primer, an intermediate coat

and a topcoat. The generic types of coatings that are frequently utilized by the oil and gas industry to protect steel surfaces include the following:

- Fusion Bonded Epoxy (FBE)
- Phenolic Epoxy
- Novolac Epoxy
- Amine-Cured Novolac Epoxy

Each type of coating has its own applications and advantages with regard to chemical resistance, durability, flexibility and abrasion resistance. For example, epoxy coatings have been used over the past decades in many critical industrial coating applications due to their outstanding adhesion properties and chemical resistance to a wide range of chemicals. Furthermore, epoxy resins exhibit good abrasive and chemical resistance in humid conditions.

Fusion-bonded epoxy (FBE) is an epoxy based powder coating, which has been used extensively by the oil and gas industries to protect steel pipelines. FBEs are thermoset polymer coatings that contain epoxy resins, pigments, plasticizers, anti-foaming agents, and curing agents. The name fusion-bonded is derived from the application method and subsequent resin cross-linking. Typical coating application temperatures range between 180 °C to 250 °C where the FBE powder is melted and transformed to a liquid that flows onto the steel surface and solidifies due to chemical cross-linking. This process is an irreversible process meaning that the coating cannot be returned to its original form once it is cured. FBE coatings have been largely used by oil and gas industries in the past decades as a cost-effective solution to mitigate corrosion. Since pipelines in the industry are usually

large in diameter and up to a hundred kilometers in length, FBE is certainly considered one of the best solutions available to prevent corrosion.

Phenolic resins produced by reacting phenol with formaldehyde are considered among the first synthetic resins that were used to synthesize coatings. Typically, phenolic coatings are heat-cured to exhibit good adhesion and resistance to chemicals, heat, and water. Furthermore, epoxy phenolic coatings are a modified version of phenolic coatings that are hard yet flexible, and are resistance to water, chemicals, solvents, abrasion and heat. The advantage of the epoxy phenolic coatings is that they do not require any heat-cure and could be formulated to dry in air. Phenolic coatings and epoxy phenolic coatings are usually used as linings due to their outstanding chemical resistance in aqueous solutions.

Novolac epoxies are resins also produced by the reaction of phenol with formaldehyde. However, these epoxy coatings have more reactive groups than phenolic epoxy coatings along their chemical backbone, resulting in a more highly cross-linked polymer. Hence, Novolac epoxy coatings offer the best chemical resistance to solvents and heat. However, due to their high-molecular weight they are very hard, dense, and brittle. Nevertheless, Novolac epoxy coatings can be cured at ambient temperature as well as high temperatures and they are usually utilized in severe service conditions.

Amine cured epoxy coatings form very hard, tightly bonded adherent films to the substrate, which provide outstanding corrosion and chemical resistance. They are typically used as linings for chemical storage tanks and may also be used in highly corrosive environments. However, amine epoxies have some disadvantages which include its toxicity and irritation to skin [20].

2.6.2 Mono Ethylene Glycol (MEG)

In natural gas producing fields, water condenses along the pipelines due to temperature gradients, and this can lead to the formation of hydrates. When gas molecules become trapped in a lattice of water molecules, a stable solid known as gas hydrates is formed. The majority of gas hydrates are formed from methane, but also other hydrocarbons (C₂ to C₄), as well as water, CO₂ and H₂S can form gas hydrates. Therefore, Mono Ethylene Glycol (C₂H₆O₂) is usually injected into the pipelines to avoid the formation of hydrates along the pipelines. MEG captures the water and makes it unavailable for hydrates to form. Besides, the polarity of the solution is reduced thereby decreasing the dissolution of CO₂ in a MEG solution.

Typically, lean MEG (80-95 wt%) is injected at the inlet where it is diluted by water to MEG (30-60 wt%) at the outlet. MEG is used because it can also be easily recycled and is less toxic than methanol due to a low vapor density. MEG absorbs water and dissolves gas molecules including CO₂, H₂S, and some heavy hydrocarbons. Gulbrandsen and Morard reported a decrease in the corrosion with 30 and 70 volume % of MEG. Also, both the anodic and cathodic reactions of CO₂ corrosion are observed to decrease in the presence of MEG as it influences protective film formation on steel surface. Dugstad et al. suggested that increasing the MEG concentration decreases the solubility of iron carbonate and therefore, facilitates the formation of the protective film [21,22].

CHAPTER 3

3.0 RESEARCH OBJECTIVES AND HYPOTHESIS

3.1 Research Justification and Objectives

3.1.1 Research Justification

- Currently, FBE coating is widely used to protect the interior of pipelines in sour gas service.
- FBE and other organic coatings have been recommended for usage in sour environment but information on in-service usage is unknown.
- Long-term testing in field conditions is required to evaluate the adhesion and durability of the coatings.

3.1.2 Research Objectives

- The main objective of this research is to evaluate the performance of selected organic coatings in sour gas media and analyze their electrochemical impedance behavior before and after exposure to the sour gas environment. The following organic coating products were selected to be tested:

- | | |
|--------------------------|--------------------------------|
| 1) FBE Coating | 2) Phenolic Epoxy Coating |
| 3) Novolac Epoxy Coating | 4) Amine Novolac Epoxy Coating |

- **Specific Tasks of Research:**

- Employ a high-temperature/high-pressure reactor (Autoclave) to simulate the sour gas environment
- Conduct Electrochemical Impedance Spectroscopy (EIS) on flawless coatings to determine their resistance and capacitance before and after the autoclave test
- Conduct EIS and Linear Polarization Resistance (LPR) to examine the behavior of artificially damaged coatings (3 mm diameter hole) before/after autoclave test
- Examine the coating degradation and the corrosion products formed in the presence of a pinhole by the use of SEM/EDS

3.2 Hypothesis

The research is driven by the following hypothesis:

- Organic coatings improve corrosion resistance of carbon steel pipelines exposed to sour gas environment.

CHAPTER 4

4.0 EXPERIMENTAL METHODS AND MATERIALS

The dimensions of all the coated steel panels used in this study were 150 mm x 50 mm. Table 1 lists the names and generic types of the coatings that were tested for corrosion resistance and bond adhesion.

Table 1: Generic types of coatings and test names.

Generic Type	Test Name	Coating Thickness (µm)	Coating Thickness Average (µm)
Fusion Bonded Epoxy	FBE	560 - 620	580
Phenolic Epoxy	Phenolic	360 - 420	400
Novolac Epoxy	Novolac	1050 - 1250	1200
Amine-Cured Novolac Epoxy	Amine Novolac	360 - 500	410

4.1 Experimental Methods and Analytical Techniques

4.1.1 Visual Inspection

All panels were visually inspected for defects (holidays) which was clearly marked if observed. Visual inspection was also conducted post autoclave testing to assess whether blisters or pinholes developed as a result of exposure to the harsh environment.

4.1.2 Coating Dry Film Thickness Measurement

The Dry Film Thickness (DFT) of each test panel was measured by a coating thickness gauge (Elcometer). The coating's DFT was measured and reported before and after the autoclave test in order to assess whether any coating degradation occurred as a result of exposure to sour gas.

4.1.3 Pull-Off Adhesion Test

This test method was used to evaluate the pull-off strength (known as adhesion) of the coating on the metallic substrate. The ability of a coating to resist tensile stress before detachment from a substrate is a measure of its adhesion strength. ASTM-D4541 Standards describes several procedures for the evaluation of adhesion strength of coatings but the basic approach of the test as well as the apparatus employed are similar. A dolly is glued to the coated surface from which a force is exerted perpendicular to the surface in order to remove both the dolly and the coating from the metal substrate. Afterwards, the force at which the coating fails as well as the type of failure are determined. Figure 6 shows the Pull-Off Adhesion tester that was used to evaluate the adhesion strength of the coatings.

The types of failure are as follows:

- 1) Adhesive Failure: failure at the coating/substrate interface
- 2) Cohesive Failure: failure within the coating film or the substrate
- 3) Glue Failure: failure within the glue



Figure 6: Pull-Off Adhesion tester.

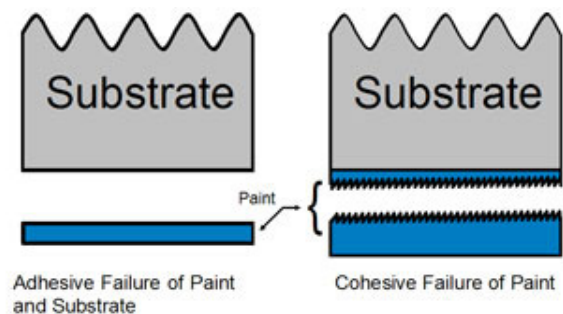


Figure 7: Adhesive and cohesive failure of coating systems [23].

Figure 7 illustrates the cohesive and adhesive failures of coating systems. The Pull-Off Adhesion test was performed in accordance with the ASTM-D4541 prior to and post the autoclave test to measure the adhesion of the coatings [24].

4.1.4 Chemical Resistance Test (Autoclave)

The chemical resistance tests using a pressurized reactor (autoclave) have been used successfully in the coating industry for over two decades. The test compares the reactions of one or more coatings to conditions that simulate an anticipated service. In essence, the coatings are exposed to liquids and gases expected in the service environment and may consist of gas phase mixtures that are corrosive, flammable, and/or inert media. In addition to the mixture of liquid and gas media, the coatings are also exposed to higher temperature and pressure. Depressurization of the test vessel can also be implemented to simulate actual events in service. These conditions help to increase the degradation rate of the coating, if any is anticipated. The coating that exhibits the least degree of degradation is considered the most reliable for use in that particular environment. The autoclave test is conducted in compliance with the NACE Standard TM0185-2006 [25].

4.1.5 Scanning Electron Microscopy (SEM) and Energy-Dispersive X-Ray Spectroscopy (EDS)

SEM uses a focused beam of electrons to scan the sample's surface. When the electrons hit the sample they generate a variety of signals that can be used to obtain information on the surface morphology and composition. EDS is a type of detector used in SEM for chemical characterization and elemental analysis of a sample. When the electron beam strikes the sample, the x-rays produced are representative of the elements present on

the sample. SEM was used to study the surface morphology and composition of the coated test panels before and after autoclave testing [16].

4.2 Electrochemical Testing Techniques

Alternating Current (AC) and Direct Current (DC) electrochemical techniques were used in this research to monitor the corrosion rate as well as to evaluate the performance of organic coatings. The DC electrochemical technique of Linear Polarization Resistance (LPR) was used to measure the corrosion rate which is typically expressed in milli-inches per year (mpy) and measurements can be obtained within a few minutes.

Electrochemical Impedance Spectroscopy (EIS) was used to evaluate the protectiveness of organic coatings since it provides a quantitative measurement of the barrier resistance properties of a coating which is related to the permeability of the coating. In EIS, an AC voltage of varying frequency is applied to the coated sample to measure the coating's impedance (Z). If the coating has a high impedance, it implies that its permeability to corrosives is low, and thus more protective. In contrast, low impedance indicates a high permeability to corrosives. EIS was conducted prior to and post the autoclave test to assess the barrier properties of the coatings [26].

4.2.1 Linear Polarization Resistance (LPR)

LPR is an electrochemical technique used to calculate the corrosion rate of a specimen by examining the linear relationship between the applied potential and the resulting current. Polarization resistance measurement is conducted by applying a potential range which is very close to the corrosion potential (E_{CORR}) and then measuring the resulting current. The applied potential ranges from 0 to -25 mV and thus only cathodic

polarization is applied in order not to interfere with the natural corrosion process. The applied potential is plotted versus the resulting current as displayed in Figure 8 [26,27].

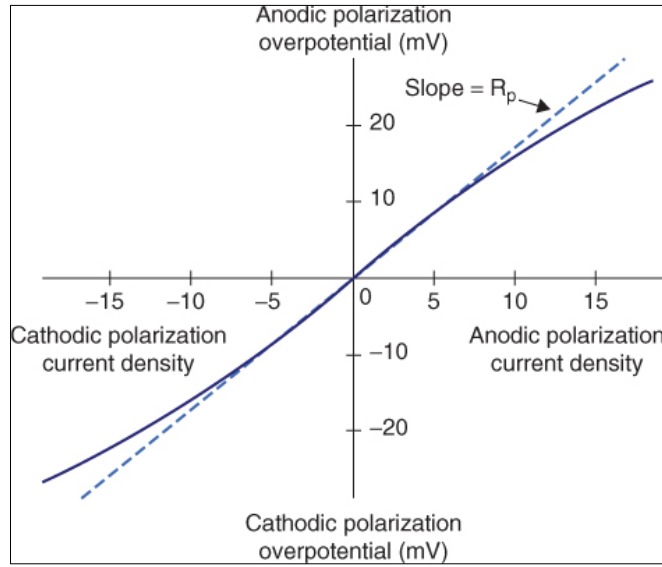


Figure 8: Applied Potential vs. Resulting Current [27].

According to Ohm's law ($R = \Delta E / \Delta i$) the ratio of the applied potential to the generated corrosion current (i_{CORR}) is defined as the polarization resistance (R_p). The slope of the plot (R_p) is related to the corrosion current (i_{CORR}) through the following Equation (1):

$$\frac{\Delta E}{\Delta i} = \frac{\beta_A \beta_C}{2.3 (i_{CORR}) (\beta_A + \beta_C)} \quad (1)$$

Where, $\Delta E / \Delta i = R_p$ = the slope of the polarization resistance plot,

ΔE is expressed in volts and Δi in μA ,

i_{CORR} is the corrosion current in μA .

B_A and B_C are anodic and cathodic Tafel constants expressed in volts/decade.

To calculate the corrosion rate, Equation (1) has to be rearranged to the following form

Equation (2):

$$i_{CORR} = \frac{\beta_A \beta_C}{2.3 (R_p) (\beta_A + \beta_C)} \quad (2)$$

Then the corrosion current can be used to calculate the corrosion rate through the following Equation (3):

$$\text{Corrosion Rate (mpy)} = \frac{0.13 I_{\text{CORR}}(\text{E.W.})}{d} \quad (3)$$

Where, E.W. = equivalent weight of the corroding specimen in grams,

d = density of the corroding species, g/cm³,

I_{CORR} = corrosion current density in μA/cm².

4.2.2 Electrochemical Impedance Spectroscopy (EIS)

4.2.2.1 Introduction

Electrochemical Impedance Spectroscopy (EIS) has been widely used in the past decades to assess and study the quality of organic coatings on metallic substrates. EIS is considered a powerful tool to examine and evaluate the degradation of coatings before any visible damage appears. In EIS experiment, the coated panel was exposed to an electrolyte solution which contained dissolved salts chosen to simulate a certain environment. Electrochemical impedance was measured by applying an AC voltage of varying frequency to the electrochemical cell and then measuring the generated current through the cell.

Ohm's law defines the concept of electrical resistance as the ability of a circuit to resist the flow of current ($R = E/I$) where R is the resistance in ohms, E is the voltage in volts and I is the current in amperes. However, systems in real world tends to exhibit a more complex behavior and as a result the simple concept of resistance is replaced by impedance (Z) which is defined as a measure of the circuit's ability to impede the flow of an AC potential. Assume a sinusoidal potential excitation signal is applied on the sample, the response to this excitation signal is the AC current signal. Electrochemical impedance is typically measured at small excitation signals in order for the cell's response to be linear.

In linear systems, the current response to the applied sinusoidal potential will be a sinusoidal at the same frequency but shifted in phase as shown in Figure 9 [26,27].

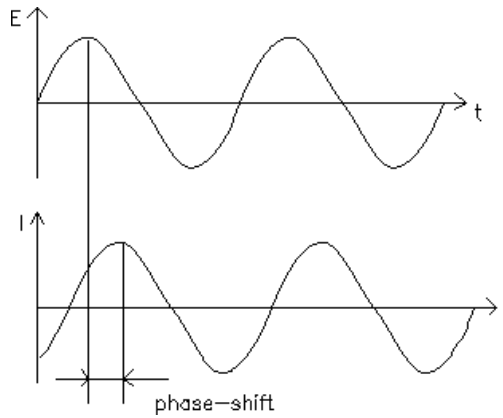


Figure 9: Sinusoidal current response to the applied AC potential in a linear system [29].

The sinusoidal potential excitation signal can be expressed as a function of time Equation (4).

$$E_t = E_0 \sin(\omega t) \quad (4)$$

Where, E_t is the potential at time t , E_0 is the amplitude of the signal, and ω is the radial frequency. Equation (5) represents the relationship between the radial frequency (ω , radians/second) and the frequency (f , hertz).

$$\omega = 2\pi f \quad (5)$$

At each frequency throughout the frequency range the corresponding phase shift (\emptyset) and the magnitude (I_0) are measured. The response signal (I_t) can be expressed by Equation (6).

$$I_t = I_0 \sin(\omega t + \emptyset) \quad (6)$$

Therefore, the impedance of a system can be expressed by Equation (7).

$$Z = \frac{E_t}{I_t} = \frac{E_0 \sin(\omega t)}{I_0 \sin(\omega t + \phi)} = Z_0 \frac{\sin(\omega t)}{\sin(\omega t + \phi)} \quad (7)$$

Thus, the impedance is expressed by a magnitude (Z) and a phase shift (ϕ). In addition, by the use of Eulers relationship expressed in the following Equation (8).

$$\exp(j\phi) = \cos(\phi) + j\sin(\phi) \quad (8)$$

The impedance then can be expressed as a complex function through Equation (9).

$$E_t = E_0 \exp(j\omega t) \quad (9)$$

Furthermore, the response current may be expressed by the following Equation (10).

$$I_t = I_0 \exp(j\omega t - \phi) \quad (10)$$

As a result, the impedance can be represented as a complex number through the following Equation (11).

$$Z(\omega) = \frac{E_t}{I_t} = Z_0 \exp(j\phi) = Z_0(\cos(\phi) + j\sin(\phi)) \quad (11)$$

4.2.2.2 Equivalent Electrical Circuit (EEC)

EIS data are normally analyzed by fitting the data to an equivalent electrical circuit representative of the electrochemical process that occurs at the sample/electrolyte interface. The common elements of the electrical circuit model include resistors and capacitors listed in Table 2.

Component	Current Vs. Voltage	Impedance
Resistor	$E = IR$	$Z = R$
Capacitor	$I = C \, dE/dt$	$Z = 1/j\omega C$

Table 2: The equivalent circuit elements, impedance [29].

common electrical and their

From Table 2 it can be observed that the impedance of a resistor does not have an imaginary component and thus the generated current through the resistor stays in phase with the applied voltage throughout the resistor. In contrast, the capacitor has an imaginary impedance component and therefore, the generated current through the capacitor has a phase shift of 90 degrees with respect to the applied voltage. The following Figure 10 illustrates the equivalent circuit of an organic coating on a metallic substrate [26].

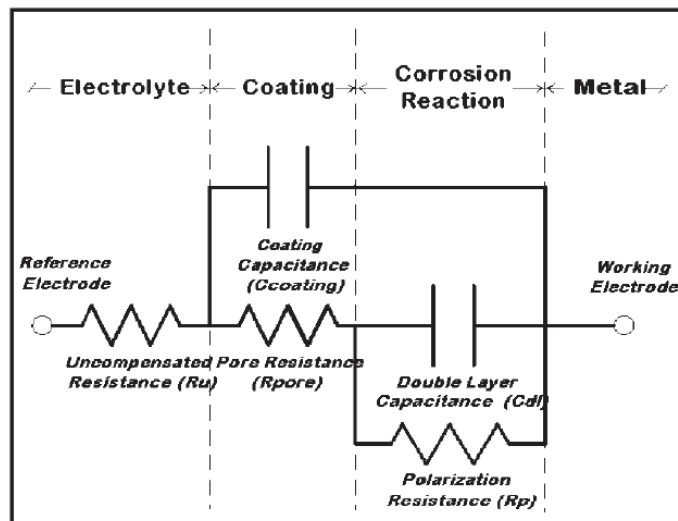


Figure 10: The equivalent circuit of an organic coating on a metallic substrate [26].

Uncompensated Resistance (Ru): Also known as solution resistance (Rs) is defined as the resistance of the electrolyte solution between the working electrode and reference electrode. In EIS measurements of organic coatings the electrolyte is conductive and thus Rs typically has a low value (1-50 ohms).

Polarization Resistance (Rp): The polarization resistance (Rp) describes the corrosion rate of the metallic substrate underneath the coating. The corrosion rate of bare metals can be determined by Polarization Resistance. Rp is inversely proportional to the corrosion rate as described by Equation (2).

Pore Resistance (Rpore): The coating's resistance normally decreases with time after exposure to the electrolyte solution as the electrolyte penetrate into the micro-pore of the coating. Initially and upon immersion of the electrolyte solution, the pore resistance (Rpore) typically has a high value and decreases with time. However, it has been observed in some cases that Rpore may experience an increase after long exposure times due to the formed corrosion products which block the micro-pores.

Coating Capacitance (C_{coating}): When two electrical conducting plates (metal substrate and electrolyte solution) are separated by a dielectric material (coatings), a capacitor is formed. Since organic coatings are thick they tend to have a low capacitance value. The capacitance of organic coatings is best described by Equation (12).

$$C_{\text{coating}} = \frac{\epsilon_0 \epsilon_r A}{t} \quad (12)$$

Where, ϵ_r = the dielectric constant of the coating, and $\epsilon_0 = 8.85 \times 10^{-14}$ Farads/cm, and A = the area in cm², and t is the thickness in cm. Equation (13) displays the relationship between the capacitance and the magnitude of the impedance (|Z|).

$$|Z| = \frac{1}{2\pi f C_{\text{coating}}} \quad (13)$$

Where f is the frequency of the applied AC potential. Table 3 lists the typical dielectric constants of some materials.

Table 3: Typical dielectric constants [29].

Material	Dielectric Constant (ϵ_r)
Vacuum	1
Water	80.1 (20°C)
Organic Coatings	2 – 7

From Table 3 it can be observed that the difference in values between the dielectric constant of organic coating and water is significantly large. The capacitance of the coating varies as it absorbs more water and hence EIS is utilized to monitor the change in its capacitance.

Double Layer Capacitance (C_{DL}): The electrical double layer is formed between the interface of the metal electrode and the electrolyte. There is a charge in the electrolyte and a charge on the metal electrode which are separated by the metal/electrolyte interface. This interface is defined as the double layer and its capacitance is known as the Double Layer Capacitance (C_{DL}). The C_{DL} is typically higher than the $C_{coating}$ and normally in the range of 10-40 $\mu F/cm^2$.

An undamaged and flawless coating normally behaves like pure capacitor and has a high impedance value. The equivalent circuit of a purely capacitive coating includes the Solution Resistance (R_s) and the Coating Capacitance ($C_{coating}$) as shown in Figure 11. When the coating is in contact with the electrolyte solution, it starts to absorb water from the electrolyte, which enters through the pores of the coating. As the coating absorbs more water, the Pore Resistance (R_p) starts to decrease. Figure 12 illustrates the Randles circuit which is one of the most common used cell models in EIS. The Randles circuit consists of solution resistance (R_s), the Double Layer Capacitance (C_{DL}) and the Charge Transfer (R_{CT}) or Polarization Resistance (R_p). After a certain time of exposure to the electrolyte, the coating begins to degrade, which enables corrosion to initiate underneath the coating at

the metal/electrolyte interface. The equivalent circuit for a damaged coating is displayed in Figure 13. It includes R_s , Pore Resistance (R_{po}), R_{CT} , C_{DL} and $C_{coating}$ [26,28].

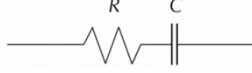


Figure 11: Purely capacitive coating [29].

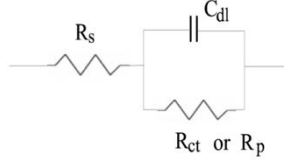


Figure 12: Simplified Randles Cell [29].

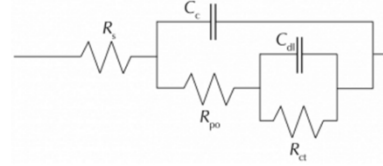


Figure 13: Equivalent circuit for a damaged coating [29].

4.2.2.3 Interpretation of EIS data: Nyquist and Bode Diagrams

The impedance data can be graphically represented in two ways:

- (a) Nyquist Plot: where $-Z_{im}$ serves as a function of Z_{re} ; and
- (b) Bode Plot: where $\log |Z|$ and the phase angle (ϕ) are expressed as a function of \log frequency.

As per Equation (11), the impedance can be represented by a complex number composed of the real impedance component (Z') and the imaginary impedance component (Z''). A plot of the real part on the X-axis and the imaginary part on the Y-axis leads to the Nyquist plot. Figure 14 displays a Nyquist plot where it can be observed that the Y-axis is negative and each point on the plot represents the impedance at a single frequency value. High frequency data are observed on the left side of the plot whereas, those at low frequency are displayed on the right side. The angle between the impedance vector and the X-axis is

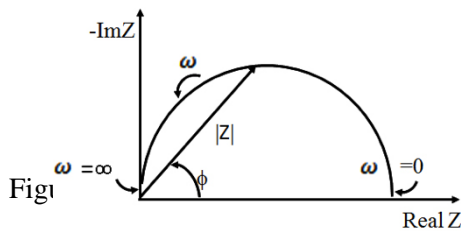


Fig 14

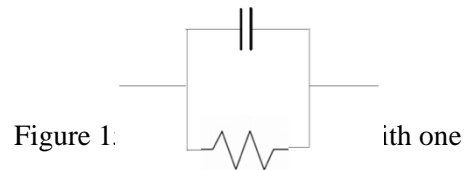


Figure 15

called the phase angle (\emptyset). Figure 15 shows the electrical equivalent circuit for the Nyquist plot in Figure 14. The semi-circle represents a single time constant [26,29].

The EIS data of coated metals may also be graphically represented by the Bode plot as shown in Figure 16. The Bode plot displays the logarithm of the impedance ($\log |Z|$) and phase angle (\emptyset) on the Y-axis versus the logarithm of the frequency on the X-axis. Thus, large variations in the impedance values can be well presented in the Bode plot.

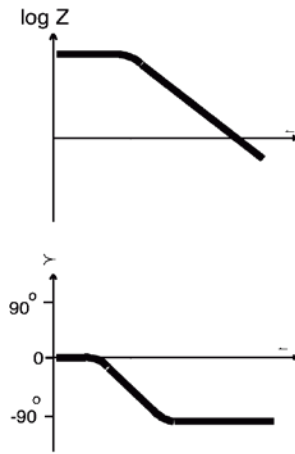


Figure 16: The Bode Plot with one time constant [29].

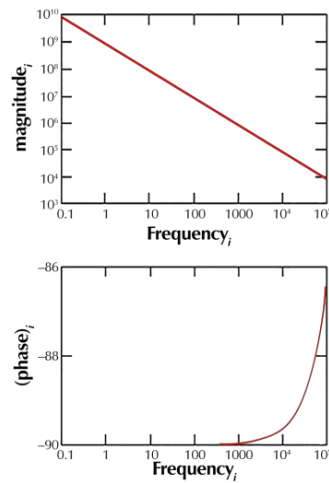


Figure 17: Bode Plot for a purely capacitive coating [29].

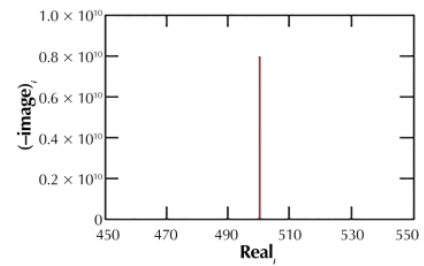


Figure 18: Nyquist Plot for a purely capacitive coating [29].

Figure 17 displays the Bode plot of a purely capacitive coating (EEC shown in Figure 11). When coatings are exposed to an electrolyte, typically high performance coatings which contain excellent barrier properties behave like perfect capacitors. The pore resistance (R_{po}) is significantly high and the Bode plot shows a straight line with slope -1. In addition, high impedance is measured at low frequency with a phase angle of -90° throughout the entire frequency range. Figure 18 shows the Nyquist plot for a purely capacitive coating and a vertical line is observed since the phase angle is always 90° . The real impedance is

zero and the total impedance is equal to the imaginary impedance. Also, the point where the curve intercepts with the X-axis can be used to estimate the solution resistance (R_s).

During the time of exposure, the electrolyte may penetrate the coatings through the micropores and as a result the pore resistance is decreased. Figure 19 illustrates the Nyquist plot for a coating that is developing a low pore resistance and it can be observed that it consists of a semi-circle like the Randles cell. The value of the solution resistance (R_s) can be estimated from the interception with the X-axis at the high frequency zone in the left region of the plot. In contrast, the interception with the X-axis at the low frequency region represents the sum of the pore resistance and the solution resistance ($R_{po} + R_s$). The Bode plot for the Randles cell is displayed in Figure 20. It should be noted that the phase angle does not reach 90° as is the case for pure capacitors.

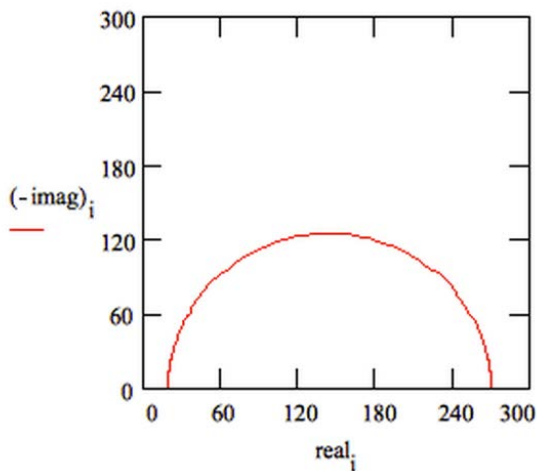


Figure 19: Nyquist Plot for Randles cell [29].

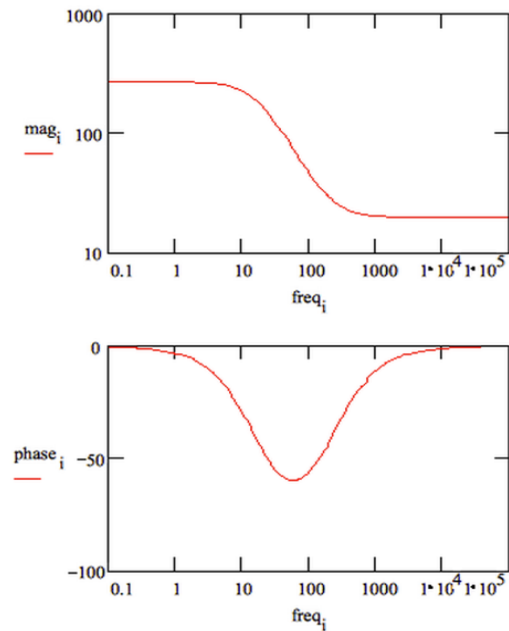


Figure 20: Bode Plot for Randles cell [29].

As the electrolyte continues to penetrate through the micropores of the coating, corrosion may occur in certain areas of the metal substrate in contact with the electrolyte. The Nyquist plot for a degraded coating is shown in Figure 21, and two semi-circles are observed that represent the two time constants. The semi-circle on the left at high frequency represents the coating capacitance while the one on the right at low frequency represents the double layer capacitance. The Bode plot for the same degraded coating is illustrated in Figure 22 and a significant drop is noticed in the total impedance of the coating at low frequency.

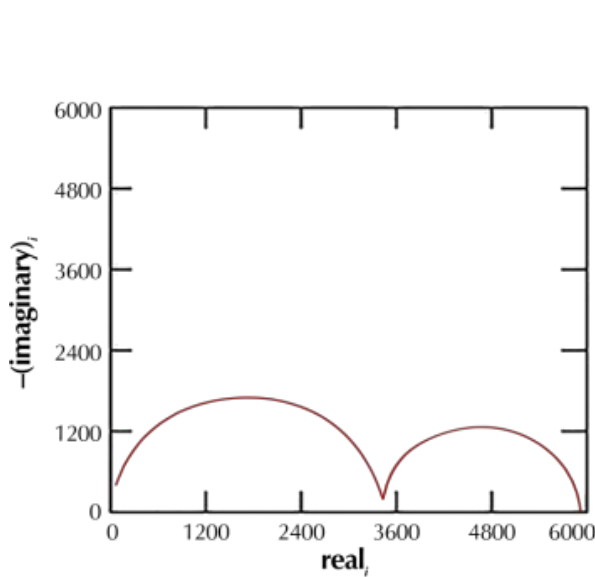


Figure 21: Nyquist Plot for a degraded coating [29].

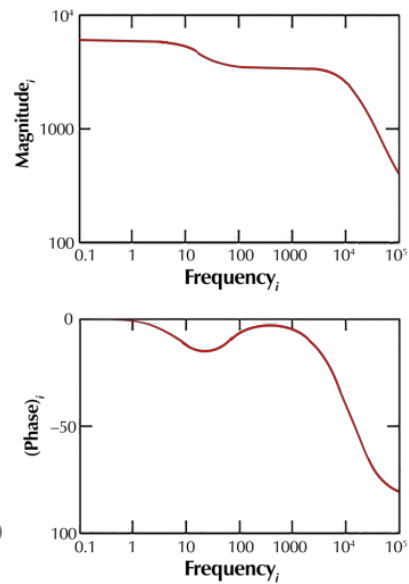


Figure 22: Bode Plot for a degraded coating [29].

In reality, all coating systems tend to degrade over time, which results in more complicated impedance behaviors. As water penetrates the coating, over time a new liquid/metal interface is formed underneath the coating, which could initiate corrosion. In Figure 13 (EEC for damaged coating), the intact coating capacitance is represented by (C_c)

and its value is usually smaller than the double layer capacitance (C_{DL}). The typical units for C_c are pF or nF whereas, the unit for C_{DL} is μF . The pore resistance (R_{po}) is defined as the resistance of the ion conducting paths that develop in the coating. The ion conducting paths represent the physical pores that are filled with electrolyte. The assumption is made that the coating becomes delaminated from the metal side of the pore, which lead to the formation of a pocket filled with electrolyte. The characteristics of this electrolyte at the interface are usually different from that of the bulk solution. As such, the double layer capacitance (C_{DL}) is modeled as the interface between this pocket of solution and the bare metal [26,29].

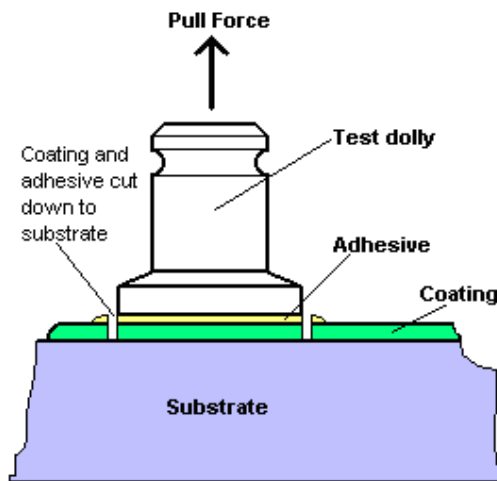
In EIS, data curves are fitted to a certain type of analog. The fit provides estimated values for the model parameters, such as pore resistance and the double layer capacitance. The impedance of the coating is defined as its ability to impede the flow of current between the anodic and cathodic areas of the metal substrate. The impedance property of the coating is considered one of the most important properties since it represents the resistance of the coating. EIS is used to characterize the impedance of coatings and according to the literature review the impedance is best characterized by measuring the low frequency limit of $|Z(\omega)|$. The reason for examining the low frequency limit for impedance measurements is that as the frequency (ω) approaches zero, the experimental noise is almost eliminated. Literature review on EIS and coatings have indicated that the low frequency (ω) ranges between 10^{-3} and 5×10^{-2} Hz [30].

4.3 Experimental Procedures and Test Panels Preparation

4.3.1 Pull-Off Adhesion Test

A dolly was glued onto the coated test panel and subjected to a force in an attempt to remove both the dolly and the coating from the metal substrate. The force at which the coating fails and the type of failure can then be determined. Figure 6 illustrates the Pull-Off Adhesion Tester (PosiTest) that was used to evaluate the adhesion strength of the coated test panels. The size of the test dolly was 20 mm and the adhesion strength (maximum pull-off pressure) was 3000 psi. A two-pack epoxy adhesive was used to glue the dollies to the coated panels. The adhesive consisted of two components; a resin and hardener that were mixed from equally weighed proportions by the use of an electronic balance. After gluing the test dolly, the glue was allowed to cure for at least 24 hours.

Figure 23 illustrates a test dolly glued on a coated substrate. The coating and adhesive are cut down to the substrate in circular shape around the test dolly. Afterwards,



the test dolly is pulled and the force required to detach the coating from the substrate is recorded. According to literature, the test results may be affected by several factors such as temperature, glue mixing, preparation of the coated panels the actual performance of the test.

4.3.2 LPR and EIS Cells, Instrumentation and Measurements

EIS and LPR measurements are performed before and after the autoclave test by employing a three-electrode corrosion cell, which included the working electrode (coated panel), a counter electrode and a reference electrode. Acrylic tubes were glued onto the

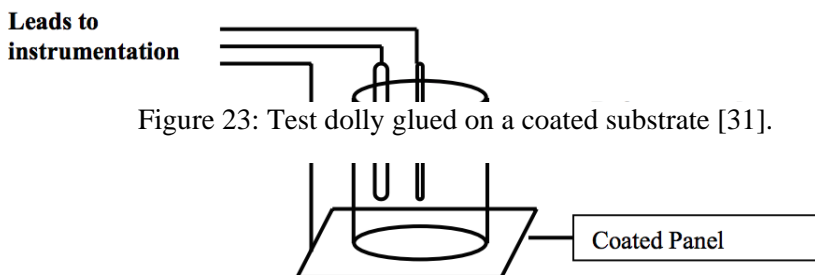


Figure 23: Test dolly glued on a coated substrate [31].

coated test panels using silicone. The tubes are then filled with electrolyte solution (50 mL of 3% NaCl) and the counter and reference electrodes were inserted into the solution. Titanium mesh was used as counter and reference electrodes. Figure 24 illustrates a schematic view of the three-electrode corrosion cell.

LPR and EIS measurements were performed by the use of Gamry's Electrochemical Multiplexer ECM8 (Reference-600/3000). As for LPR measurements, the test cell was cathodically polarized and the applied potential ranged from 0 to -25 mV vs. E_{OC} (Open Circuit

Figure 24: Schematic view of the three-electrode corrosion cell [13].

Potential) with a scan rate of 0.05 mV/s. As for EIS experimental parameters, the applied frequency ranged from 100,000 to 0.01 Hz. The DC voltage was at 0 V vs. E_{OC} and the AC voltage was at 10 mV.

Each coated test panel was divided equally into two parts; upper and lower. The upper part was exposed to the gas phase during the autoclave testing while the lower part

was exposed to the liquid phase. Therefore, this arrangement enabled an investigation of the coating's performance in both phases. Thus, two acrylic tubes (OD: 1.75 in, ID: 1.5 in, and 6 cm in height) were glued on each test panel; one in the lower part (liquid phase) and the other one in the upper part (gas phase). LPR and EIS measurements in 3% NaCl electrolyte solution were conducted on samples before and after one week of exposure to simulated sour gas in the autoclave test.

Figure 26 displays the Gamry Electrochemical Multiplexer ECM8 with eight possible connections to coated panels for conducting EIS testing. Figure 25 shows two coated test panels with the acrylic cylinders glued on both panels.



Figure 25: Acrylic tubes glued on coated panels

Figure 27 shows the titanium mesh used as reference and counter electrodes since titanium is a very stable metal. The Open Circuit Potential (E_{OC}) of the titanium reference electrode was measured vs. the Saturated Calomel Electrode (SCE) on a daily basis to ensure the stability of titanium as a reference electrode. Figure 28 illustrates the experimental setup for EIS and LPR measurements where the eight corrosion test cells are connected to the eight channels of the Gamry ECM8 Multiplexer.

4.3.3 Autoclave Test

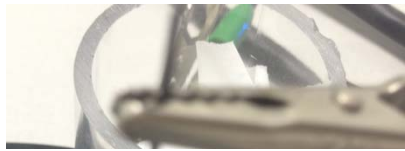
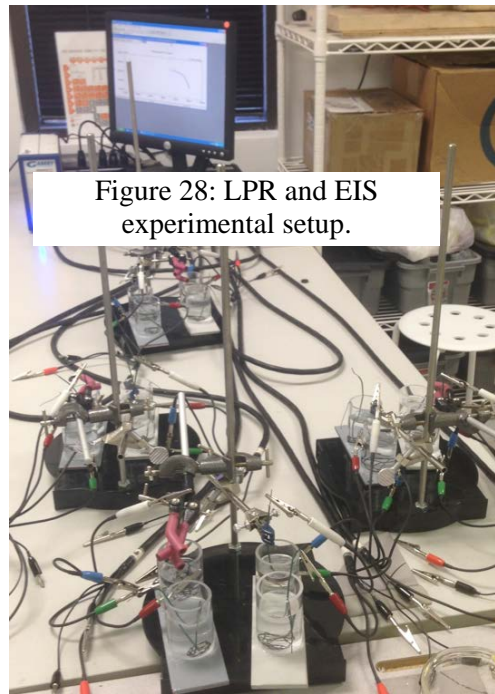


Figure 27: Titanium mesh as counter and reference electrodes.



Figure 26: Gamry Electrochemical Multiplexer ECM8



Parr Bench Top Reactor (Series 4525) which is shown in Figure 29 was used to simulate the sour gas environment. A 1000 mL autoclave with a maximum pressure rating of 1900 psig was employed to conduct the test at a maximum temperature of 350 °C. A Parr Model 4842 Temperature Controller was used to control and monitor the autoclave temperature.



Figure 29: Parr Bench Top Reactor and Temperature Controller.

The test panels were cut to a length of 13 cm in order to fit inside the autoclave. An epoxy was applied on the surface of steel that was exposed after cutting each panel. The autoclave was capable of accommodating up to 4 coated panels in each test run. But, only half of the autoclave (500 mL) was filled with MEG/water mixture of 50/50 % by volume (volume/volume %). The coated panels were exposed to the following liquid and gas phases:

Gas Phase (Mole %): 5% of H₂S, 8% of CO₂ and 87% of CH₄.

Liquid Phase (Volume %): 50% of MEG and 50% Brine (3% NaCl).

First, the autoclave is pressurized with Nitrogen and monitored for 48 hours to observe if there is a pressure drop over time. After ensuring that there is no pressure drop the

autoclave is then filled with 500 mL of liquid mixture (Water = 250 mL, MEG = 250 mL). Afterwards, 4 panels are placed inside the autoclave and then it is assembled and Nitrogen is purged through the autoclave for 24 hours to remove any contaminants. Following that the autoclave is sealed and the sour gas is injected from a premixed gas cylinder via a stainless steel pressure regulator (CGA-330, Delivery Pressure 0-500 psi) and the autoclave is pressurized to 430 psi. The autoclave test parameters are listed below in Table 4.

Table 4: Autoclave test parameters.

Test Parameter	Temperature (°C)	Pressure (psi)	Test Duration (Hrs)	Release time (mins)
Autoclave	50	430	48	15 – 30

After injecting the sour gas, the autoclave was then sealed and the temperature was set to 50 °C. The test is conducted in accordance with the NACE Standard TM0185-2006 which states that the test shall be performed for a sufficient amount of time (not less than 16 hours) at the designated temperature and pressure. In addition, the autoclave should be depressurized to atmospheric pressure at a uniform rate within 15 to 30 minutes. Once the autoclave test is over the test panels should be inspected immediately in both phases for apparent changes in the coating. Furthermore, the coated test panels shall be compared with untested coated panels to observe if any blistering, softening or swelling have formed. The examination of the coated panels shall be performed according to ASTM-D714 (Standard Test Method for Evaluating Degree of Blistering of Paints) [24,25].

4.3.4 SEM/EDS

In order for the panels to fit inside the SEM/EDS chamber they need to be cut to a length and a width of 1 cm. Thus, to minimize sample deformation a low-speed saw was used to cut the cross-sectional area of interest. Then, the samples were mounted in molds by two-part epoxy: resin and hardener. 2:1 resin to hardener ratio was used and about 15 grams of mix was needed for each sample. The resin and hardener were mixed gently for approximately two minutes and then poured into molds. A releasing agent was sprayed on the walls of the molds to prevent the epoxy gluing to molds' walls. The samples were labeled and allowed for 24 hours for epoxy to cure. Figure 30 shows two samples that are labeled and molded in epoxy.

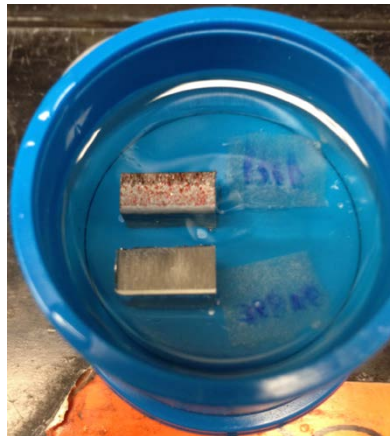


Figure 30: Two samples molded in epoxy.

Once the samples are cured, they are then grinded and polished. A common grinding and polishing sequence starts with 320, 400, 600 Silicone Carbide (SiC) grit papers and then followed by 1 μm , 0.3 μm , 0.05 μm alumina polishing compounds [16].

4.4 Test Matrix

The test matrix is divided into two categories: 1) As-Received Coatings, 2) Artificially Damaged Coatings. The first category includes testing the coated panels as-received from the coating manufacturers. On the other hand, the second category includes

applying an artificial pinhole (3 mm in Diameter) to the coated panels in both liquid and gas phases. The selection of the pinhole is based on the fact that pitting corrosion is the most common type of corrosion failure found in sour gas pipelines according to literature.

Table 5 below demonstrates the test matrix.

Table 5: Test Matrix.

Product/ # of Panels	# of Panels As Received Coatings	# Of Panels Artificially Damaged Coatings
FBE	2	2
Phenolic	2	2
Novolac	2	2
Amine Novolac	2	2
Total # of Panels	8	8

Figures 31 and 32 displays the as-received coated panels of the four products. Furthermore, Figures 33 and 34 illustrate the four products with the applied pinhole (3 mm Diameter Hole). The depth of the pinholes is measured by the use of Vernier Caliper.



Figure 31: Phenolic Epoxy & FBE as received.

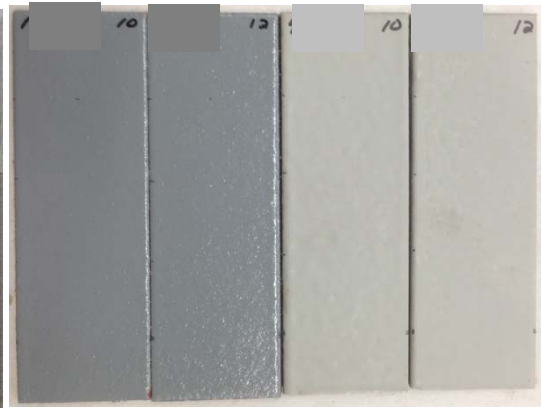


Figure 32: Amine Novolac & Novolac Epoxy as received.

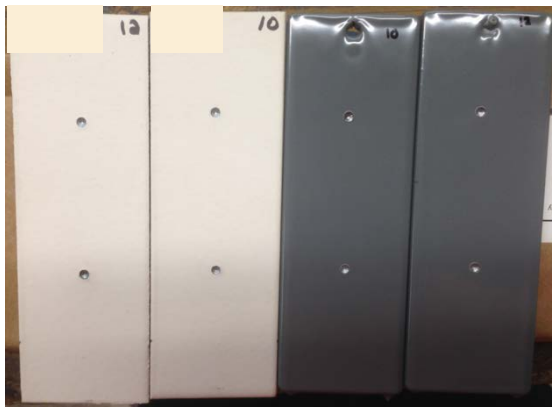


Figure 33: Phenolic Epoxy & FBE with defect.

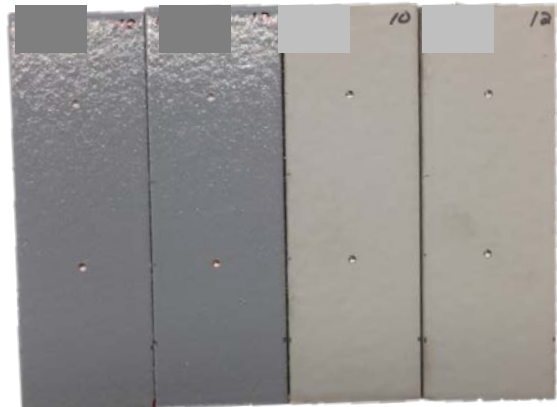


Figure 34: Amine Novolac & Novolac Epoxy with defect.

CHAPTER 5

5.0 RESULTS AND DISCUSSION

5.1 EIS & LPR Results Before Autoclave

EIS and LPR measurements were performed by the use of Gamry's Electrochemical (Reference-600/3000) Multiplexer ECM8. In EIS experiments, the applied frequency was in the range of 100,000 to 0.01 Hz. The DC voltage was at 0 V vs. E_{OC} (Open Circuit Potential) and the AC voltage was at 10 mV. As for LPR measurements, the test cell was cathodically polarized and the applied potential ranged from 0 to -25 mV vs. E_{OC} with a scan rate of 0.05 mV/s. EIS and LPR measurements were performed for a week prior and post the autoclave test in 3% NaCl solution at room temperature. In addition, it was very essential to determine the initial impedance of the coatings before exposure to sour conditions in the autoclave. Moreover, the hydration conditions which include the electrolyte concentration, hydration time, and temperature (typically room temperature) were used as reference conditions for pre and post the autoclave test.

5.1.1 EIS Results

In EIS measurements, the impedance of a coating represents the electrical resistance of the coating which is measured by an alternating current (AC) electricity. If the coating has a high impedance, it indicates that its permeability to water is low. In contrast, low impedance values imply that the coating permeability is high and corrosion might occur under the coating film. Furthermore, the impedance of coatings typically decreases over time when coatings are exposed to aggressive aqueous environments. The decrease in impedance is related to the water uptake of coatings as well as the increase in their permeability to electrolytes.

The Bode plot results of the as-received coatings for panel #1 in the gas phase is shown in Figure 35. All the results were replicated and the Bode plot results of all coatings for panel #3 in the gas phase is included in the appendices. From the Bode plot it can be observed that the measured impedance for both the FBE and Novolac coatings were high significantly in the lower ranges of frequency and remained steady over the seven days of EIS testing. Also, the Amine Novolac coating had excellent impedance however, it decreased with time whereas the Phenolic coating had very low impedance compared to the other 3 coatings and it decreased over time. Figure 36 displays the Bode plot for panel #1 in the liquid phase. The impedance results of the liquid phase were very close to the results of the gas phase since measurements were taken before the autoclave test.

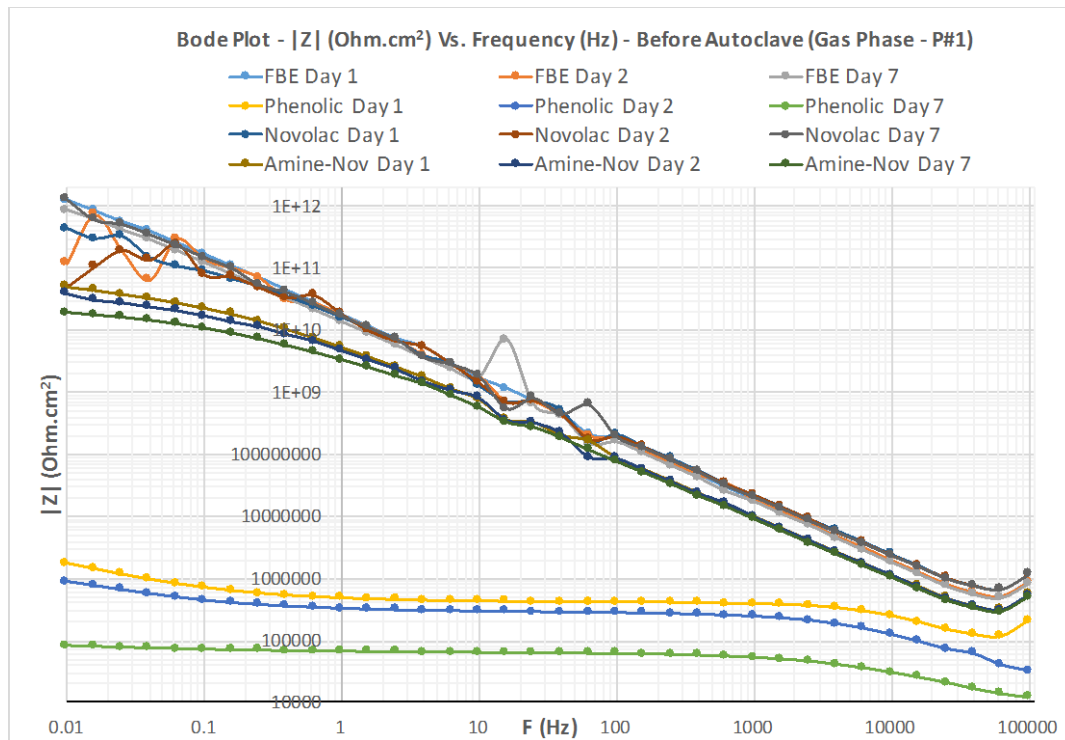


Figure 35: Bode Plot of all coatings for panel #1 in the gas phase.

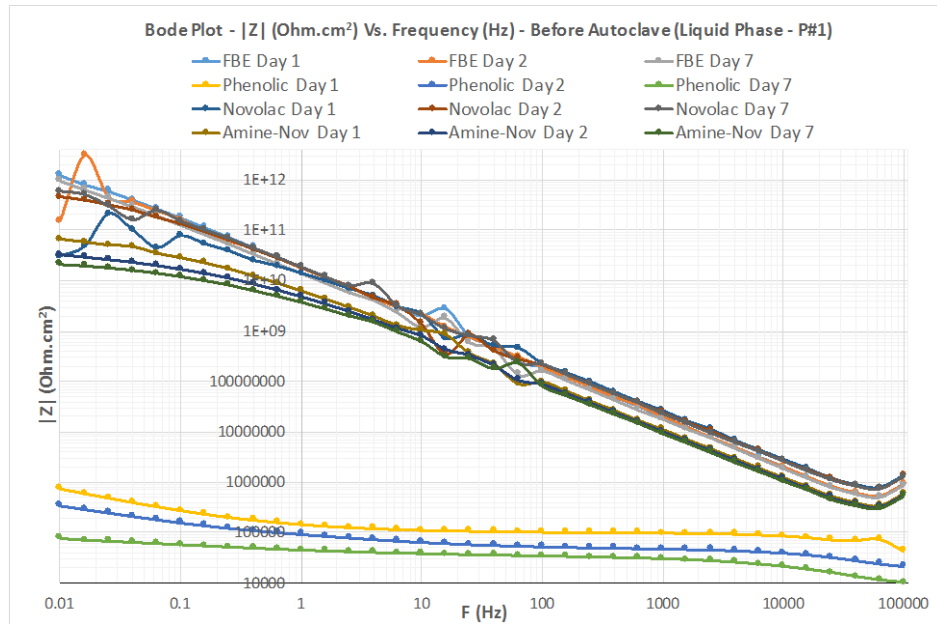


Figure 36: Bode Plot of all coatings for panel #1 in the liquid phase.

Figure 37 shows the Nyquist plot for panel #1 in the gas phase. It can be noted that both the FBE and Novolac coatings behaved like almost perfect capacitors and this behavior was represented by a vertical line in the Nyquist Plot. Additionally, the Amine Novolac

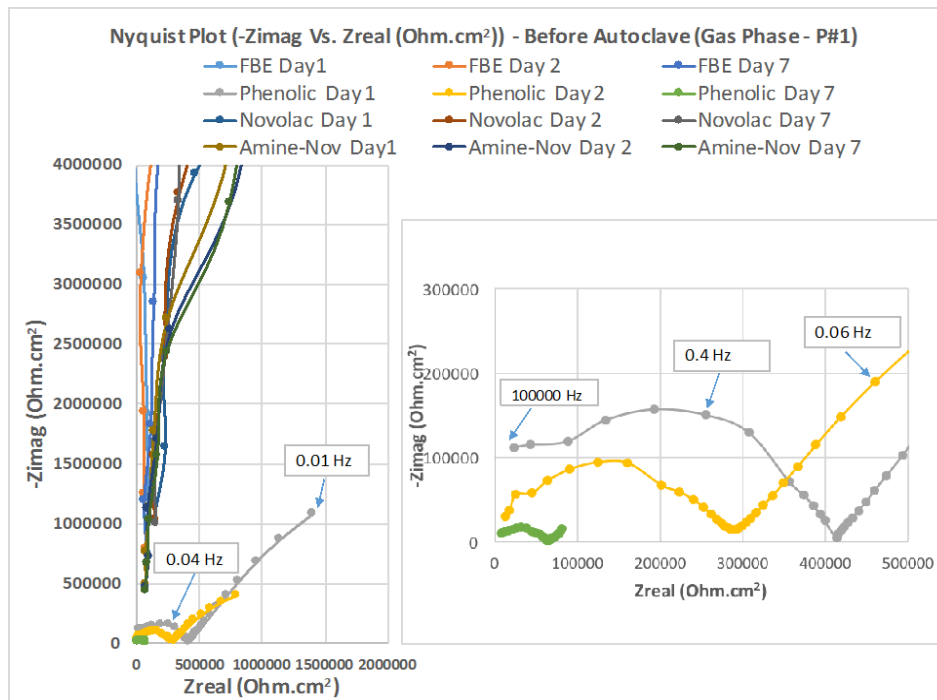


Figure 37: Nyquist Plot of all coatings for panel #1 in the gas phase.

coating showed capacitive behavior and had high impedance. In contrast, the Phenolic coating had low impedance and the pore resistance significantly decreased over time. The decrease in pore resistance (R_{po}) indicate that the electrolyte penetrated through the coating and reached the metal surface. This behavior of a degraded coating is usually represented with two semi-circles in the Nyquist plot which was the case for the Phenolic coating. Figure 38 demonstrates the Nyquist plot for panel #1 in the liquid phase and it can be observed that the results were similar to the gas phase results. The FBE and Novolac coatings behaved like capacitors and the Amine Novolac coating had also high impedance. While the Phenolic coating behaved like a degraded coating with two semi-circles in the Nyquist plot and had low impedance which decreased over time.

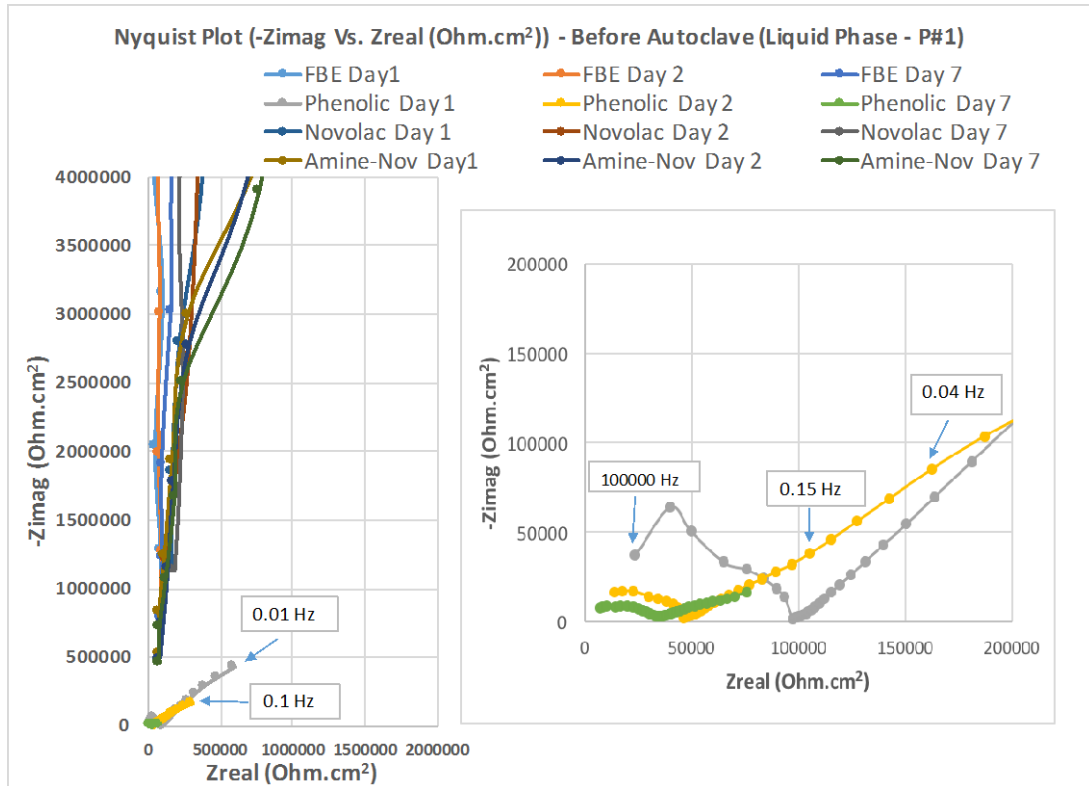


Figure 38: Nyquist Plot of all coatings for panel #1 in the liquid phase.

The EIS results of the as-received coatings were fitted to the appropriate electrical equivalent circuit (EEC) and the coating capacitance (C_c) and pore resistance (R_{po}) of each coating were determined over the week of EIS testing. The coating capacitance is a measure of the water and electrolyte ingress in the coating. Figure 39 displays the capacitance of each coating for panel #1 in the gas phase. The FBE and Novolac coatings exhibited low coating capacitance which indicated that there was no significant water absorption by both coatings. Additionally, the coating capacitance of the Amine Novolac was also low yet, it slightly increased over time. On the other hand, the Phenolic coating had relatively low capacitance over the first few days however, it increased with time which suggested that water and ions may have penetrated the coating through the pores. Figure 40 illustrates the coating capacitance for panel #1 in the liquid phase. The results were very similar to the results of the gas phase and the Phenolic capacitance increased with time.

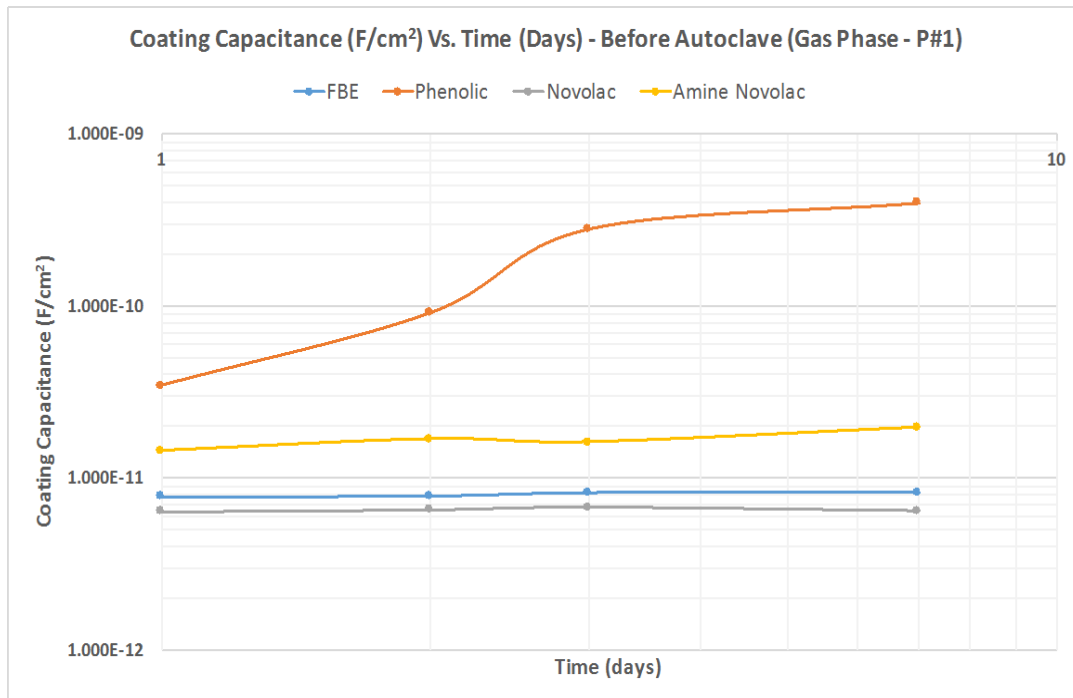


Figure 39: Coating Capacitance (F/cm^2) for panel #1 in the gas phase.

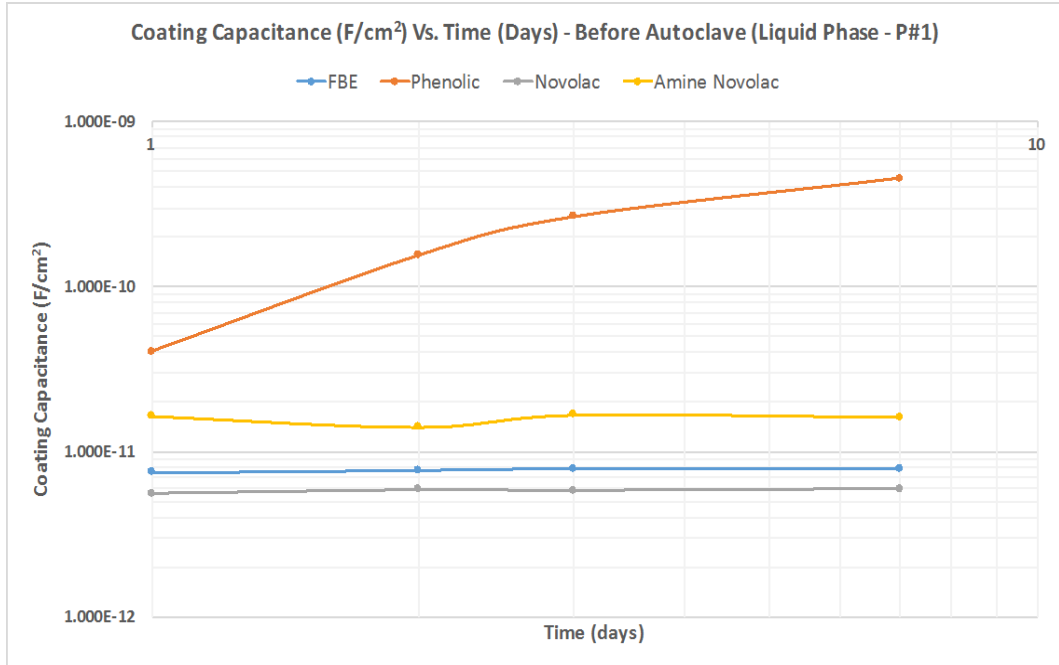


Figure 40: Coating Capacitance (F/cm²) for panel #1 in the liquid phase.

Figure 41 demonstrates the determined pore resistance (R_{po}) of all coatings for panel #1 in the gas phase over the week of EIS testing in 3% NaCl solution. It can be observed that the FBE and Novolac coatings had high pore resistance which implied that the micropores of both coatings had high ability to resist the flow of current and electrolytes.

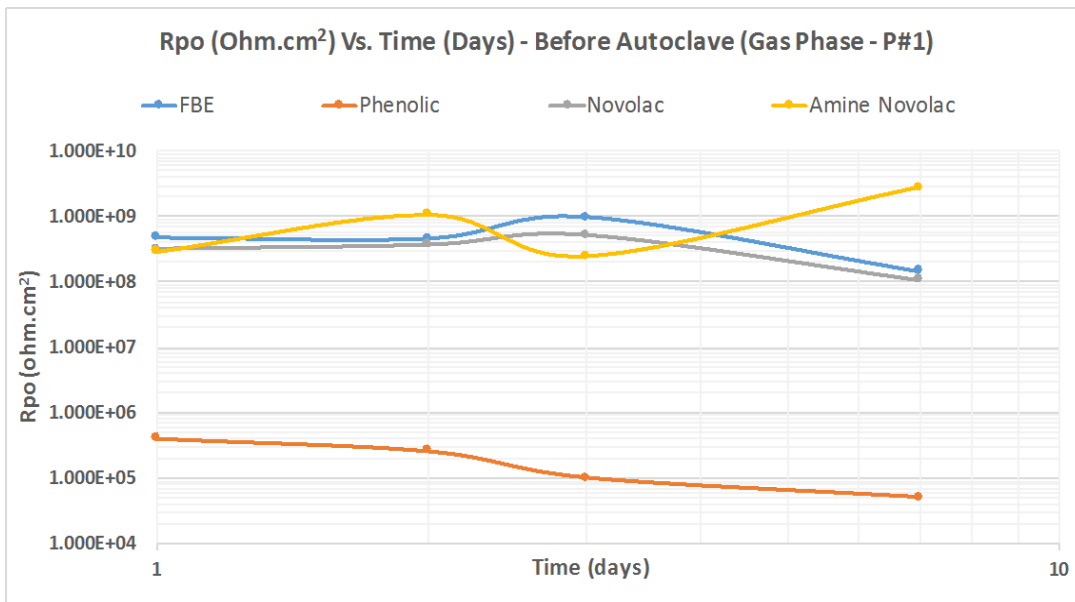


Figure 41: Pore Resistance (R_{po}) for panel #1 in the gas phase.

In addition, the Amine Novolac coating had high pore resistance over the time of exposure which indicated that the Amine Novolac was considered a high performance coating before exposure to the sour gas environment. On the other hand, the Phenolic coating exhibited low pore resistance and it decreased over time which implied that the electrolyte may have penetrated through the coating layers and reached the metal surface. Figure 42 displays the determined pore resistance (Rpo) of all coatings for panel #1 in the liquid phase and it can be observed that the trends are similar to the gas phase trends.

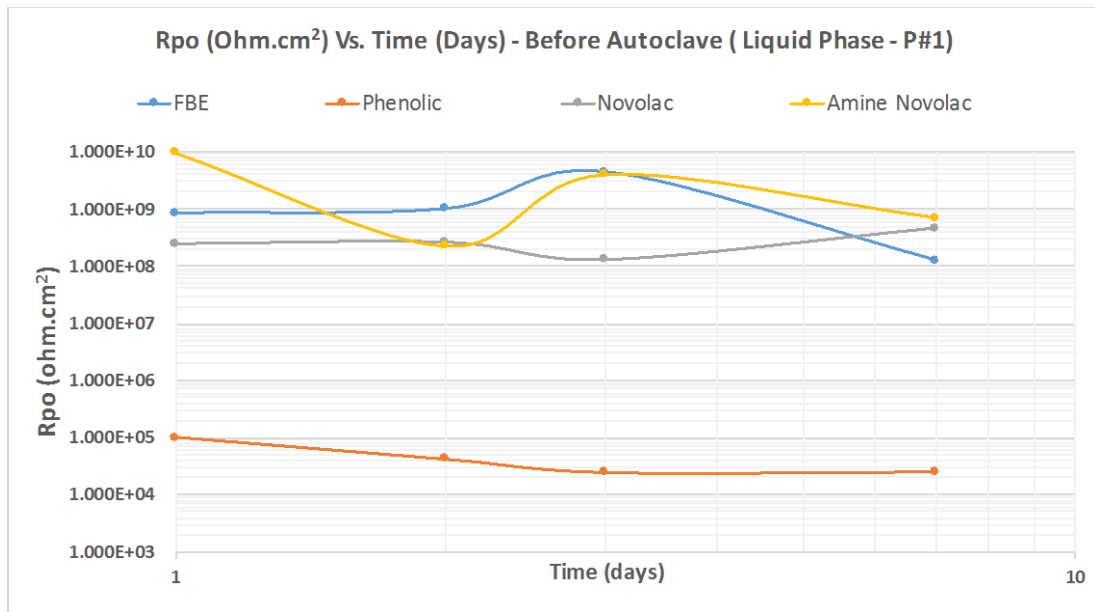


Figure 42: Pore Resistance (Rpo) for panel #1 in the liquid phase.

Furthermore, the water uptake by each coating was estimated by the use of Brasher-Kingsbury equation (shown in the appendices) which is considered the most common equation used to estimate the water uptake by coatings. Moreover, the water uptake by each coating was determined at the last day #7 of EIS testing in 50 mL of 3% NaCl solution before the autoclave test. The FBE coating absorbed 0.608 mL of water in the gas phase and 0.623 mL in the liquid phase which implied that only small amount of water was

absorbed by the FBE coating. Also, the Novolac coating absorbed small amount of water with 0.159 mL in the gas phase and 0.823 mL in the liquid phase. While the Amine Novolac coating absorbed 3.62 mL of water in the gas phase and 0.257 mL in the liquid phase. On the other hand, the Phenolic coating absorbed 27.9 mL of water in the gas phase and 27.6 mL in the liquid phase which indicated that significant amount of water was absorbed by the Phenolic coating [26].

5.1.2 LPR Results

The LPR measurements were conducted to the artificially damaged coatings (3 mm diameter hole) to determine the corrosion current density (i_{corr} , $\mu\text{A}/\text{cm}^2$). Figure 43 displays the Linear Polarization Resistance (LPR) results of all coatings for panels #10 and #12 in the gas phase before the autoclave test. The Phenolic coating had the highest corrosion current density (i_{corr}) and it increased with time. The FBE and Amine Novolac coatings had similar values of i_{corr} with a slight increase over time. In contrast, the

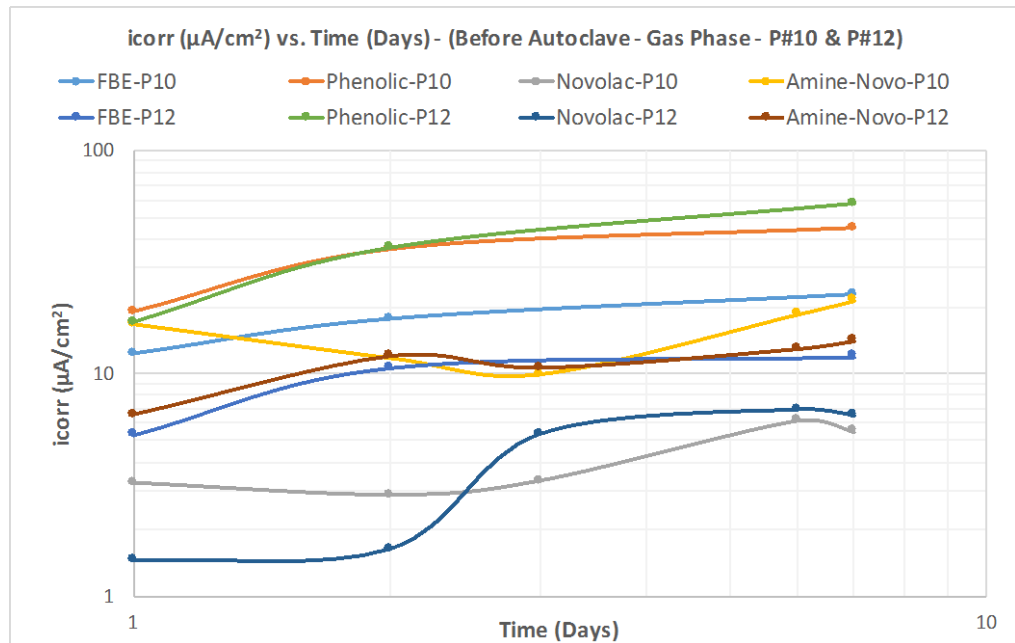


Figure 43: i_{corr} vs. Time for panels #10 & #12 in the gas phase.

Novolac coating had the lowest icorr and it remained stable over a week of exposure to 3% NaCl electrolyte solution. The LPR results for panels #10 and #12 in the liquid phase are shown in Figure 44 and the results are very similar to the gas phase results.

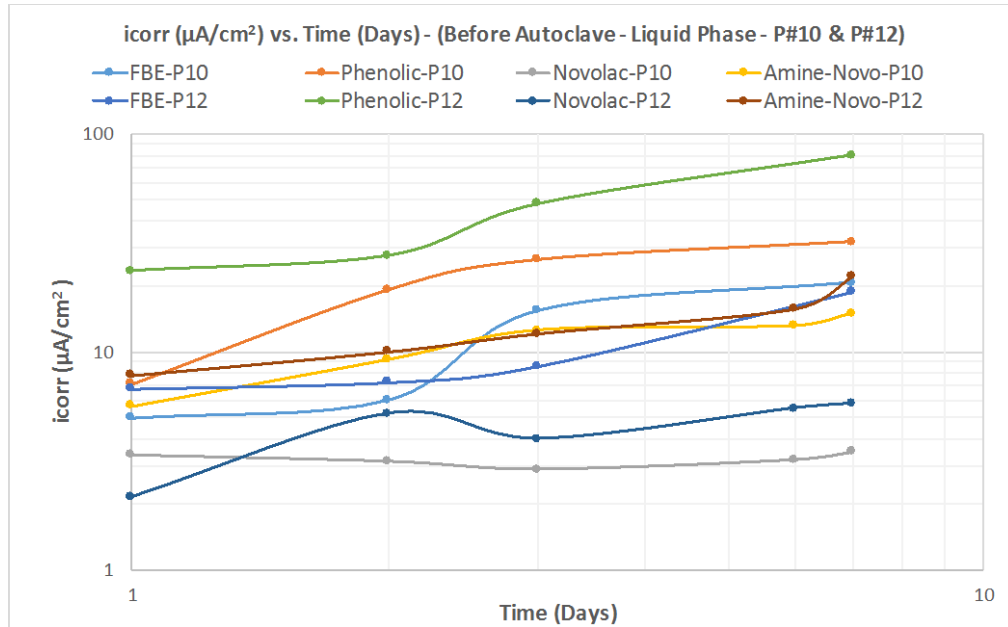


Figure 44: icorr vs. Time for panels #10 & #12 in the liquid phase.

5.2 Chemical Resistance (Autoclave Test) Results

The coated panels were placed inside the autoclave and pressurized with sour gas up to 430 psi for 48 hours and the temperature was set at 50°. Once the autoclave test was over, the panels were immediately inspected in the gas and liquid phases for apparent changes in the coating. Furthermore, the coated panels were compared with untested coated panels to observe if any blistering, softening or swelling have formed. The examination of the coated panels was performed in accordance with ASTM-D714 (Standard Test Method for Evaluating Degree of Blistering of Paints). Figures 45 and 46 display some of the coated panels after the autoclave test. It can be observed that blisters were formed on both the Phenolic and Amine Novolac coatings in both phases, liquid and gas. In addition, more

blisters were observed in the liquid phase than in the gas phase for both coatings. The formation of blistering is usually attributed to the breakdown in the protective nature of the coating. Moreover, blisters indicate that the coating may have lost adherence from the steel which may lead to water accumulation and corrosion might occur. On the other hand, the FBE and Novolac coatings did not experience any blistering which suggested that both coatings had excellent adhesion properties after exposure to the sour environment.

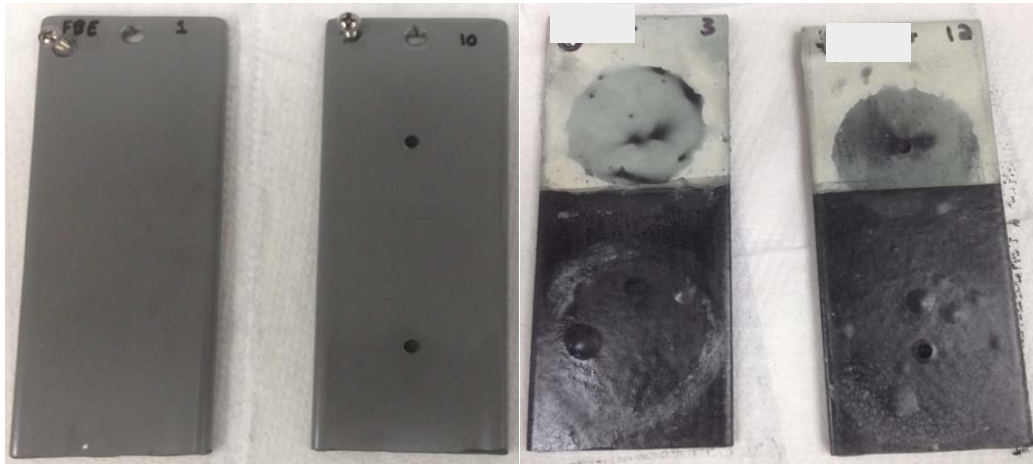


Figure 45: FBE and Phenolic Epoxy coated panels after the autoclave test.



Figure 46: Amine Novolac and Novolac Epoxy coated panels after the autoclave test.

5.3 EIS & LPR Results After Autoclave

5.3.1 EIS Results

The Bode plot results of all coatings after the autoclave test for panel #1 in the gas phase is illustrated in Figure 47. It can be noticed that the measured impedance for both the FBE and Novolac coatings remained significantly high even after being exposed to the sour environment as well as stable over the week of EIS testing in 3% NaCl solution.

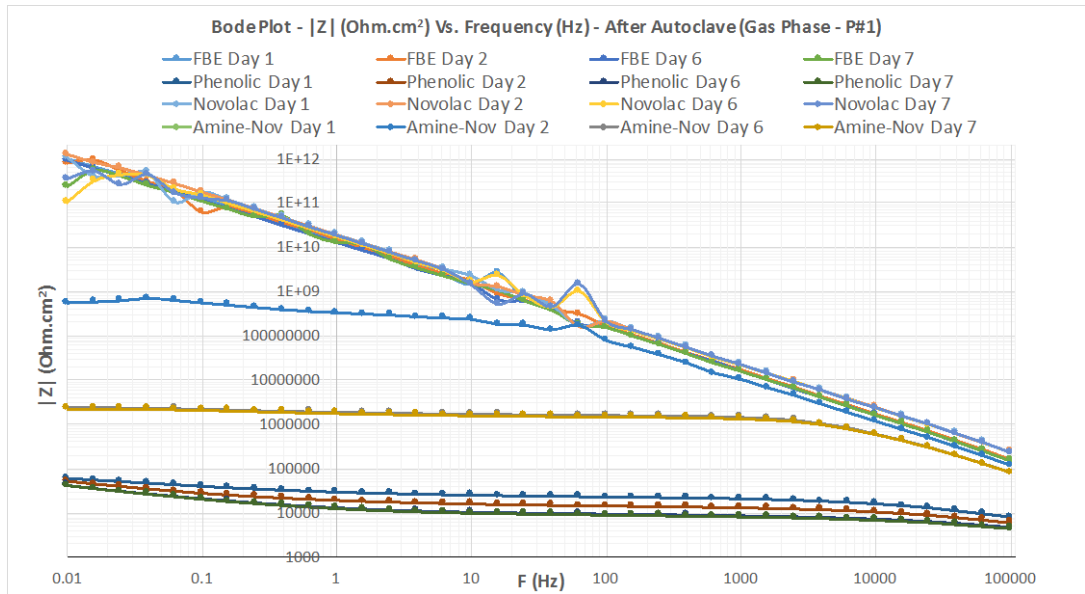


Figure 47: Bode Plot of all coatings for panel #1 in the gas phase.

As for the Amine Novolac coating, the measured impedance was lower than before the autoclave and it drastically declined with time. Similarly, the impedance values for the Phenolic coating were lower than before the autoclave and decreased over time. Figure 48 displays the Bode plot of all coatings after the autoclave test for panel #1 in the liquid phase. The FBE and Novolac coatings exhibited high impedance even in the liquid phase and remained steady over time. In contrast, the Amine Novolac coating had lower impedance than before the autoclave and significantly decreased over time. Moreover, the Phenolic coating also showed low impedance in the liquid phase and declined over time.

Furthermore, it can be observed that the Phenolic and Amine Novolac coatings had lower impedance in the liquid phase as compared to the gas phase.

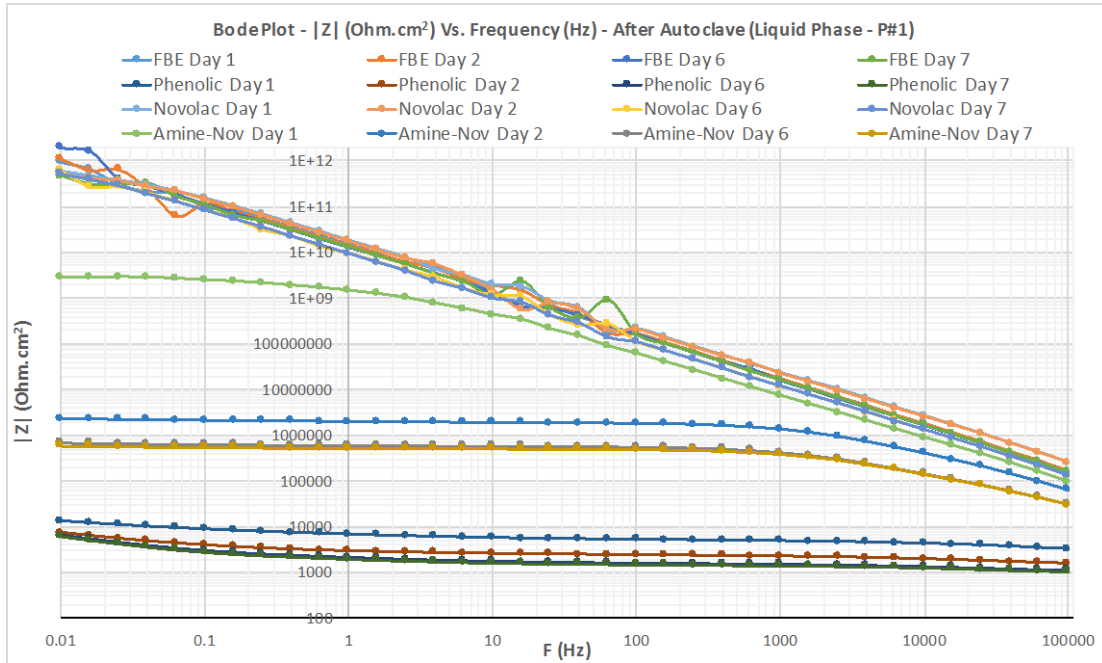


Figure 48: Bode Plot of all coatings for panel #1 in the liquid phase.

Figure 49 illustrates the Nyquist plot for panel #1 in the gas phase after the autoclave test.

The FBE and Novolac coatings continued to behave like pure capacitors and exhibited

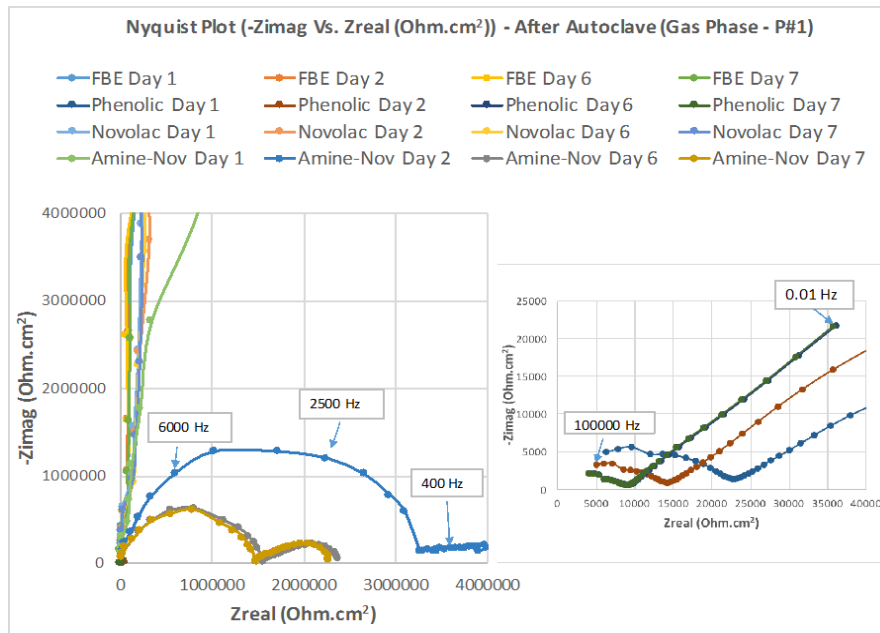


Figure 49: Nyquist Plot of all coatings for panel #1 in the gas phase.

significantly high impedance over the week of EIS testing in 3% NaCl solution. In contrast, the Amine Novolac impedance decreased over time and it exhibited the behavior of a degraded coating with two semi-circles in the Nyquist plot. Also, the Phenolic coating had very low impedance and it declined with time. Figure 50 shows the Nyquist plot for panel #1 in the liquid phase. The FBE and Novolac coatings also exhibited a capacitive behavior in the liquid phase over the EIS testing period. While the Amine Novolac showed low impedance in the liquid phase with a significant decrease over time. Additionally, the Phenolic coating had very low impedance and it declined with time. Furthermore, it can be observed that the Phenolic and Amine Novolac coatings had lower impedance in the liquid phase as compared to the gas phase which suggest that both coatings showed higher signs of degradation in the liquid phase during the autoclave test.

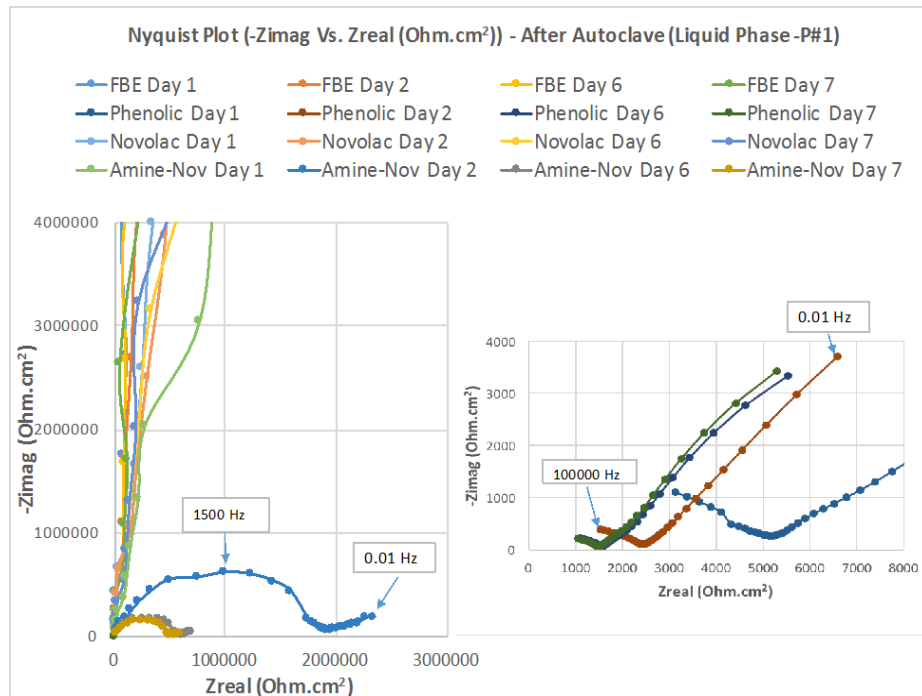


Figure 50: Nyquist Plot of all coatings for panel #1 in the liquid phase.

Figure 51 displays the capacitance of all coatings after the autoclave test for panel #1 in the gas phase over the week of EIS testing. The FBE and Novolac coatings demonstrated low capacitance which implied that there was no significant water absorption by both coatings during exposure to the sour environment in the autoclave. In addition, the Amine Novolac coating had also low capacitance however, it slightly increased over time.

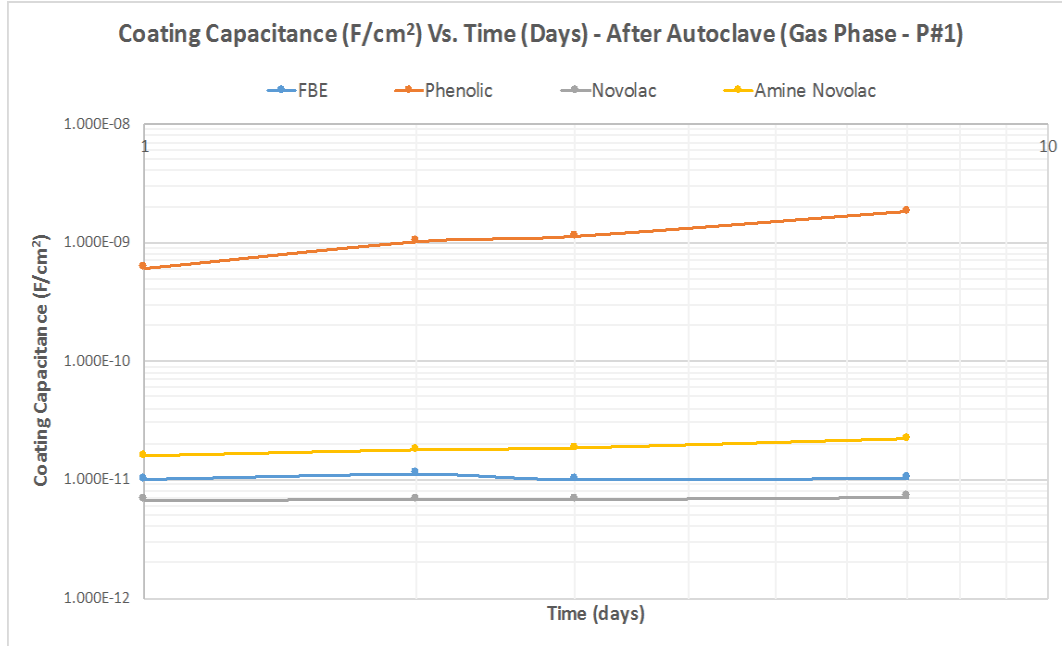


Figure 51: Coating Capacitance (F/cm²) for panel #1 in the gas phase.

In contrast, the Phenolic coating had the highest capacitance which increased over time and exceeded the typical capacitance value of an undamaged coating (1×10^{-9} F/cm²). Figure 52 displays the capacitance of all coatings for panel #1 in the liquid phase and similar results were observed for both the FBE and Novolac with low coating capacitance. Moreover, the Amine Novolac coating had also low capacitance, yet it noticeably increased over time. While the Phenolic coating had very high capacitance compared to the other coatings and it significantly increased over time. Furthermore, it can be observed that the Phenolic and Amine Novolac had higher coating capacitance in the liquid phase as

compared to the gas phase which suggest that both coatings absorbed more water in the liquid phase during the autoclave test.

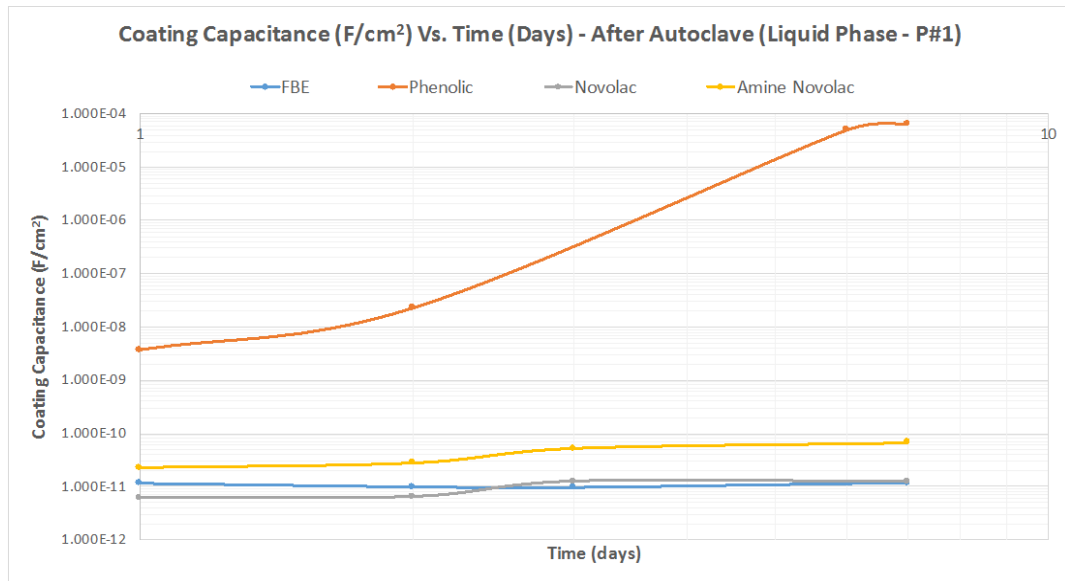


Figure 52: Coating Capacitance (F/cm²) for panel #1 in the liquid phase.

Figures 53 and 54 illustrate the determined pore resistance (R_{po}) of all coatings for panel #1 in the gas and liquid phases over the week of EIS testing in 3% NaCl solution. The FBE coating had the highest pore resistance in both phases and it remained high and steady over time. In addition, the Novolac coating revealed high pore resistance in both phases as well

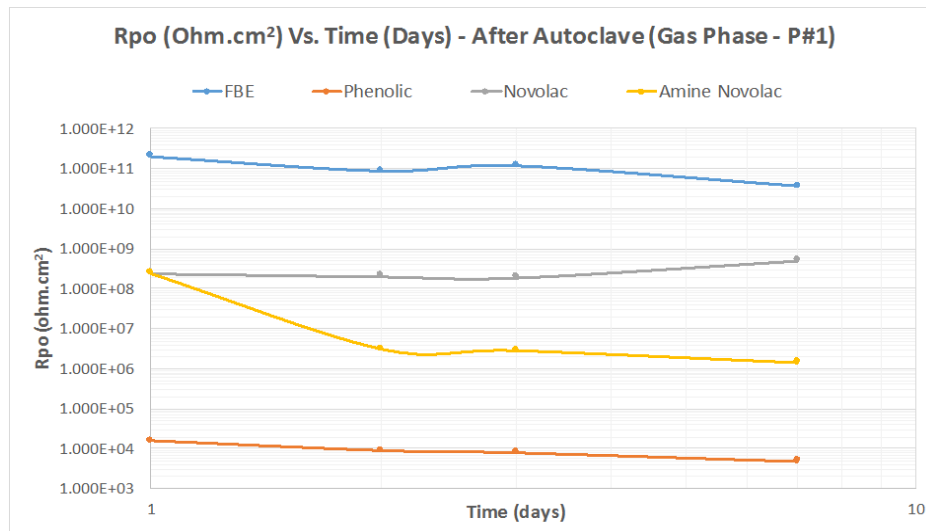


Figure 53: Pore Resistance (R_{po}) for panel #1 in the gas phase.

and it remained stable over time. In contrast, a decrease of two to three orders of magnitude is observed in the pore resistance of the Amine Novolac coating which suggest that the electrolytes may have penetrated the coating layers through the micropores. Additionally, the Phenolic coating exhibited low pore resistance which indicate that the electrolyte continued to penetrate through the micropores of the coating which lead to the corrosion of the metal surface under the coating. Moreover, the determined pore resistance of the Phenolic and Amine Novolac coatings were lower in the liquid phase than the gas phase.

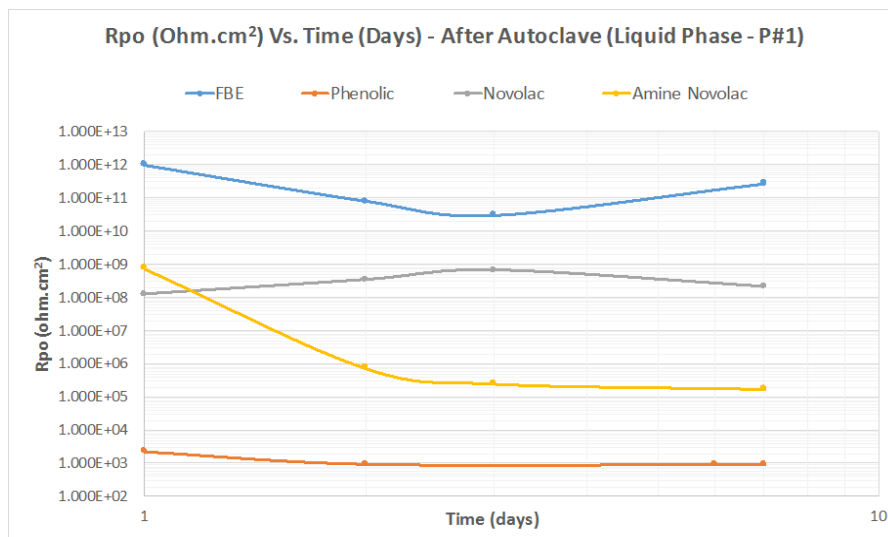


Figure 54: Pore Resistance (Rpo) for panel #1 in the liquid phase.

Furthermore, the water uptake by each coating was determined at the last day #7 of EIS testing in 50 mL of 3% NaCl solution after the autoclave test. The FBE coating absorbed 3.04 mL of water in the gas phase and 5.14 mL in the liquid phase which implied that only small amount of water was absorbed by the FBE coating. Also, the Novolac coating absorbed small amount of water with 1.21 mL in the gas phase and 9.19 mL in the liquid phase. Whereas the Amine Novolac coating absorbed 4.72 mL of water in the gas phase and 16.1 mL in the liquid phase. On the other hand, the Phenolic coating absorbed significant amount of water with 45.2 mL in the gas phase and 163 mL in the liquid phase.

Furthermore, in this study the impedance of coatings (Log Z) at 0.1 Hz is tabulated and used to evaluate the performance of the coatings and assess their corrosion protection properties. The selection of Log Z at 0.1 Hz is rather arbitrary, yet considered very reliable to distinguish between the performance of different coatings. Figure 55 displays the logarithmic coating impedance scale which predict the performance of organic coatings based on the coating impedance (Log Z) at 0.1 Hz. The scale was generated according to large number of literature of laboratory and fieldwork on coating impedance studies [32].

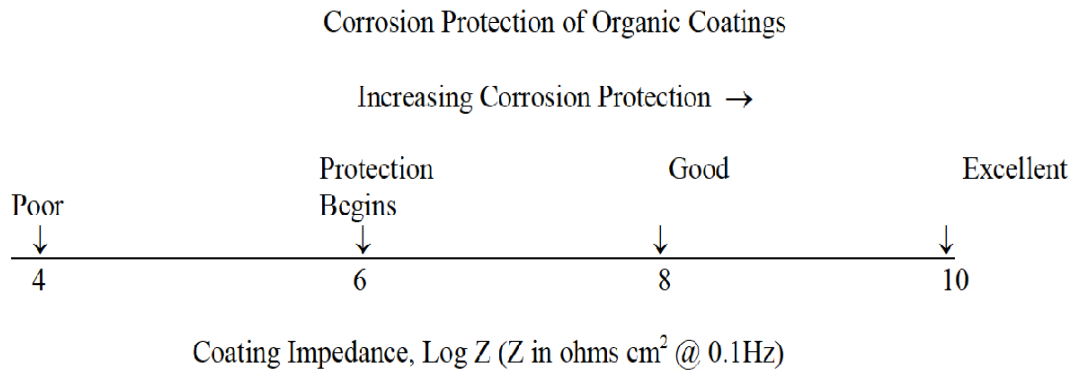


Figure 55: Logarithmic Coating Impedance Scale [32].

High performance coatings possess excellent barrier properties and low permeability to water and as a result, they have high impedance ($>10^{10}$ ohm.cm²) at low frequency (0.1 Hz) and behave such as pure capacitors. In contrary, poor performance coatings typically have high permeability to water and thus exhibit low impedance ($<10^6$ ohm.cm²) at low frequency (0.1 Hz). The decrease in impedance is attributed to the water uptake of the coating as well as the increase in its permeability to water. Furthermore, the performance of coatings in EIS is usually evaluated over a sufficient amount of time which give the electrolytes a chance to penetrate through the micropores of the coatings [13].

Figures 56 and 57 show the determined coating impedance (Log Z in ohm.cm²) at 0.1 Hz for panels #1 and #3 in both phases (liquid and gas) before and after exposure to the sour gas environment at the seventh day of EIS testing. It can be seen that both the FBE and Novolac coatings had excellent impedances with Log Z ranging from 10.92 to 11.18 for both the liquid and gas phases prior and post exposure to the autoclave environment.

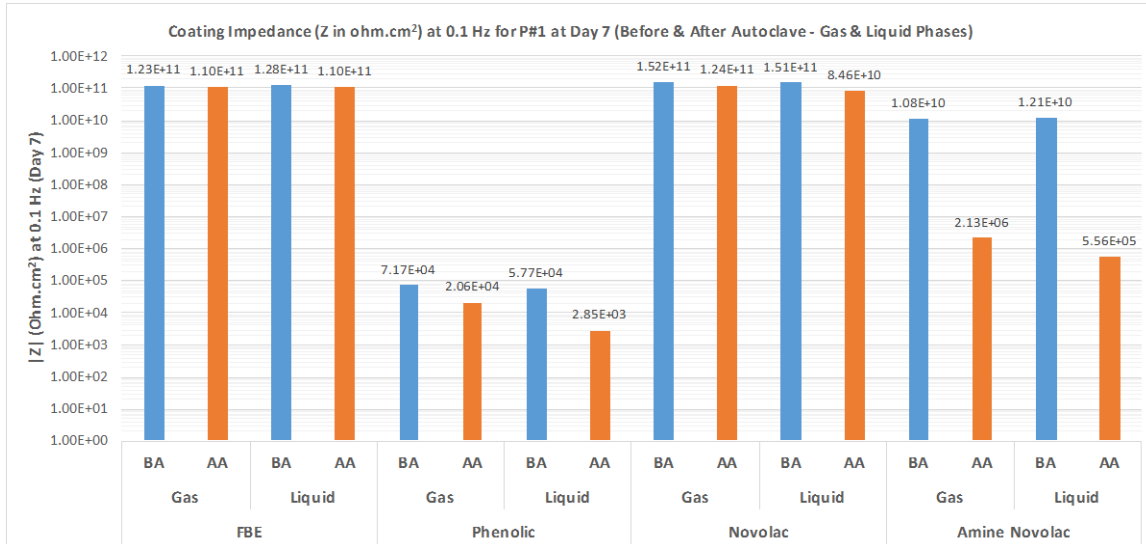


Figure 56: Coating Impedance (ohm.cm²) at 0.1 Hz for panel #1 in gas/liquid phases before/after autoclave.

In addition, the Amine Novolac coating showed also excellent impedances before the autoclave with Log Z ranging from 10.03 to 11.21. However, a significant decrease was observed in the coating impedance of the Amine Novolac after being exposed to the sour media and Log Z varied from 5.71 to 9.45. This substantial drop in the coating impedance might be attributed to the degradation of the coating which occurred during exposure to the autoclave test conditions. On the other hand, the Phenolic coating exhibited low coating impedances even before the autoclave test with Log Z ranging from 4.76 to 4.92. Additionally, the coating impedances of the Phenolic coating continued to decrease after the autoclave test and Log Z ranged from 3.45 to 4.31. Furthermore, the coating

impedances in the liquid phase had lower values than the gas phase for both the Phenolic and Amine Novolac coatings. This implies that more coating deterioration had occurred in the liquid phase compared to the gas phase during exposure to the autoclave test conditions.

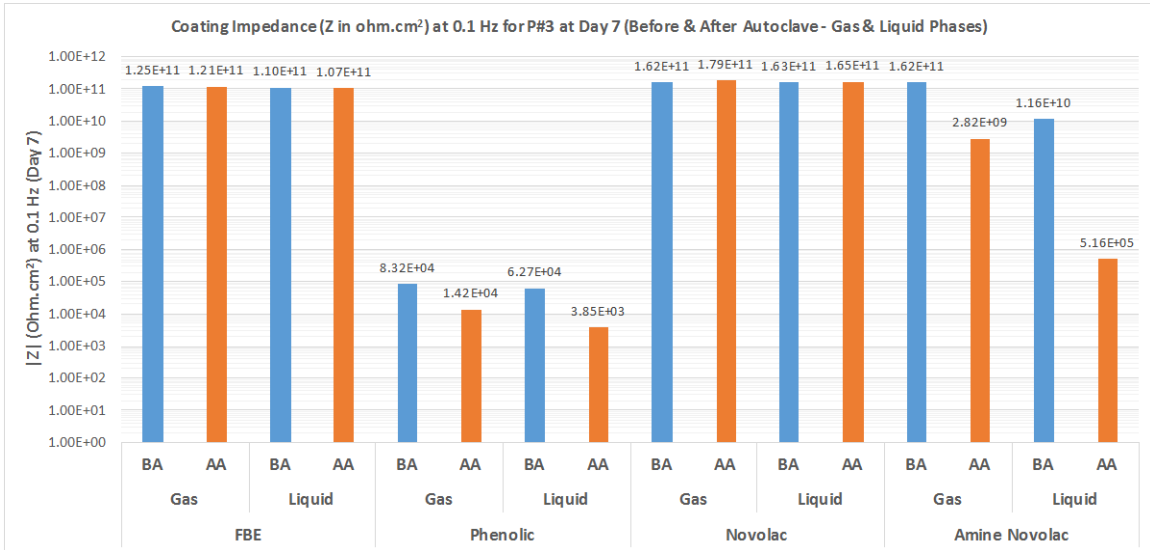


Figure 57: Coating Impedance (ohm.cm²) at 0.1 Hz for panel #3 in gas/liquid phases before/after autoclave.

5.3.2 LPR Results

The LPR measurements were performed to the coatings with defect (3 mm diameter hole) to determine the corrosion current density (i_{corr} , $\mu\text{A}/\text{cm}^2$) after exposure to the autoclave test conditions in 3% NaCl electrolyte solution. Figure 58 displays the Linear Polarization Resistance (LPR) results of all the coatings for panels #10 and #12 in the gas phase after the autoclave test. In similar manner to prior the autoclave, the Phenolic coating had the highest corrosion current density (i_{corr}) whereas the Novolac coating had the lowest i_{corr} . The FBE and Amine Novolac coatings had similar values of i_{corr} and remained steady over time. Figure 59 shows the Linear Polarization Resistance (LPR) results of all coatings for panels #10 and #12 in the liquid phase after the autoclave test.

For all coatings the determined corrosion current density (i_{corr}) in the liquid phase were slightly higher in comparison to the gas phase. This imply that during exposure to the gas and liquid phases in the autoclave, the 3 mm defect holes which were exposed to the liquid phase have suffered more corrosion than the ones in the gas phase.

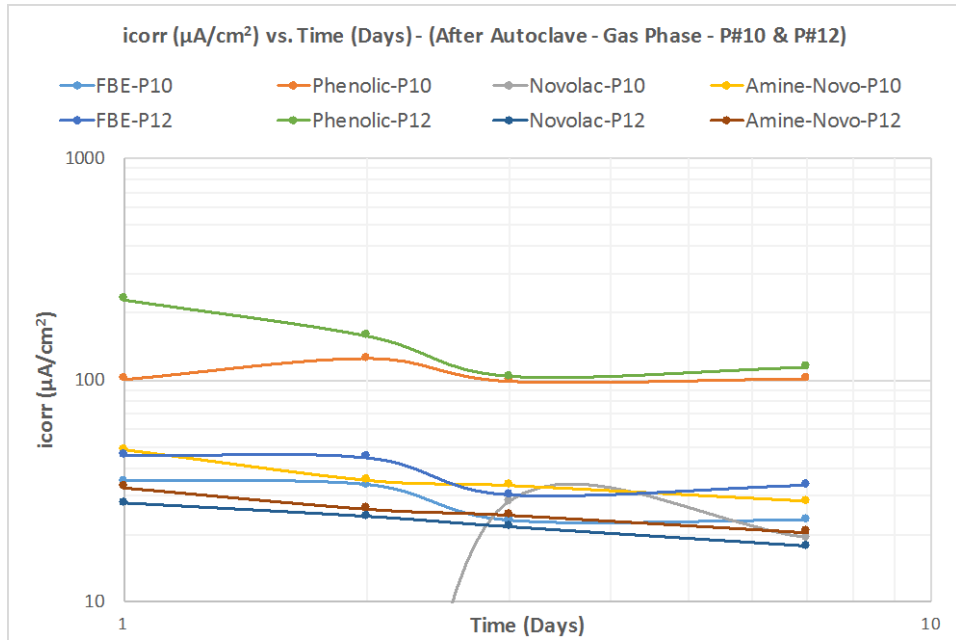


Figure 58: i_{corr} vs. Time for panels #10 & #12 in the gas phase.

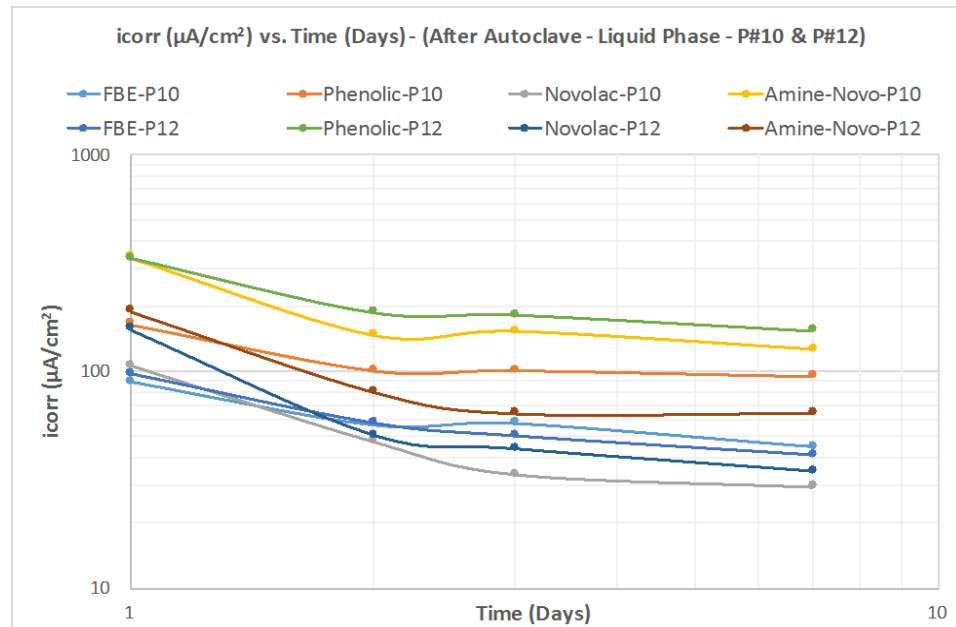


Figure 59: i_{corr} vs. Time for panels #10 & #12 in the liquid phase.

5.4 Pull-Off Adhesion Test Results

5.4.1 Before Autoclave

The pull-off adhesion test was performed to all the coatings in as received conditions. Figure 60 shows the results of the pull-off adhesion test for the as-received coatings. Two types of failures were observed including glue failure and cohesive failure. The blue columns represent glue failures whereas the dotted columns represent cohesive failures. It can be observed that for both the FBE and Novolac coatings, all the adhesion test failures were recorded as glue failures and the measured pull-off force was over 1000 psi, which indicated that both coatings possess excellent adhesion properties. On the other hand, the Amine Novolac coating exhibited cohesive failures and the pull-off force was below 1000 psi. In addition, the Phenolic coating also showed cohesive failures in some cases however, the pull-off adhesion force was over 1000 psi.

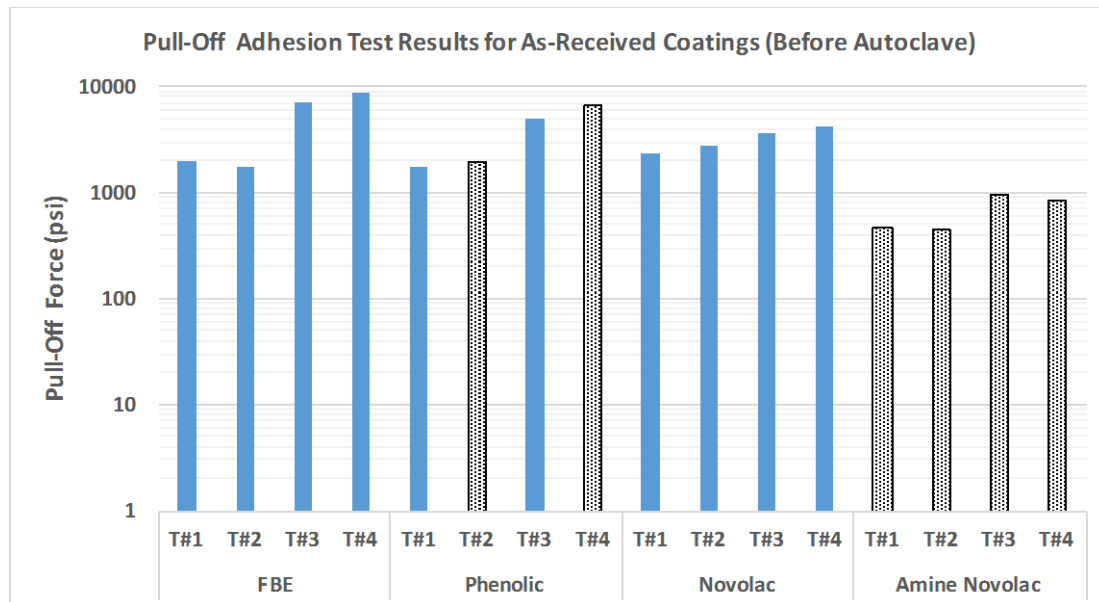


Figure 60: Pull-Off Adhesion Test results for as-received coatings before autoclave.

Figure 61 shows samples of the four coatings after the pull-off adhesion test. It can be observed that the Amine Novolac coating had cohesive failures and the topcoat was entirely

removed from the substrate. In addition, the Phenolic coating also had cohesive failures and the coating was partly detached as shown.

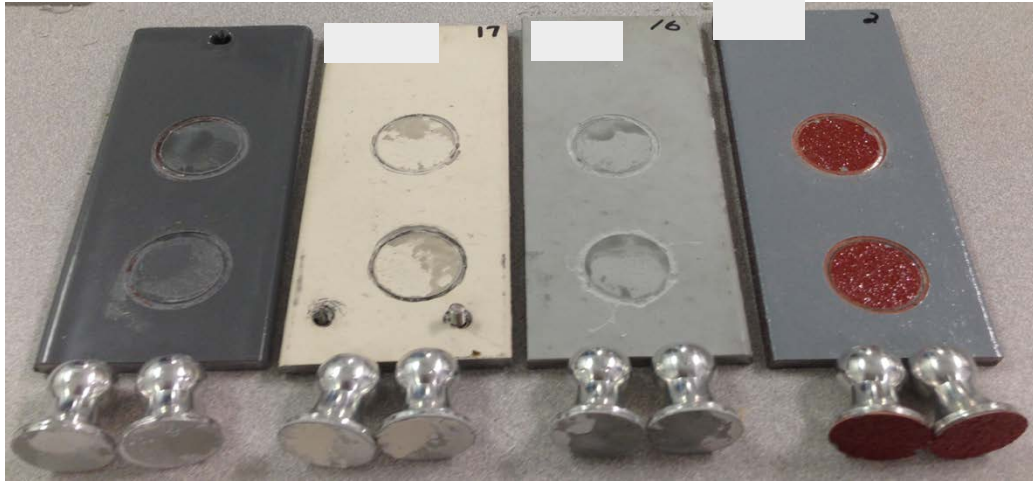


Figure 61: FBE, Phenolic, Novolac, and Amine Novolac coated panels after the pull-off test.

5.4.2 After Autoclave

After the autoclave test and the week of EIS testing in 3% NaCl solution, the pull-off adhesion test was conducted on all test panels including the as-received and artificially damaged coatings. Figure 62 demonstrates the pull-off adhesion test results of the as-received coatings for panel #1 in the gas and liquid phases. The blue columns represent

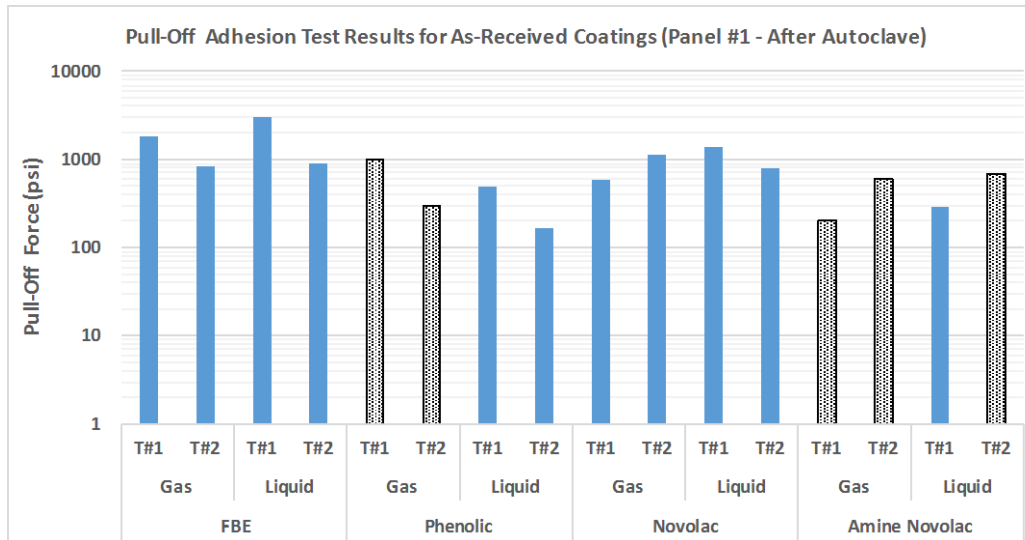


Figure 62: Pull-Off Adhesion Test results for panel #1 after autoclave.

glue failures while the dotted columns represent cohesive failures. It can be observed that for both the FBE and Novolac coatings, all the test failures were recorded as glue failures which suggest that both coatings exhibited outstanding adhesion properties even after being exposed to the sour environment. On the other hand, the majority of failures were identified as cohesive failures for both the Phenolic and Amine Novolac coatings. In addition, both coatings were detached at lower pressures as compared to before the autoclave test which suggest that both coatings have severely deteriorated during exposure to the sour environment. Figure 63 illustrates the pull-off adhesion test results of the pin-holed coatings for panel #10 in the gas and liquid phases. The measured pull-off force for all pin-holed coatings were lower than the as-received coatings. Furthermore, glue failures were recorded for FBE and Novolac coatings while the Phenolic and Amine Novolac coatings revealed cohesive failures in both phases, liquid and gas.

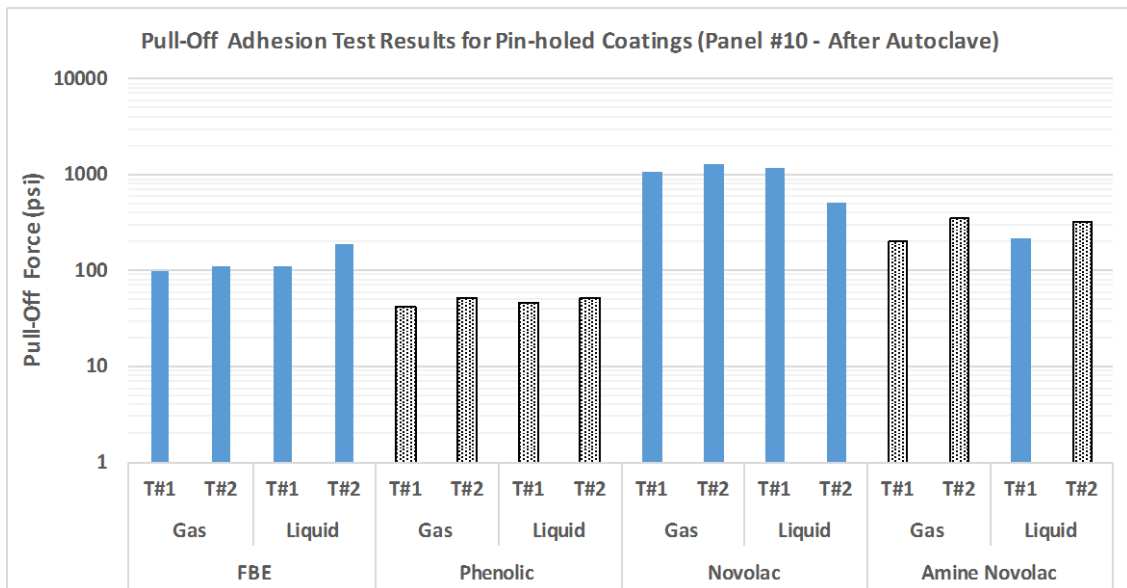


Figure 63: Pull-Off Adhesion Test results for panel #10 after autoclave.

Figure 64 shows the pull-off adhesion test results of the pin-holed coatings for panel #12 in the gas and liquid phases. Glue failures were observed for the FBE and Novolac coatings whereas cohesive failures were noted for the Phenolic and Amine Novolac coatings. In addition, Figure 65 displays some of the coated panels after the pull-off adhesion test.

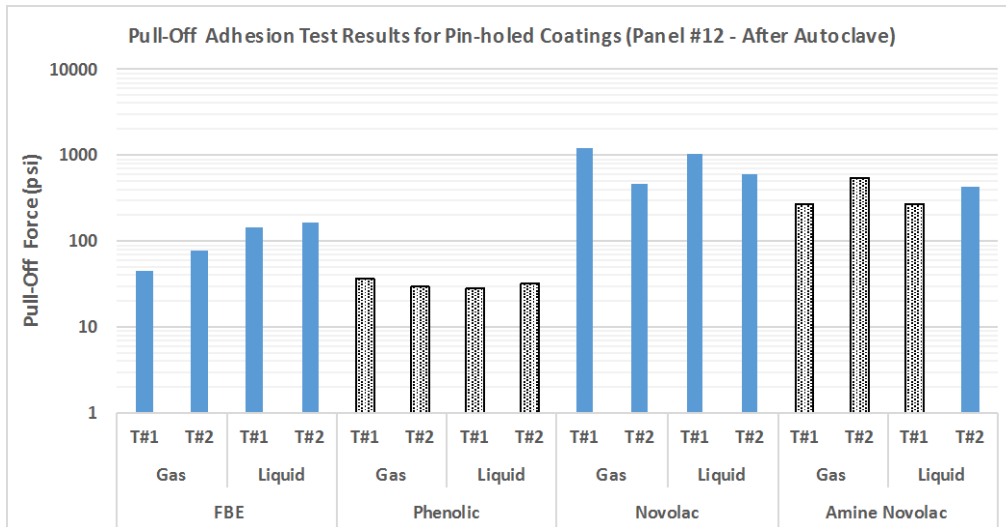


Figure 64: Pull-Off Adhesion Test results for panel #12 after autoclave.

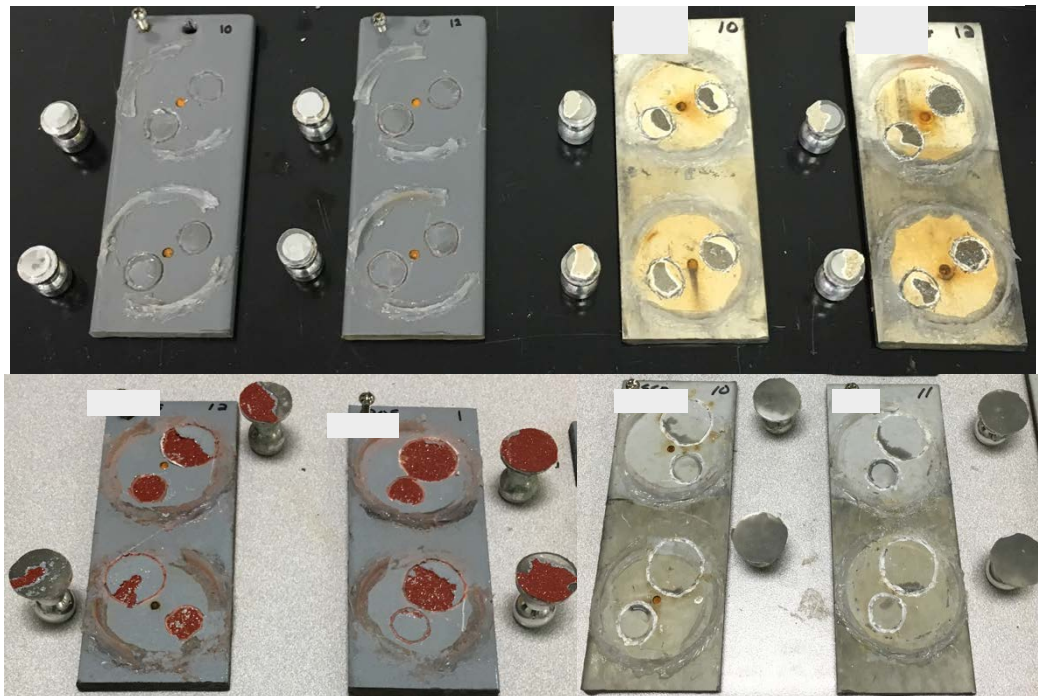


Figure 65: FBE, Phenolic, Amine Novolac, and Novolac coated panels after the pull-off test.

5.5 SEM/EDS Results

Analytical techniques such as Scanning Electron Microscopy (SEM) and Energy Dispersive Spectroscopy (EDS) were used to examine the surface morphology and the composition of the corrosion products that were formed in the presence of a pinhole after exposure to the sour environment. Several corrosion products were formed in the pinhole during the EIS and autoclave testing. Figure 66 display the SEM images of the cross-sectional area of the pinholes for the four coatings.

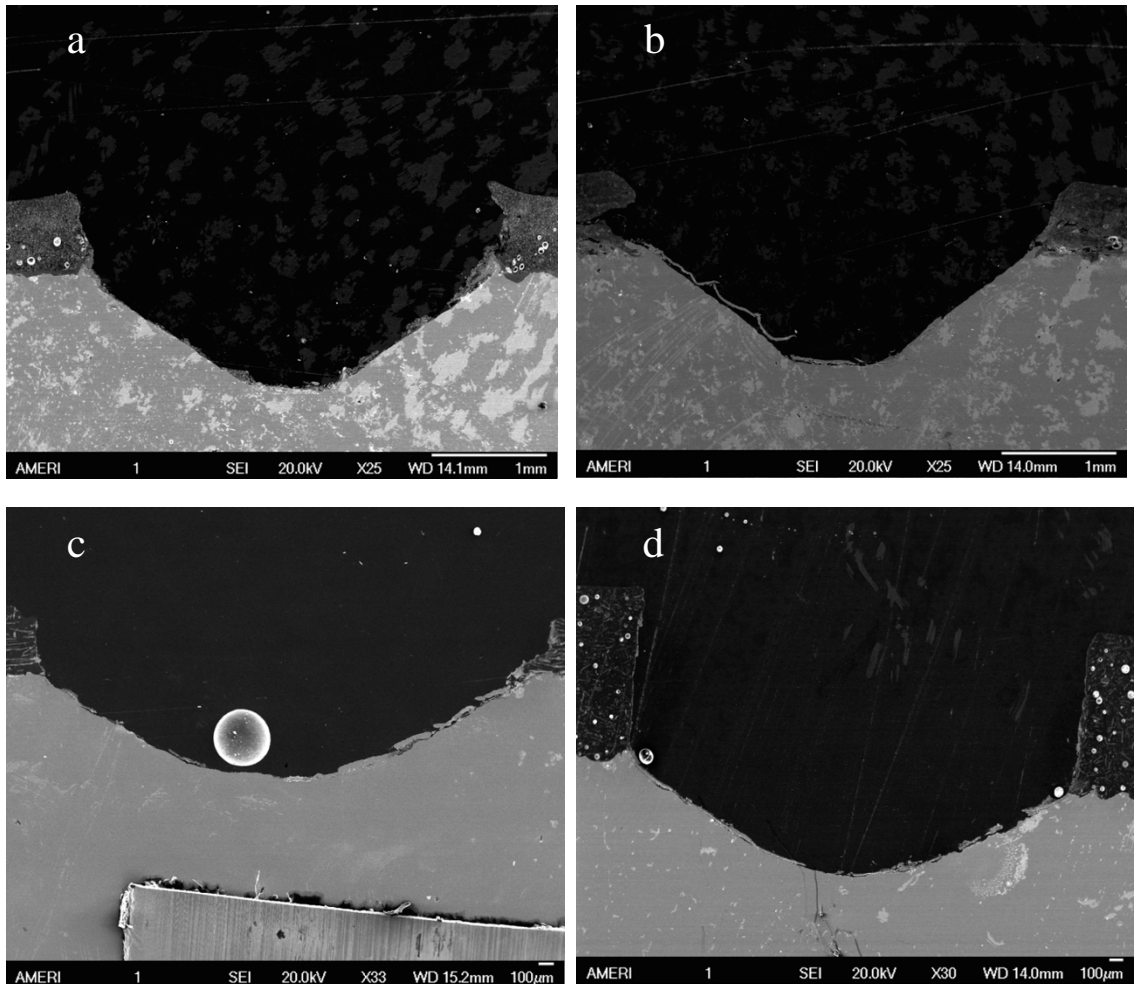


Figure 66: SEM images of the cross-sectional area of the pinholes. (a) FBE (b) Phenolic (c) Amine Novolac (d) Novolac.

The SEM images result of the cross-sectional area of the artificial pinhole in the FBE coating is demonstrated in Figure 67 along with the EDS spectrum. The EDS results revealed elements including C, Fe, O and Cl which suggest that the corrosion products consist mainly of iron oxide. The presence of chloride (Cl) is attributed to the chloride ions in the 3% NaCl electrolyte solution.

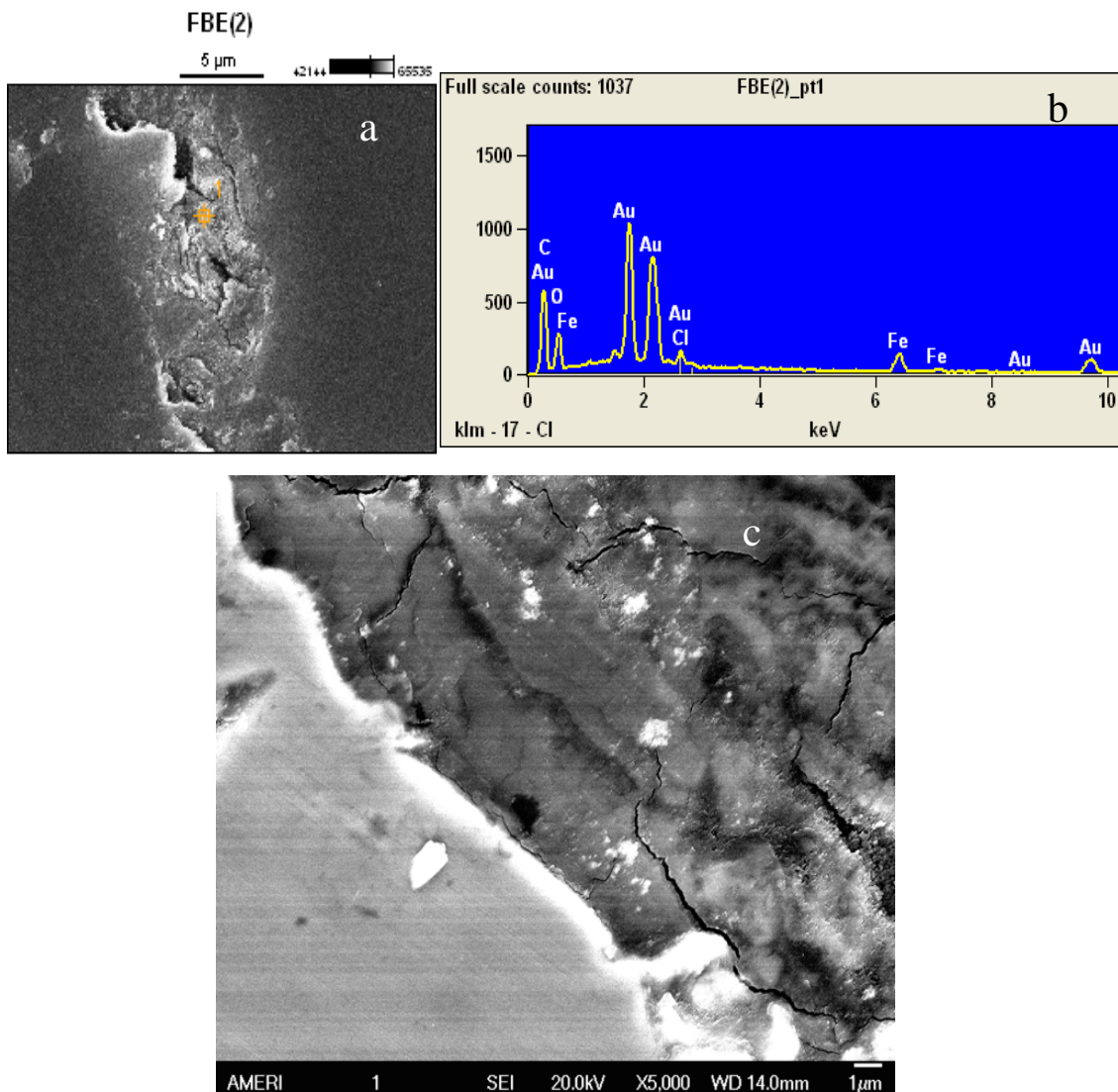


Figure 67: (a) and (c): SEM image of corrosion products in pinhole. (b) EDS spectrum illustrating the elemental composition of the region marked in (a).

The SEM/EDS results of the pinhole for the Phenolic coating is illustrated in Figure 76. The EDS results revealed the presence of elements including C, Fe, O and Cl which imply that the corrosion products consist mainly of iron oxide. Similar to FBE, the chloride (Cl) is present as a result of the chloride ions in the 3% NaCl solution. In addition, Figure 68 (c) shows the SEM image of the pinhole near the interfacial layer between the coating and steel. It can be observed that the coating has delaminated from the steel substrate near the pinhole areas.

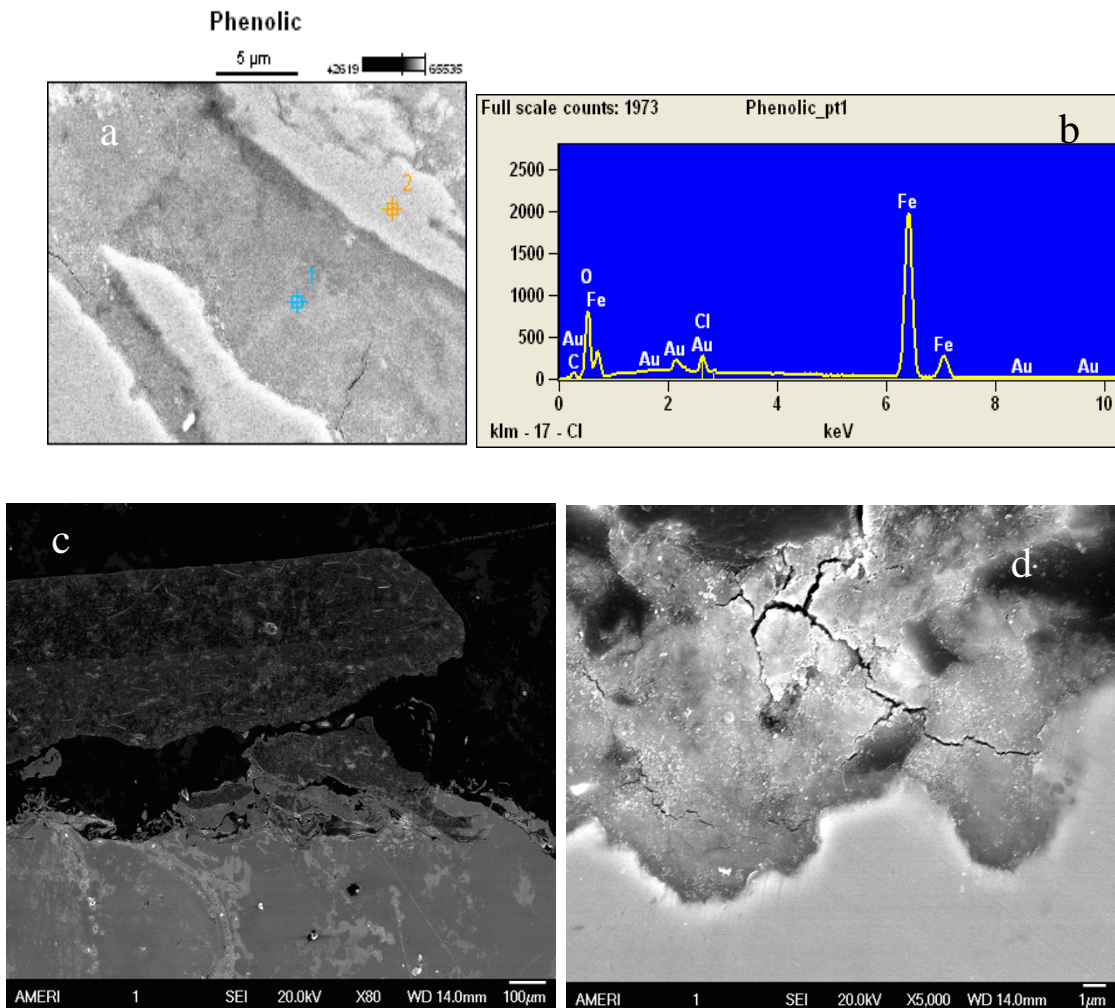


Figure 68: (a), (c) and (d): SEM image of corrosion products in pinhole. (b) EDS spectrum illustrating the elemental composition of the region marked in (a).

The SEM images result of the cross-sectional area of the pinhole for the Novolac coating is demonstrated in Figure 69 with the EDS spectrum result. The EDS results revealed elements including C, Fe, O, Cl and S which suggest that the corrosion products consist of mixtures of iron oxide and iron sulfide. The chloride (Cl) is present as a result of the chloride ions in the 3% NaCl solution. In addition, the presence of sulfur (S) in corrosion products is associated with exposure to the sour environment and hydrogen sulfide (H₂S) gas during the autoclave test.

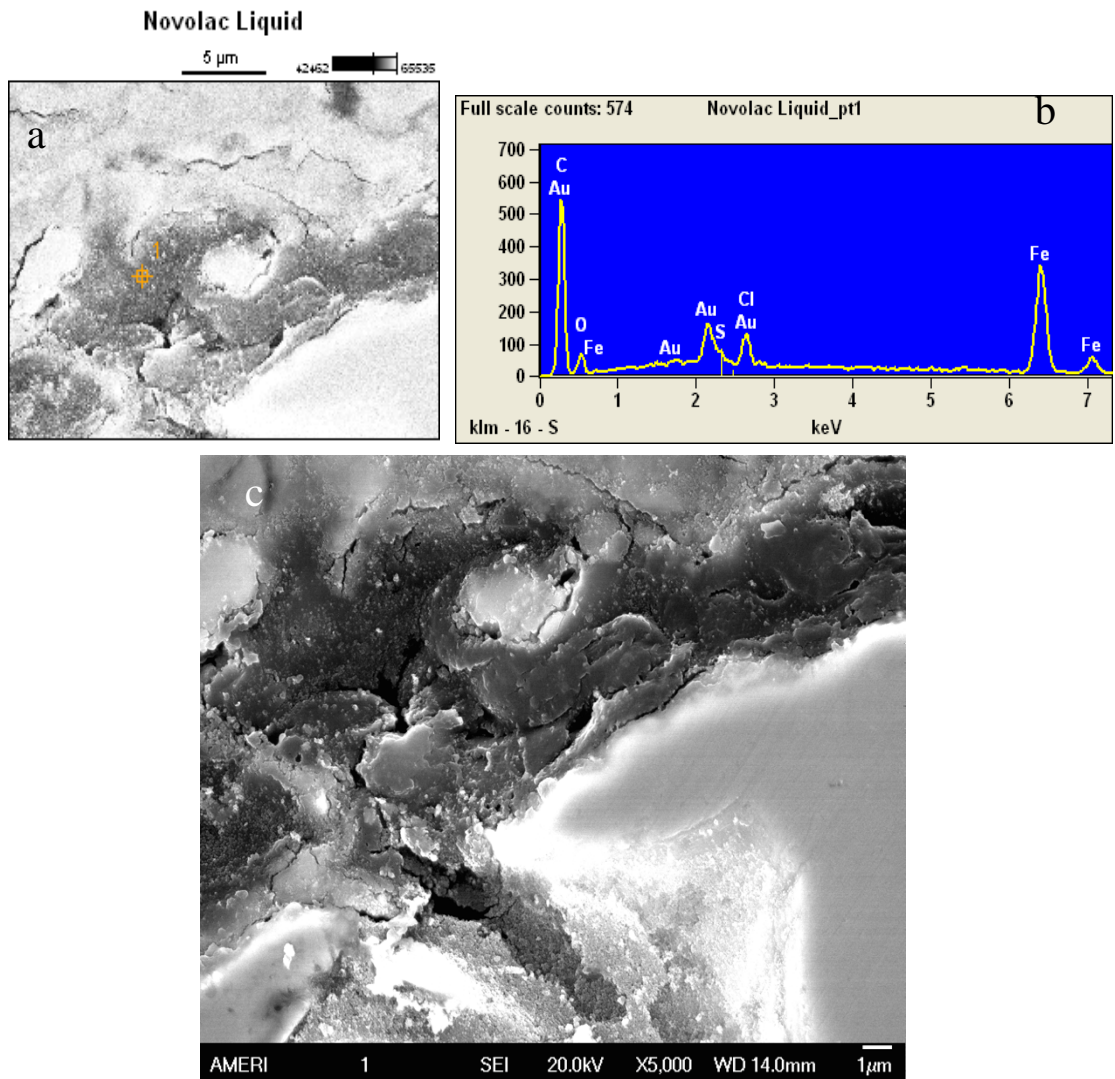


Figure 69: (a) and (c): SEM image of corrosion products in pinhole. (b) EDS spectrum illustrating the elemental composition of the region marked in (a).

For the Amine Novolac coating, the SEM images result of the cross-sectional area of the pinhole is presented in Figure 70 with the EDS spectrum result. The EDS results were similar to the Novolac coating results and revealed elements including C, Fe, O, Cl and S which suggest that the corrosion products consist of mixtures of iron oxide and iron sulfide. The chloride (Cl) is present as a result of the chloride ions in the 3% NaCl solution. Similarly, the presence of sulfur (S) in corrosion products is due to exposure to the sour gas environment during the autoclave test.

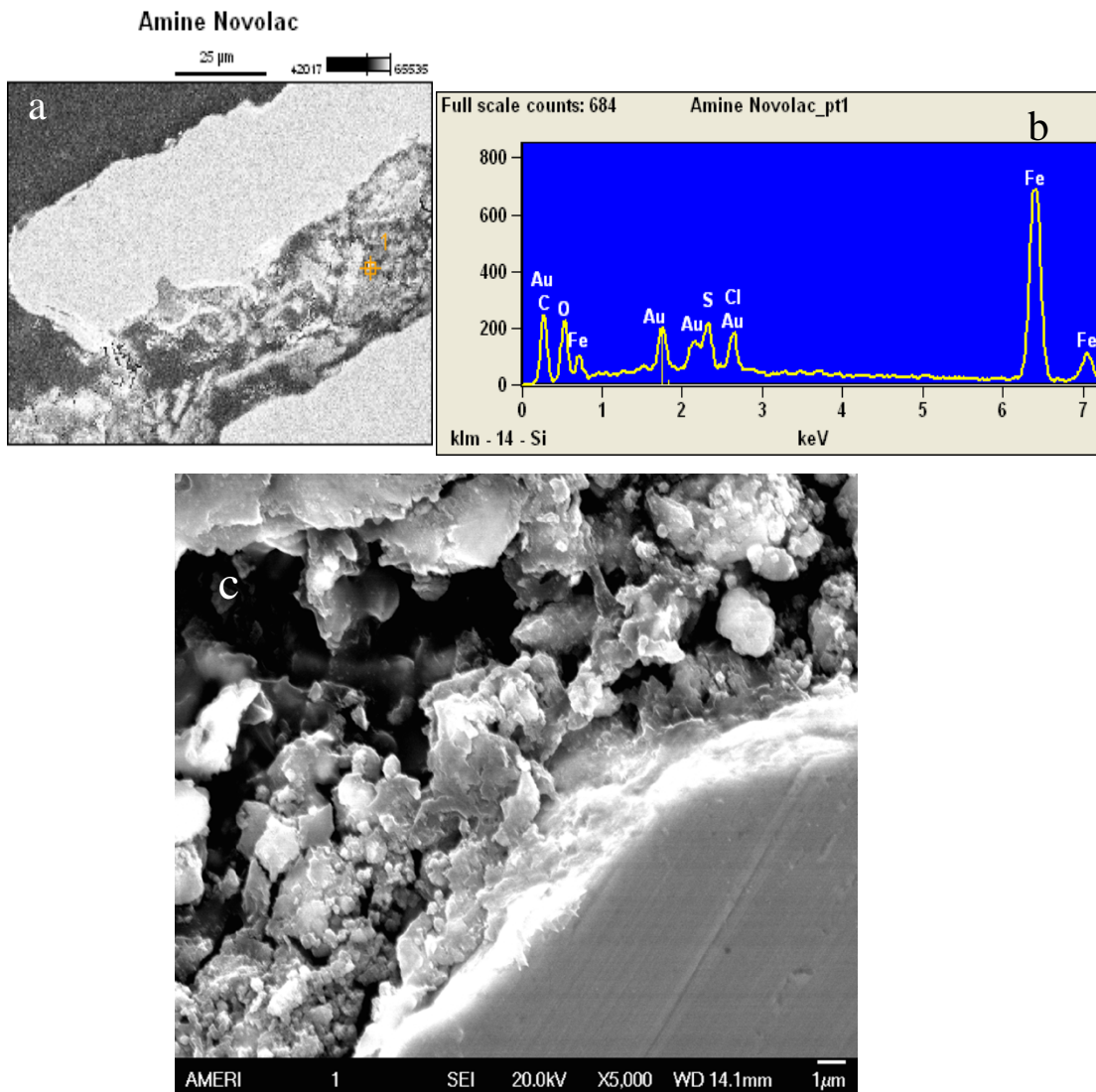


Figure 70: (a) and (c): SEM image of corrosion products in pinhole. (b) EDS spectrum illustrating the elemental composition of the region marked in (a).

CHAPTER 6

6.0 CONCLUSIONS AND RECOMMENDATIONS

6.1 Conclusions

The results of the as-received coatings revealed that both the FBE and Novolac Epoxy coatings exhibited excellent adhesion properties and superior chemical resistance to the sour environment. The measured coating impedances for both the FBE and Novolac were significantly high and remained steady throughout the EIS testing period before and after the autoclave test. In addition, the FBE and Novolac coatings exhibited low coating capacitance which indicated that there was no significant water absorption by the coatings. Moreover, the FBE and Novolac coatings did not experience any blistering during exposure to the sour environment which imply that both coatings had excellent adhesion properties. Furthermore, all the pull-off adhesion test failures were recorded as glue failures for both coatings before and after the autoclave test, which indicated that both coatings had outstanding adhesion properties and were considered high performance coatings.

The Amine Novolac Epoxy coating had excellent coating impedance before the autoclave test and was considered a high performance coating before exposure to the sour gas environment. In addition, the coating capacitance of the Amine Novolac coating was low but it slightly increased over time. Additionally, the Amine Novolac coating had high pore resistance over the week of EIS testing in 3% NaCl solution before the autoclave. However, after the autoclave test, blisters were formed on the coating and the measured impedance of the Amine Novolac coating was lower than before the autoclave and significantly decreased over time. Moreover, the capacitance of the Amine Novolac coating started to remarkably increase particularly in the liquid phase. In addition, a decrease of

two to three orders of magnitude was observed in the pore resistance of the Amine Novolac coating which suggest that the electrolytes have penetrated the micropores of the coating.

The Phenolic epoxy coating had significantly low impedance as compared to the other coatings since the first day of EIS testing and it significantly decreased over time. Moreover, the determined pore resistance of the Phenolic coating was low which indicated that the electrolytes have penetrated through the coating and reached the metal surface even before the autoclave test. Besides, the Phenolic coating had relatively low capacitance over the first few days however, it significantly increased with time especially after the autoclave test which indicated that water and ions have penetrated the coating through the pores and corrosion initiated under the coating.

The results of the pin-holed coatings revealed that the Phenolic coating had the highest corrosion current density (i_{corr}) before and after the autoclave test whereas the Novolac coating had the lowest i_{corr} . In addition, the FBE and Amine Novolac coatings had similar values of i_{corr} and they slightly increased over time. Furthermore, the determined corrosion current density (i_{corr}) in the liquid phase were slightly higher in comparison to the gas phase. This imply that during exposure to the gas and liquid phases in the autoclave, the pinholes which were exposed to the liquid suffered more corrosion.

6.2 Recommendations and Future Work

- The use of the autoclave and EIS testing on the coatings demonstrated the need to use elevated temperatures and pressures to examine the stability and adhesion properties of the coatings.
- In EIS experiments, the use of Faraday's cage is recommended to reduce noise.

- Laboratory testing cannot duplicate all of the chemical and process conditions that occur in the field. Therefore, field testing is recommended to be done as the final qualification of a coating.

REFERENCES

- [1] Alexandre Rojey, Claude Jaffret. (1994). Natural Gas Production Processing Transport. Editions Technip, Paris, p. 18-24.
- [2] R. Winston Revie. (2011). Uhlig's Corrosion Handbook. By John Wiley & Sons.
- [3] A. S. Khanna. (2008). High-Performance Organic Coatings. Woodhead Publishing Limited.
- [4] The Economist Intelligence Unit. (September 6th, 2013). Saudi Arabia gas: Saudi Aramco accelerates its gas development programme. Natural Gas, Saudi Aramco.
- [5] Al Wasit Gas Program, Saudi Arabia. offshore-technology.com.
- [6] Najmiddin Yaakob, Marc Snger and David Young. (2014). Top of the Line Corrosion Behavior in Highly Sour Environment Effect of Gas Temperature. Corrosion 2014, Paper No. 3807 (San Antonio, Texas, USA).
- [7] Sankara Papavinasam. (2014). Corrosion Control in the Oil and Gas Industry. Elsevier Inc.
- [8] Sergio Kapusta. (2008). Managing Corrosion In Sour Gas Systems: Testing, Design, Implementation And Field Experience. Corrosion 2008, Paper No. 08641.
- [9] D. Martíneza, R. Gonzalezb, K. Montemayor a, A. Juarez-Hernandeza, G. Fajardob, M.A.L. Hernandez-Rodrigueza. (2009). Amine type inhibitor effect on corrosion–erosion wear in oil gas pipes” Wear 267 (2009) 255–258.
- [10] D.G. Enos, J.A. Kehr, C.R. Guilbert. A High Performance, Damage Tolerant Fusion Bonded Epoxy Coating. 3M Company, 3M Austin Technical Center.
- [11] Qiang Liu. (2012). Elemental sulphur uptake and corrosion protection in sour gas systems. Corrosion 2012, Paper No. 0001090.
- [12] Rolf Nyborg. (2010). CO₂ Corrosion Models For Oil And Gas Production Systems” Corrosion 2010, Paper No. 10371.
- [13] Mike O’Donoghue, Ph.D., Ron Garrett, Jamie Garrett. (2003). Field Performance Versus Laboratory Testing: A Study Of Epoxy Tank And Vessel Linings Used In The Canadian Oil Patch. Corrosion 2003, Paper No. 03051 (Edmonton, Alberta, Canada).
- [14] Larry Chen, Nihal Obeyesekere, Jonathan Wylde. The Effect of Surfactant Additions on the Mechanism of Sulfur Corrosion in Aqueous Sour Systems. Corrosion, Paper No. 3828.

- [15] Justin Beck, Serguei Lvov, Ruishu Feng, Margaret Ziomek-Moroz. (2014). Study of Dissolved H₂S in Deaerated Brine Environments on the Corrosion Behavior of High Strength Low Alloy Carbon Steel. Corrosion 2014, Paper No. 4191.
- [16] Bruce Brown, David Young, and Srdjan Nešić. Localized Corrosion In An H₂S / CO₂ Environment” NACE International. Paper No. 2704.
- [17] <http://susris.com/wp-content/uploads/2013/02/eia-4.gif>. (Figure 1: Natural Gas Offshore Fields in Arabian Gulf).
- [18] Lekan Taofeek Popoola¹, Alhaji Shehu Grema, Ganiyu Kayode Latinwo, Babagana Gutti and Adebori Saheed Balogun. (2013). Corrosion problems during oil and gas production and its mitigation” International Journal of Industrial Chemistry 2013, 4:35.
- [19] Saudi Aramco. DOCUMENT No. 01-LF-E-D94817CA
- [20] Robert Heidersbach. (2011). Metallurgy and Corrosion Control in Oil and Gas Production. Wiley.
- [21] Dugstad A, Seiersten M, Nyberg R. (March 2003). Flow Assurance of pH Stabilized Wet Gas Pipelines. Corrosion 2003 Conference and Expo; San Diego, CA: NACE International; paper no. 03314.
- [22] Gulbrandsen E, Morard J. (1998). Why Does Glycol Inhibit CO₂ Corrosion? Corrosion 98 Conference and Expo; Houston, TX: NACE International; 1998, paper no. 98221.
- [23] <http://www.lpdlabsservices.co.uk/>. (Figure 7: Adhesion and cohesive failure of coatings systems).
- [24] ASTM Standard-D4541. Standard Test Method for Pull-Off Strength of Coatings Using Portable Adhesion Testers.
- [25] NACE Standard-TM0185. TM0185-2006, Evaluation of Internal Plastic Coatings for Corrosion Control of Tubular Goods by Autoclave Testing.
- [26] David Loveday, Pete Peterson, and Bob Rodgers. (August 2004). Evaluation of Organic Coatings with Electrochemical Impedance Spectroscopy: Part 1: Fundamentals of Electrochemical Impedance Spectroscopy, Part 2: Application of EIS to Coatings, and Part 3: Protocols for Testing Coatings with EIS. Gamry Instruments, JCT CoatingsTech.
- [27] Mars G. Fontana (1987). Corrosion Engineering. McGraw-Hill Book Company.
- [28] Princeton Applied Research. Basics of Electrochemical Impedance Spectroscopy. Application Note AC- 1.

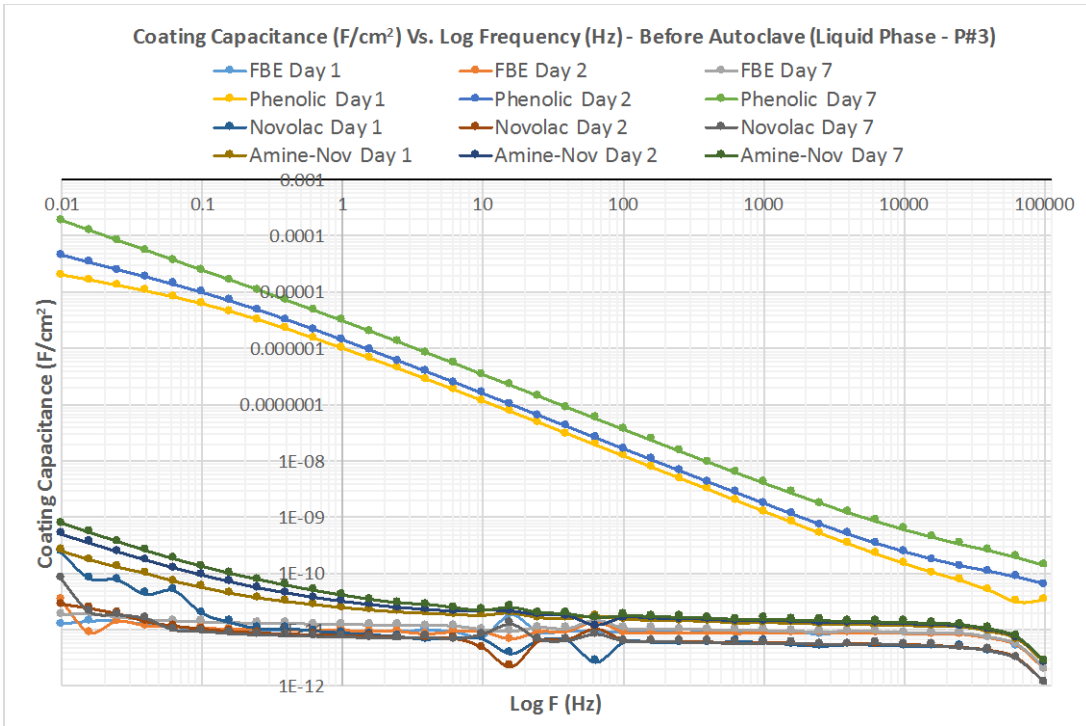
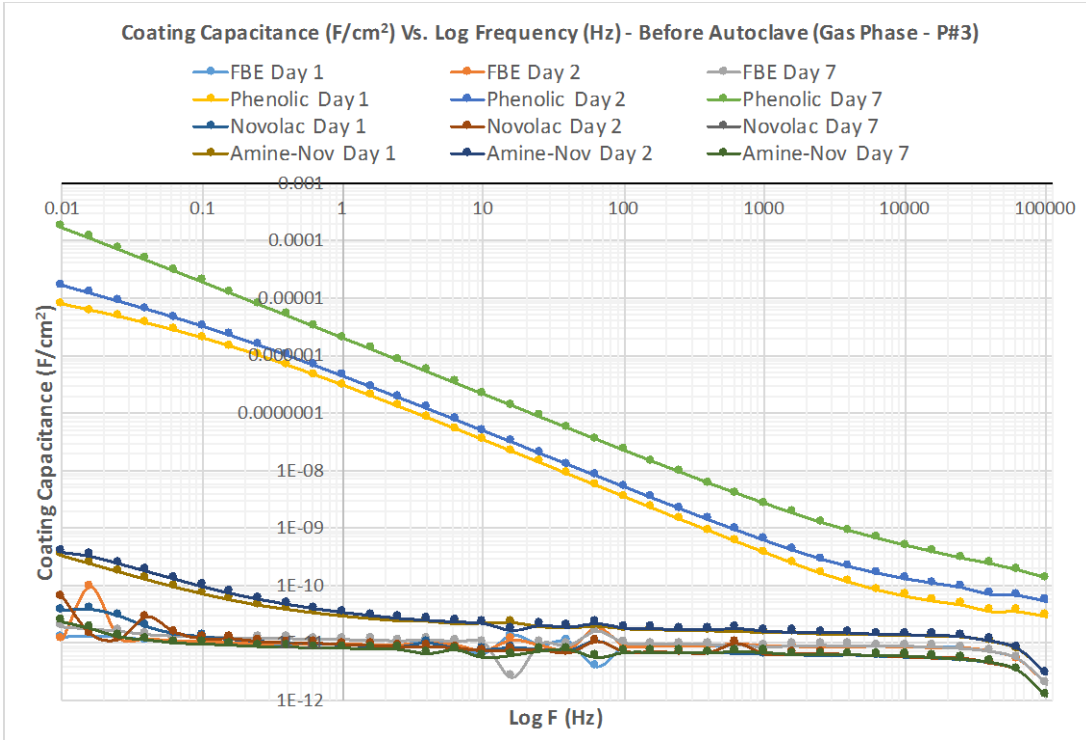
[29] <http://www.gamry.com/application-notes>. Basics of Electrochemical Impedance Spectroscopy.

[30] Gordon Bierwagen, Dennis Tallman, Junping Li, Lingyun He, Carol Jeffcoate. (2003) EIS studies of coated metals in accelerated exposure” Progress in Organic Coatings 46 (2003) 148–157.

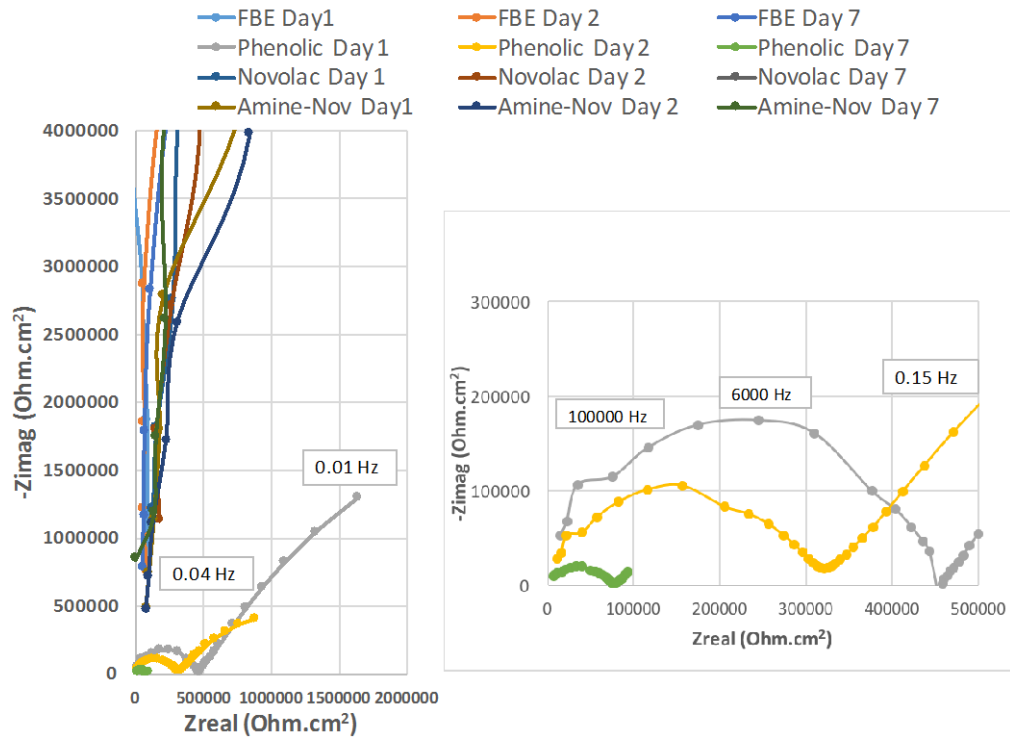
[31] <http://www.dfdinstruments.co.uk/topics/Study5-ASTM-D4541.htm>. (Figure 23: Test dolly glued on a coated substrate).

[32] Vaughn O'Dea and Remi Briand, Tnemec Co.; and Linda Gray. (April, 2008). Assessing Coatings & Linings for Wastewater: Accelerated Test Evaluates Resistance to Severe Exposures. KTA-Tator (Canada) Inc.

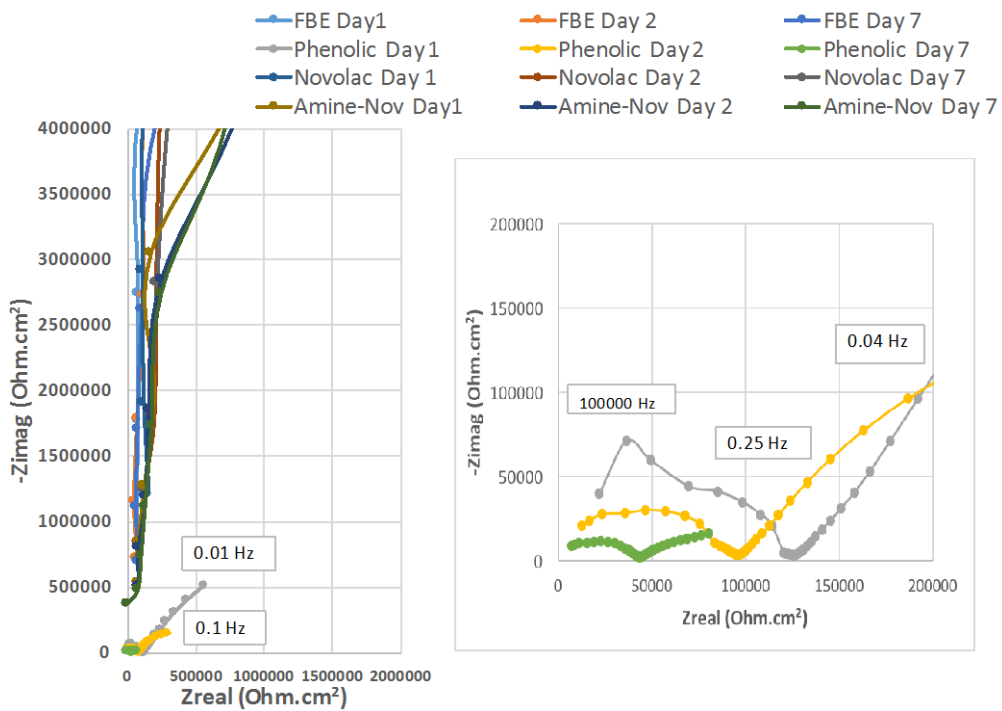
APPENDICES

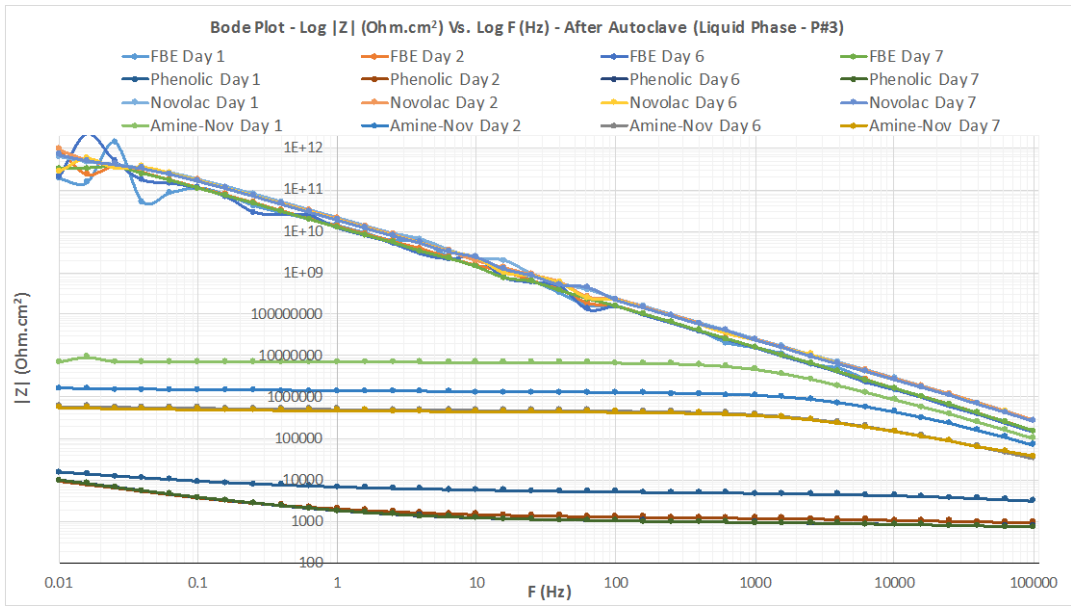
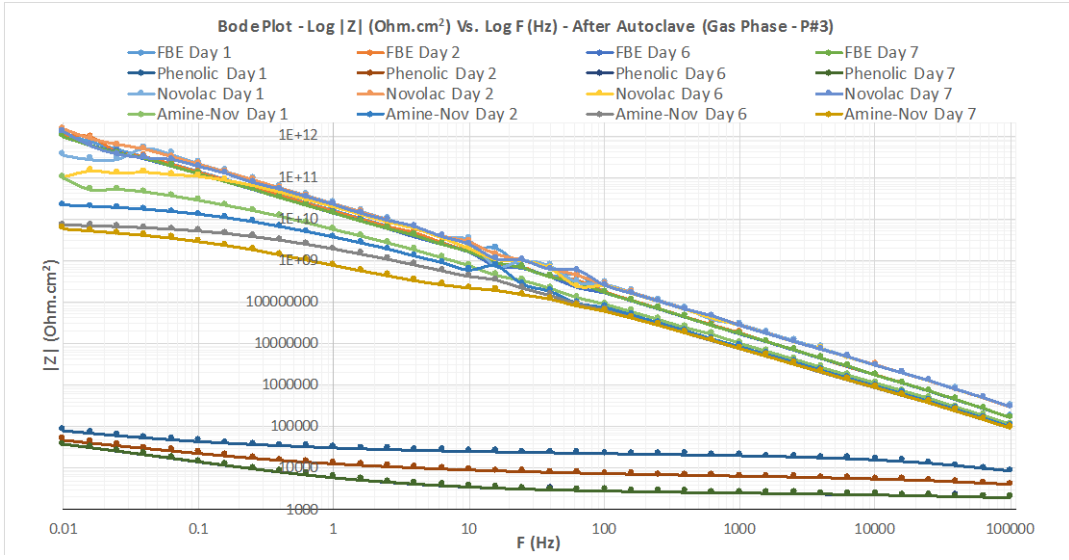


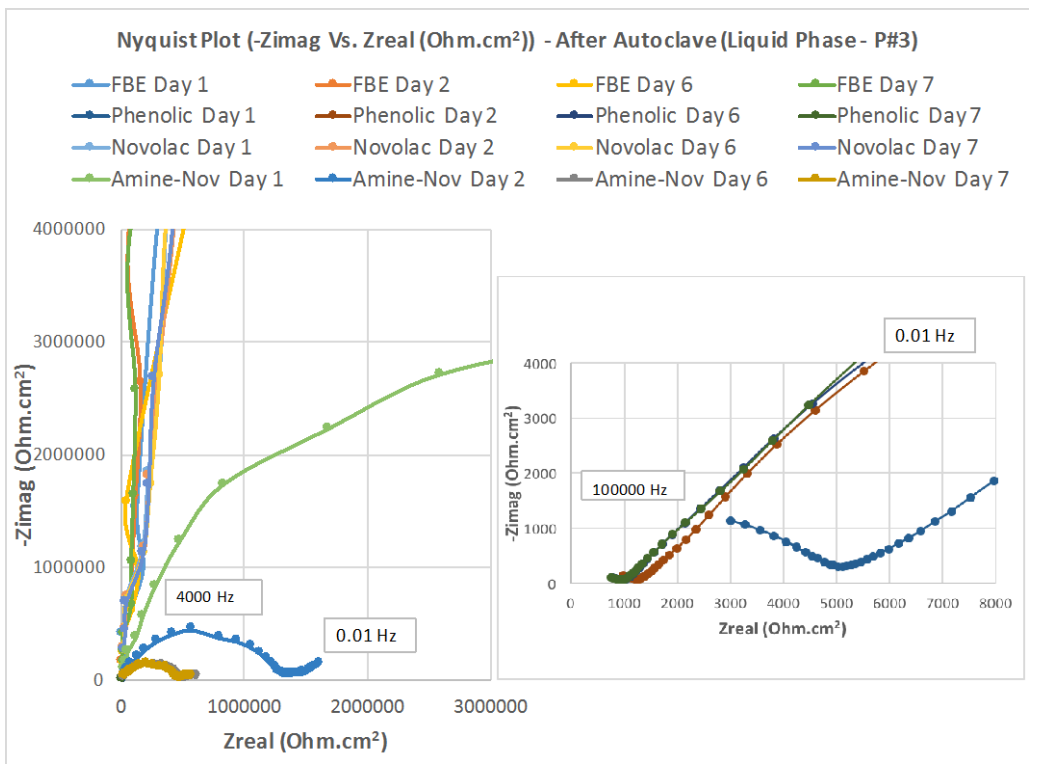
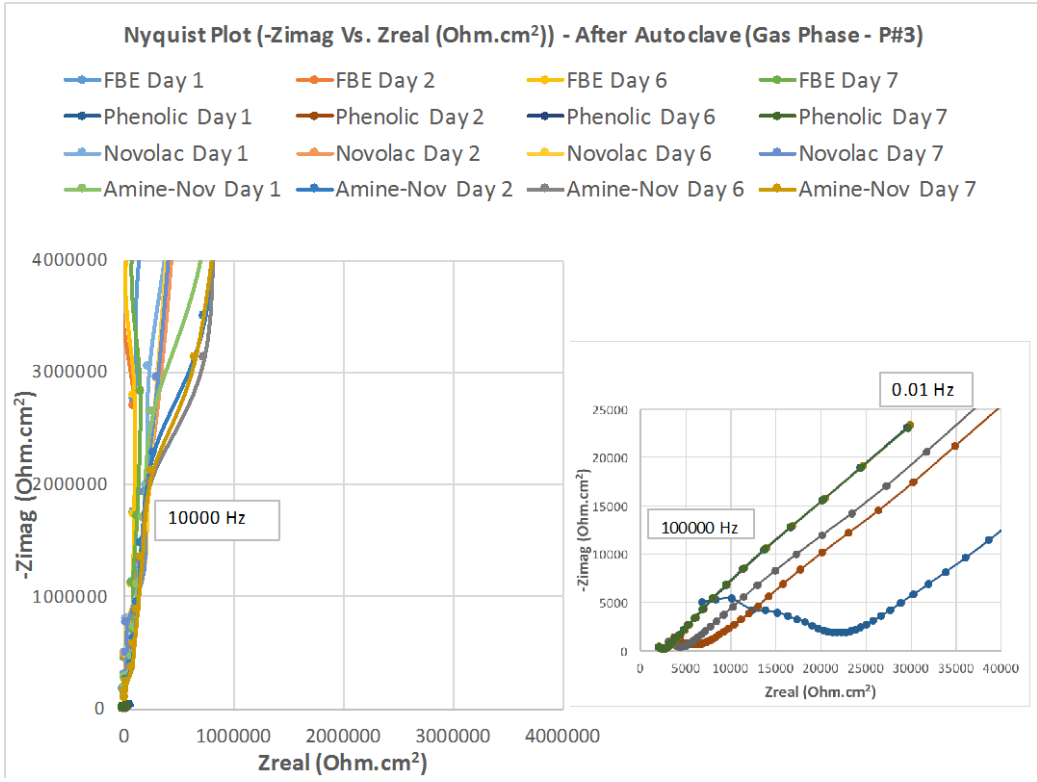
Nyquist Plot (-Zimag Vs. Zreal (Ohm.cm²)) - Before Autoclave (Gas Phase - P#3)

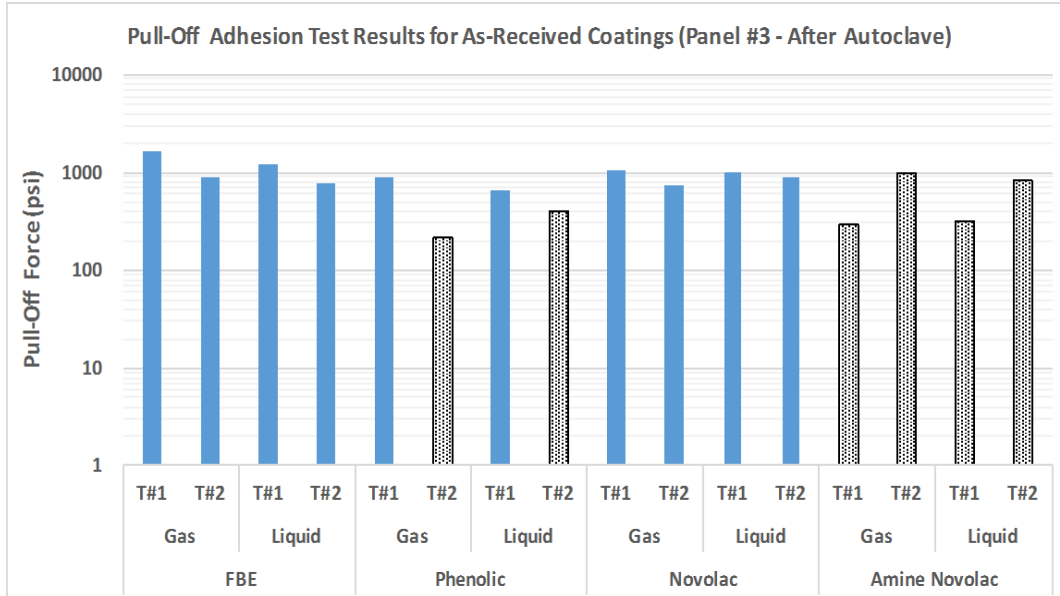


Nyquist Plot (-Zimag Vs. Zreal (Ohm.cm²)) - Before Autoclave (Liquid Phase - P#3)









Brasher-Kingsbury Equation:

$$\text{Volume Fraction H}_2\text{O} = (\log C_t / C_o) / \log \epsilon_w$$

Where C_t = coating capacitance at time t
 C_o = initial coating capacitance
 ϵ_w = dielectric constant of water (80)